PSU-IRL-SCI-438

Classification Numbers 1.5.2, 1.5.3, 1.9.4, 1.9.6

THE PENNSYLVANIA
STATE UNIVERSITY

IONOSPHERIC RESEARCH

Scientific Report 438

ELECTRIC FIELDS IN THE IONOSPHERE

by

Volker W. J. H. Kirchhoff

October 3, 1975

The research reported in this document has been supported by The National Science Foundation under Grant No. 33446X2 and The National Aeronautics and Space Administration under Grant No. 39-009-003.

IONOSPHERE RESEARCH LABORATORY

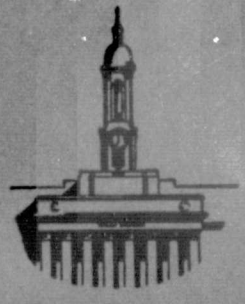

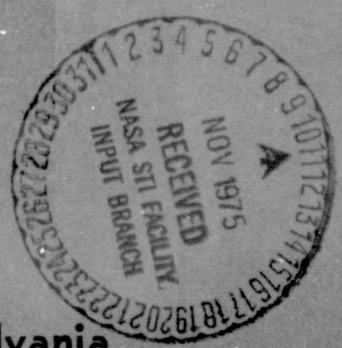

University Park, Pennsylvania

Security Classification

DOCUMENT CONTROL DATA - R & D

(Security classification of title, body of abstract and indexing annotation must be entered when the overall report is classified)

1. ORIGINATING ACTIVITY (Corporate author)	2a. REPORT SECURITY CLASSIFICATION
The Ionosphere Research Laboratory	2b. GROUP

3. REPORT TITLE

Electric Fields in the Ionosphere

4. DESCRIPTIVE NOTES (Type of report and, inclusive dates)

Scientific Report

5. AUTHOR(S) (First name, middle initial, last name)

Volker W. J. H. Kirchhoff

6. REPORT DATE	7a. TOTAL NO. OF PAGES	7b. NO. OF REFS
October 3, 1975	139	

8a. CONTRACT OR GRANT NO.	9a. ORIGINATOR'S REPORT NUMBER(S)
NSF GA 33446X2 b. PROJECT NO. NASA NGL 39-009-003	PSU-IRL-SCI-438
c.	9b. OTHER REPORT NO(S) (Any other numbers that may be assigned this report)
d.	

10. DISTRIBUTION STATEMENT

Supporting Agencies

11. SUPPLEMENTARY NOTES	12. SPONSORING MILITARY ACTIVITY
	National Science Foundation The National Aeronautics and Space Administration

13. ABSTRACT

F-region drift velocities, measured by the Millstone Hill incoherent-scatter radar have been analyzed in terms of diurnal, seasonal, magnetic activity, and solar cycle effects.

A comprehensive electric field model has been developed that includes the effects of the E and F-region dynamos, magnetospheric sources, and the ionospheric conductivities, for both the local and conjugate regions. Through its use the importance of the different sources is determined. The E-region dynamo dominates during the day but at night the F-region and convection are more important. This model provides much better agreement with observations of the F-region drifts than previous models.

Measurements and calculations indicate larger magnitudes at night, and the daily variation is dominated by the diurnal mode. Seasonal variations introduced through variations in conductivities and thermospheric winds indicate a reversal in direction in the early morning during winter, from south to northward. On magnetic perturbed days the drifts deviate rather strongly from the quiet days average, especially around 13 L.T. for the northward and 18 L.T. for the westward component.

PSU-IRL-SCI-438
Classification Numbers 1.5.2, 1.5.3, 1.9.4, 1.9.6

Scientific Report 438

Electric Fields in the Ionosphere

by

Volker W. J. H. Kirchhoff

October 3, 1975

The research reported in this document has been supported by The National Science Foundation under Grant No. 33446X2 and The National Aeronautics and Space Administration under Grant No. 39-009-003.

Submitted by:

L. A. Carpenter, Assistant Professor of Electrical Engineering

Approved by:

J. S. Nisbet, Director
Ionosphere Research Laboratory

Ionosphere Research Laboratory
The Pennsylvania State University
University Park, Pennsylvania 16802

ACKNOWLEDGEMENTS

I wish to express my gratitude to Dr. Lynn Carpenter for his guidance and support during the course of this research. Dr. Carpenter and Dr. John Nisbet, who served as co-chairmen of the doctoral committee, closely followed the main steps of this work and I benefited from many useful discussions. Dr. Nisbet as Director of the Ionosphere Research Laboratory provided facilities for a number of trips to Millstone Hill and scientific meetings. Drs. R. Greenfield, G. McMurtry and J. Mentzer served as members of the thesis committee and their interest is greatly appreciated.

During many trips to the Millstone Hill Incoherent Scatter Station I had the privilege to participate in a number of discussions on current research with Drs. J. V. Evans and J. E. Salah whose kind and friendly attitude has induced very much appreciation.

The Brazilian Institute for Space Research (INPE) provided me with financial support. I thank its director, Dr. F. de Mendonça, for his efforts to improve the support to Brazilian students abroad.

TABLE OF CONTENTS

Page

LIST OF TABLES

LIST OF FIGURES

ABSTRACT

F-region drift velocities, measured by the Millstone Hill incoherent-scatter radar, have been analyzed in terms of diurnal, seasonal, magnetic activity, and solar cycle effects.

A comprehensive electric field model has been developed that includes the effects of the E and F-region dynamos, magnetospheric sources, and the ionospheric conductivities, for both the local and conjugate regions. Through its use the importance of the different sources is determined. The E-region dynamo dominates during the day but at night the F-region dynamo and convection are more important. This model provides much better agreement with observations of the F-region drifts than previous models.

Measurements and calculations indicate larger magnitudes at night, and the daily variation is dominated by the diurnal mode. Seasonal variations introduced through variations in conductivities and thermospheric winds indicate a reversal in direction in the early morning during winter, from south to northward. On magnetic perturbed days the drifts deviate rather strongly from the quiet days average, especially around 13 L. T. for the northward and 18 L. T. for the westward component.

CHAPTER I

INTRODUCTION

1.1 General Statement of the Problem

The general aim of this research is to determine the electric field in the F-region at midlatitudes and to study the factors controlling its variations.

The origin of the earth's geomagnetic fluctuations and their relation to currents flowing in the ionosphere have been studied for over a century. These currents can be directly related to electric fields through the ionospheric conductivities if these are known. This relationship between geomagnetic variations measured on the ground, electric currents flowing in the lower ionosphere, and the associated electric fields was called the atmospheric dynamo theory and in this work this mechanism will be referred to as the E-region dynamo. While the geomagnetic fluctuations provided an indication of the currents, it did not give a good indication of the electric fields because the conductivity is very much lower at night than during the day and because only the current variations could be sensed with no indication of the zero level.

More recently other sources for the electric field have been recognized, notably magnetospheric convection electric fields and F-region dynamo fields. Measurement techniques have been developed which allow the electric field itself to be measured. Ground based measurements using whistlers and the incoherent backscatter radars and air borne measurements using balloons, rockets and satellites have been made.

Ionospheric electric fields are of great interest because of the information they provide on the physics of the solar-terrestrial interactions. They have great practical interest because of the large effect they have on the transport in the F-region of the ionosphere, the associated effect on electron densities and on the wind systems which control the behavior of the thermosphere.

1.2 Historical Summary

The prediction that electric currents flow in the upper atmosphere dates back to the early studies of the variations of the geomagnetic field components. Stewart (1882) postulated that the quiet daily magnetic variations are caused by currents flowing in the upper atmosphere and proposed that they are established by the sun's heating action on the upper parts of the atmosphere. This theory is now known as the atmospheric dynamo theory since the action described is similar to that of a dynamo or current generator in which the earth is the magnet and the moving air the armature.

Quantitatively the dynamo theory was first studied by Shuster (1889, 1908) who showed that indeed the currents could be explained by tidal air motions. Chapman (1913, 1919) extended the treatment using spherical harmonics as the basic mathematical tool and the daily geomagnetic variations as the main measured input parameter. Worldwide equivalent current systems were calculated and thoroughly discussed in Chapman and Bartels (1940).

The effects of the geomagnetic field on the electric conductivity was studied by Hirono (1950, 1952, 1953) and atmospheric tides in the ionosphere were considered by Martyn (1948). Horizontal wind

systems in the E-region were deduced by Maeda (1955) and these studies served as a basis for the subsequent deduction of F-region ionization drifts (Maeda, 1963) presented as a function of latitude and local time and which served as a theoretical model for comparisons with measured drift velocities.

Matsushita (1969, 1971) also calculated F-region electric fields often used as a standard for comparison with experimental data, and more recently Stening (1973) produced a model of electric fields allowing for seasonal and longitudinal variations.

1.2.1 Electric Field Models

From the analysis of the measured variations of the components of the geomagnetic flux density vector $\vec{B}(x, y, z)$, it was concluded that the variations could not be caused directly by the sun but that an overhead current system in the upper atmosphere could account for them. It is now well established that such a conducting layer, where currents flow, exists in the E-region of the ionosphere. This atmospheric dynamo region extends from about 90 km to 150 km in altitude and is that region which has the highest values of conductivity. Wind motions triggered by the daily heating action of the sun transfer momentum to ions and electrons which in presence of the magnetic field move in different directions thus giving origin to an electric current.

The basic tensor equation for dynamo theory studies is the generalized Ohm's law

$$\vec{J} = \sigma \vec{E}' = \sigma (\vec{E} + \vec{U} \times \vec{B}) \qquad (A/m^2) \qquad (1.2.1)$$

where

$\vec{J}$ is the current density (A/m^2),

σ is the conductivity tensor ($\Omega^{-1}m^{-1}$),

$\vec{E}'$ is the total electric field vector,

$\vec{E}$ is the polarization electric field vector (V/m) established through charge separation, and

$\vec{U} \times \vec{B}$ is the induced or dynamo electric field, U being the neutral air velocity vector (m/sec) and B the magnetic flux density vector ($T = 10^{-9}\ \gamma$ = Weber/m^2).

In studying ionospheric electric fields, it is convenient to separate the electric field vector into components perpendicular ($\vec{E}'_{\perp}$) and parallel ($\vec{E}'_{//}$) to the magnetic field. The ionospheric current vector can then be expressed by

$$\vec{J} = \sigma_o \vec{E}'_{//} + \sigma_1 \vec{E}'_{\perp} + \sigma_2 (\vec{B} \times \vec{E}'_{\perp})/B \qquad (1.2.2)$$

where $\vec{E}'_{//}$ is the total electric field parallel to $\vec{B}$, and $\vec{E}'_{\perp}$ is the total electric field perpendicular to $\vec{B}$. The dynamo problem can be solved with the additional conditions

$$\nabla \cdot \vec{J} = 0$$

$$\nabla \times \vec{E}' = \nabla \times (\vec{U} \times \vec{B})$$

Basically, two approaches have been used to this end. One uses the Sq current system derived from the quiet daily magnetic variations to calculate winds and electric fields, while the other assumes a neutral wind model and calculates the resulting currents. Using the first

approach Maeda (1963) deduced a model of drift velocities for the F-region, while Matsushita (1971) and Stening (1973) used the second approach.

The Maeda model represents drift velocities in the F-region of the ionosphere (Maeda, 1963), as a function of latitude and local time. These velocities are based on electric field calculations (Maeda, 1955) based on the Sq distribution calculated for the Second Polar Year, 1932-33. Since drift velocities and electric fields in the F-region are simply related by (see Section 1.2.4)

$$\vec{V} = \frac{\vec{E} \times \vec{B}}{B^2} \qquad (1.2.3)$$

these drift velocities also represent electric field information. This drift velocity model is shown in Figure 1.2.1.

Since the vertical dimension is much smaller than the horizontal one, the equivalent current system obtained from geomagnetic variations is considered the flow in a thin shell around the earth. Therefore, it does not provide information on the vertical structure of the winds that generate it, and only an equivalent height-independent wind system can be deduced. Tarpley (1970a, b), Matsushita and Tarpley (1970) and Matsushita (1971) assume the wind field to be known and calculate the resulting current distribution. Tarpley studied the current generating properties of different tidal modes of the neutral wind with different height variations, concluding that neutral winds of the diurnal mode are the ones that reproduce the Sq pattern more closely, which is in disagreement with most experimental results which favor the semi-diurnal mode.

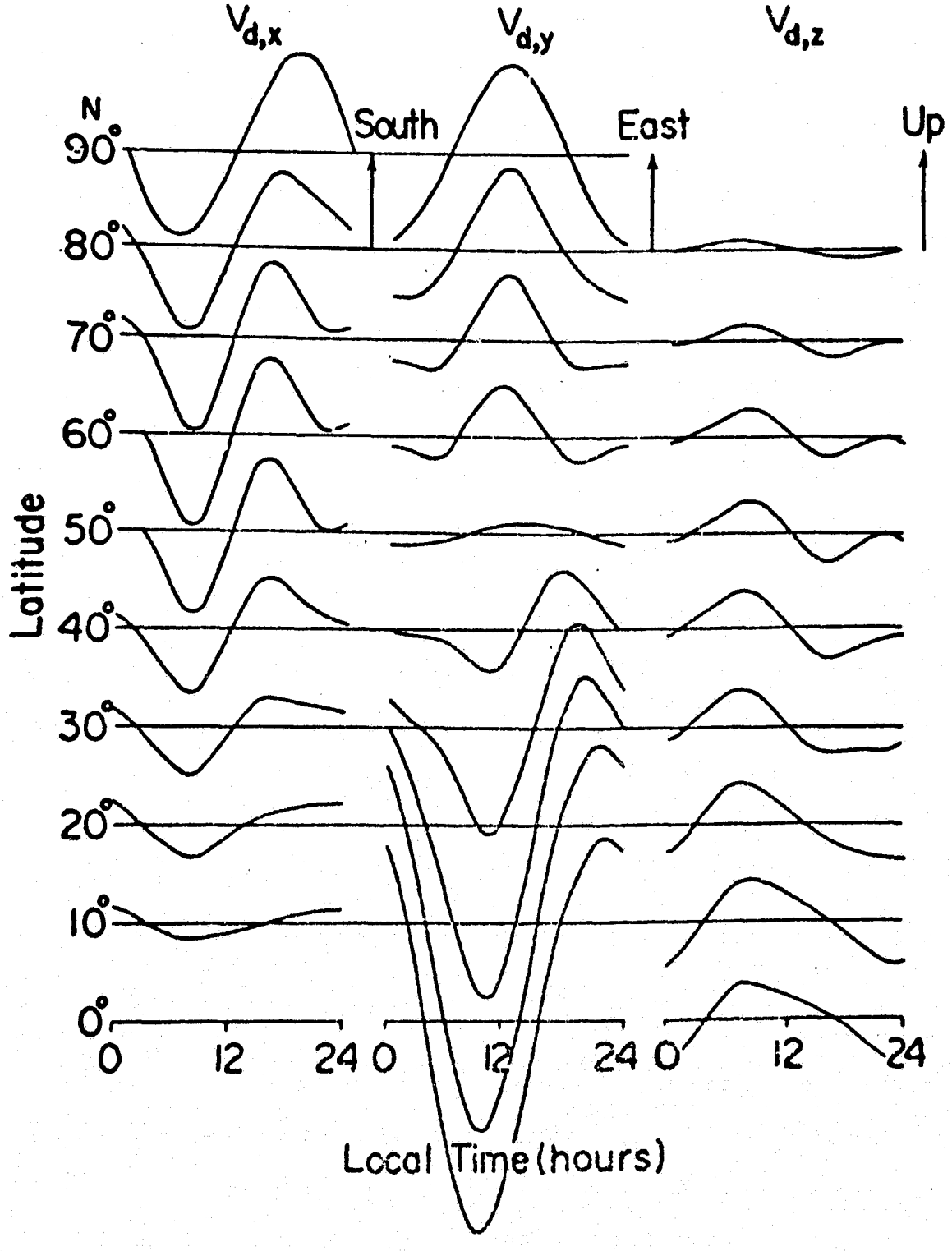

Figure 1.2.1 The drift velocity model of Maeda (1963) Arrows represent magnitudes of 50 m/sec

Matsushita (1971, 1972) has investigated the possibility that Sq-type electric currents in the dynamo region (90-150 km) can be produced from the electric fields originating from the magnetospheric motions that are conducted down the magnetic field. He calculated the F-region motions perpendicular to the magnetic field as a function of latitude and local time based on this assumption. The dynamo region electrostatic field is shown in Figure 1.2.2a, mapped to 300 km. In Figure 1.2.2b the plasmaspheric electric fields due to magnetospheric motions are shown also mapped to 300 km, according to Matsushita (1972). Either of these two mechanisms can reproduce the Sq current system assumed to cause the magnetic field variations as measured on the ground.

A somewhat different approach for the calculations of dynamo currents in the E-region has been developed by Stening (1968). The ionosphere is represented as a large circuit network for which the conductivities and neutral winds are assumed known. In this way, Stening (1969) studied the different contributions of tidal wind components to the overall measured Sq current system. From this he concluded that the diurnal mode dominates at the higher latitudes.

Longitudinal and seasonal variations of the Sq current system were studied by Stening (1971), and electric field distributions are given in Stening (1973). The electric field model is shown in Figure 1.2.3 (Stening, 1973) and Figure 1.2.4 (private communication, Stening, 1974).

a)

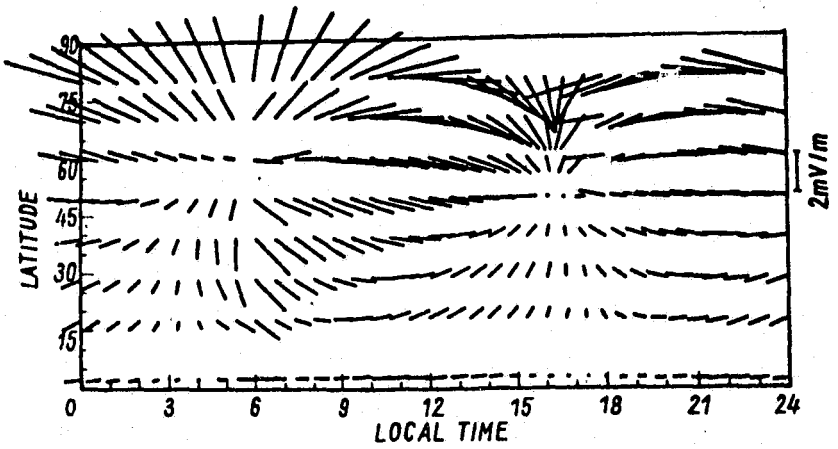

DYNAMO-REGION ELECTROSTATIC FIELD

b)

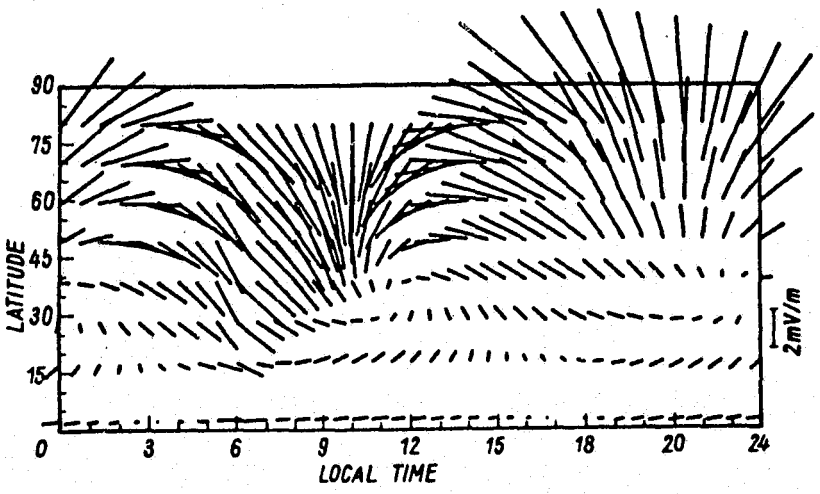

PLASMASPHERIC ELECTROSTATIC FIELD

Figure 1.2.2 The electric field models of Matsushita (1972)

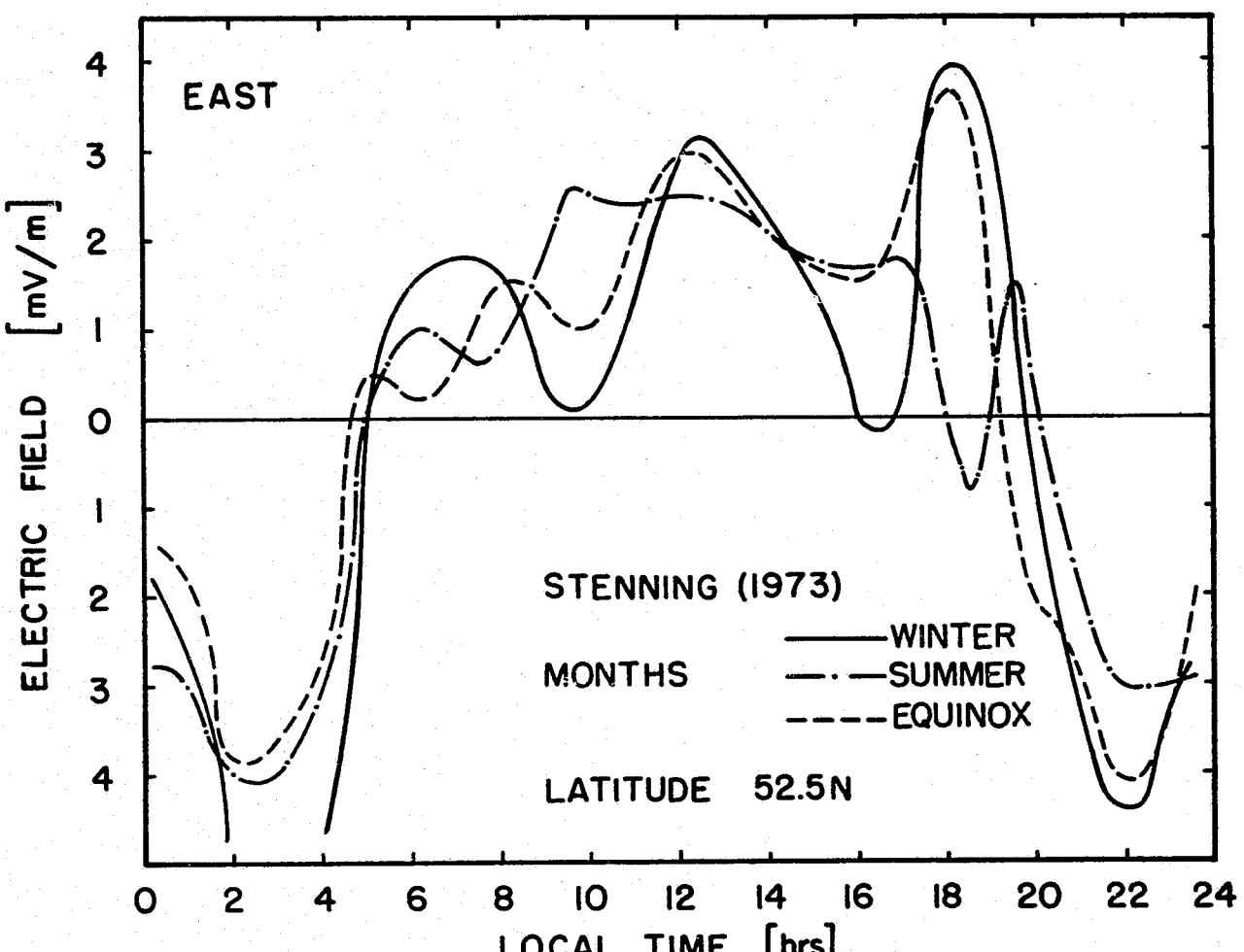

Figure 1.2.3 The electric field model of Stening (1973), eastward component

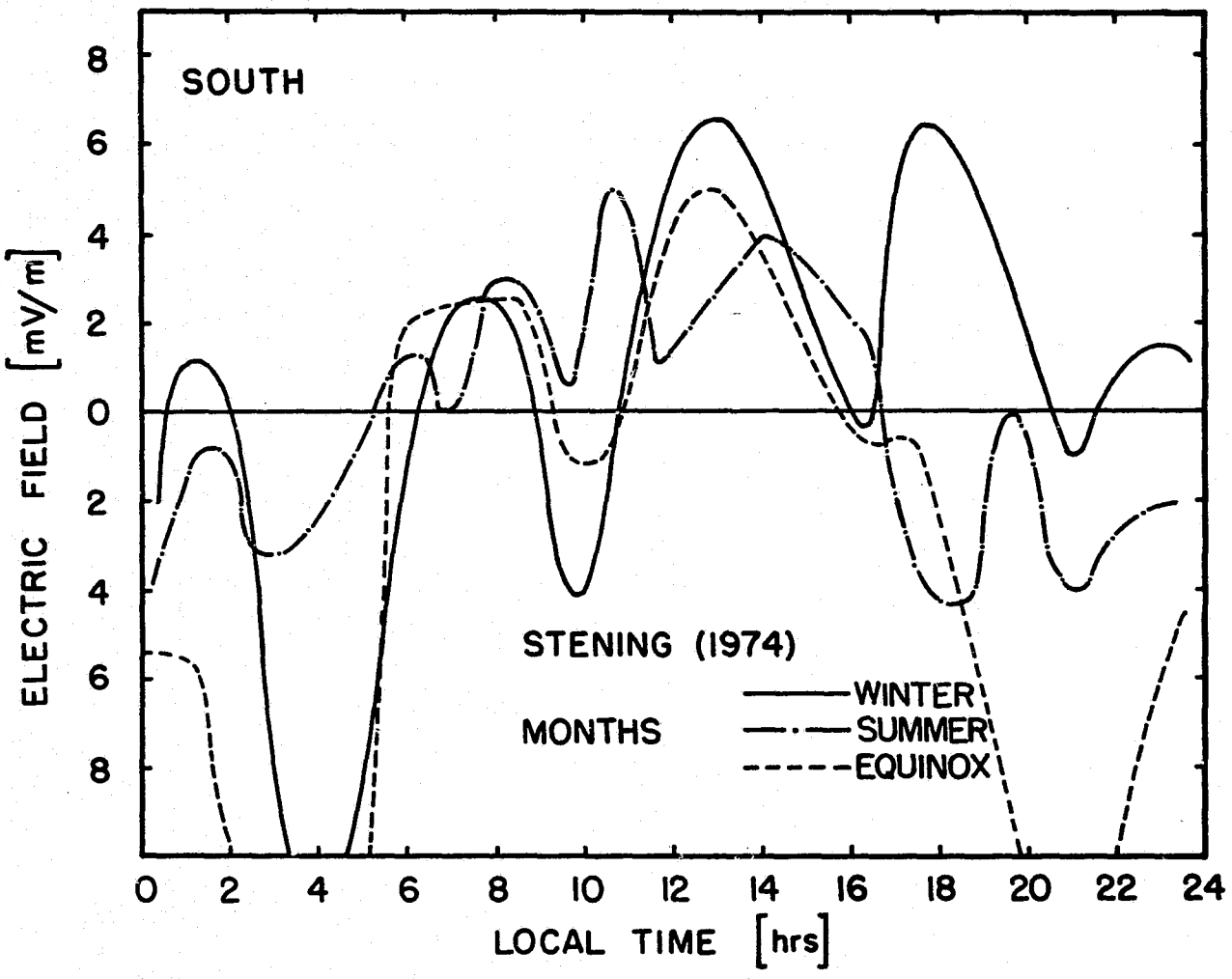

Figure 1.2.4 The electric field model of Stening (1974), southward component

1.2.2 Electric Field Variations

The electric field models of the previous section are dominated by the diurnal mode, i.e. the basic frequency component is the one with a 24-hour period.

Seasonal variations have not been studied adequately, although Stening (1973) allows his conductivity model to vary as $\cos^{1/2}\chi$, where χ is the solar zenith angle. Irregular variations have been studied mainly connected with substorm phenomena at high latitudes. Some of the characteristics of the electric field variations are discussed by Evans (1972) for Millstone Hill; Behnke and Harper (1973) and Hagfors and Behnke (1974) for Arecibo; at Malvern by Taylor (1974); at Jicamarca by Woodman (1970, 1972); at Chatanika by Banks et al. (1973, 1974) and Brekke et al. (1974).

Electric fields from the ionosphere are attenuated little as they are conducted down to lower heights. This has been studied by Mozer and Serlin (1969), Volland (1972), Park and Dejnakarintra (1973) and Chiu (1974).

The basic principle of the mapping process is that the potential difference along magnetic field lines is practically zero (Farley, 1959; Spreiter and Briggs, 1961). Therefore the potential difference between two magnetic field lines remains the same at different locations in the magnetosphere. Since the magnetic field lines tend to spread out in the outer parts of the magnetosphere, the magnitude of the electric field is increased in the mapping process from the magnetosphere to the ionosphere. Due to the particular geometry of the essentially dipole magnetic field lines the meridional ratio is

larger by almost a factor of two than the east-west ratio. Mozer (1970) gives the mapping factors from the magnetospheric equatorial plane to the ionosphere in terms of the L value of the magnetic field line; Matsushita (1971) extended the calculations to include any point in the magnetosphere.

With respect to solar activity, current variations show larger amplitudes at times of high solar activity (Tarpley, 1970) and there is evidence to suggest that substorm related electric fields are more frequent during low solar cycle periods. Irregular pulsations of the magnetic field (Pi 2 pulsations) of period 40-150 seconds (Jacobs et al., 1964) accompany the onset of a substorm on a one-to-one basis (Saito, 1961). Based on an extensive statistical analysis of Pi 2 pulsations, Saito and Matsushita (1968), have shown that their frequency of occurrence is maximum at solar cycle minimum. It is deduced, therefore, that substorm electric field perturbations are more frequent during low solar cycle periods. Large geomagnetic storms, however, are more frequent during high solar cycle periods and as shown by Bhargava and Yacob (1974) the largest variation in the magnetogram H trace occurs during solar maximum.

1.2.3 F-Region Electric Fields

Although the F-region conductivities are much smaller than those of the E-region, Rishbeth (1971) has suggested that large electrostatic fields may develop in the F-region, particularly at night. Essentially this situation is created by the neutral winds which, driving currents that cannot close their circuit, build up polarization

charges creating an electric field. These polarization electric fields in the F-region can be estimated in the following way.

The drift velocity of ions induced by neutral winds in a coordinate system where x is toward east, y north and z up are given by (Rishbeth and Garriott, 1969).

$$V_x = -U_y \frac{\nu}{\omega} \sin I; \qquad V_{y\perp} = U_x \frac{\nu}{\omega}; \qquad V_z = U_x \frac{\nu}{\omega} \cos I \tag{1.2.4}$$

where

I is the dip angle,

ν is the ion-neutral collision frequency,

ω is the gyro frequency,

U is the neutral wind, and

$\perp$ indicates perpendicular to the magnetic field.

The currents associated with these velocities are then

$$j_x = -Ne\, U_y \frac{\nu}{\omega} \sin I; \qquad j_{y\perp} = Ne\, U_x \frac{\nu}{\omega} \tag{1.2.5}$$

where N is the ion density and e the electronic charge. Thus the polarization field E_p is given by

$$E_{px} = U_y B \sin I$$

$$E_{py} = -U_x B \tag{1.2.6}$$

and the associated drift velocities by

$$V_x = U_x$$

$$V_y = U_y \sin I \qquad (1.2.7)$$

It was assumed that a neutral wind was the only driving force, thus electric fields of other origins (E-region dynamo, magnetospheric) and diffusion were neglected. The result in Equation 1.2.7 is highly significant because it implies a strong coupling between the neutral wind and the ion drift velocities, brought about by the polarization field created in the F-region. Further analysis of this situation is discussed in Chapter III.

1.2.4 Magnetospheric Convection

The magnetosphere of the earth is that region of space where the geomagnetic field exerts a strong control on the dynamics of ionized matter. Its lower boundary may be identified with the ionosphere whereas the outer boundary is determined by the interaction of the geomagnetic field and the interplanetary gas. The outer boundary is closest to the earth on the side toward the sun because of the effect of the solar wind compressing the magnetic field, while it is farthest from the earth's surface on the opposite side.

The theory on magnetospheric convection is still in its infancy and it has only been developed to the point of giving a qualitative description. Even so, its implications both in the magnetosphere and ionosphere are extremely important.

Several mechanisms have been proposed to drive the convective motion. The earliest, proposed by Axford and Hines (1961), assumes

that the motion is impressed on the magnetosphere by a viscous-like interaction with the solar wind. Some of the solar wind momentum is transferred to the outer magnetosphere setting magnetospheric particles into motion. These are carried to the tail region on the outer edge of the magnetosphere, the return flow being in the interior of the magnetosphere (Figure 1.2.5). Rotation of the earth is included in Figure 1.2.6. Dungey (1961) proposed the reconnection of interplanetary magnetic field lines with geomagnetic field lines as an alternative driving mechanism for convection. This is shown schematically in Figure 1.2.7. The important fact to be realized however, is that no matter what the driving mechanism is, a convection motion like the one described (Figure 1.2.5) will occur, and has actually been detected by several measurement techniques. The motion of magnetic field lines over the polar cap implies an electric field there, directed from dawn to dusk, thus the electric potential is positive on the dawn side and negative on the dusk side. Mathematical models of convection have been discussed by Vasyliunas (1970).

The magnetosphere is a medium of high electric conductivity where, as pointed out by Gold (1959), in addition to the simple concept of lines of force, the magnetic field lines have an individual identity. The original concept of magnetic field line represented only the direction of the field at each point in space. In a perfectly conducting fluid, however, the particles that are at one time on a line of force remain on it throughout the motion of the magnetic field line. Thus each line has an identity established through the identity possessed by a set of fluid particles. It is concluded, therefore, that in the

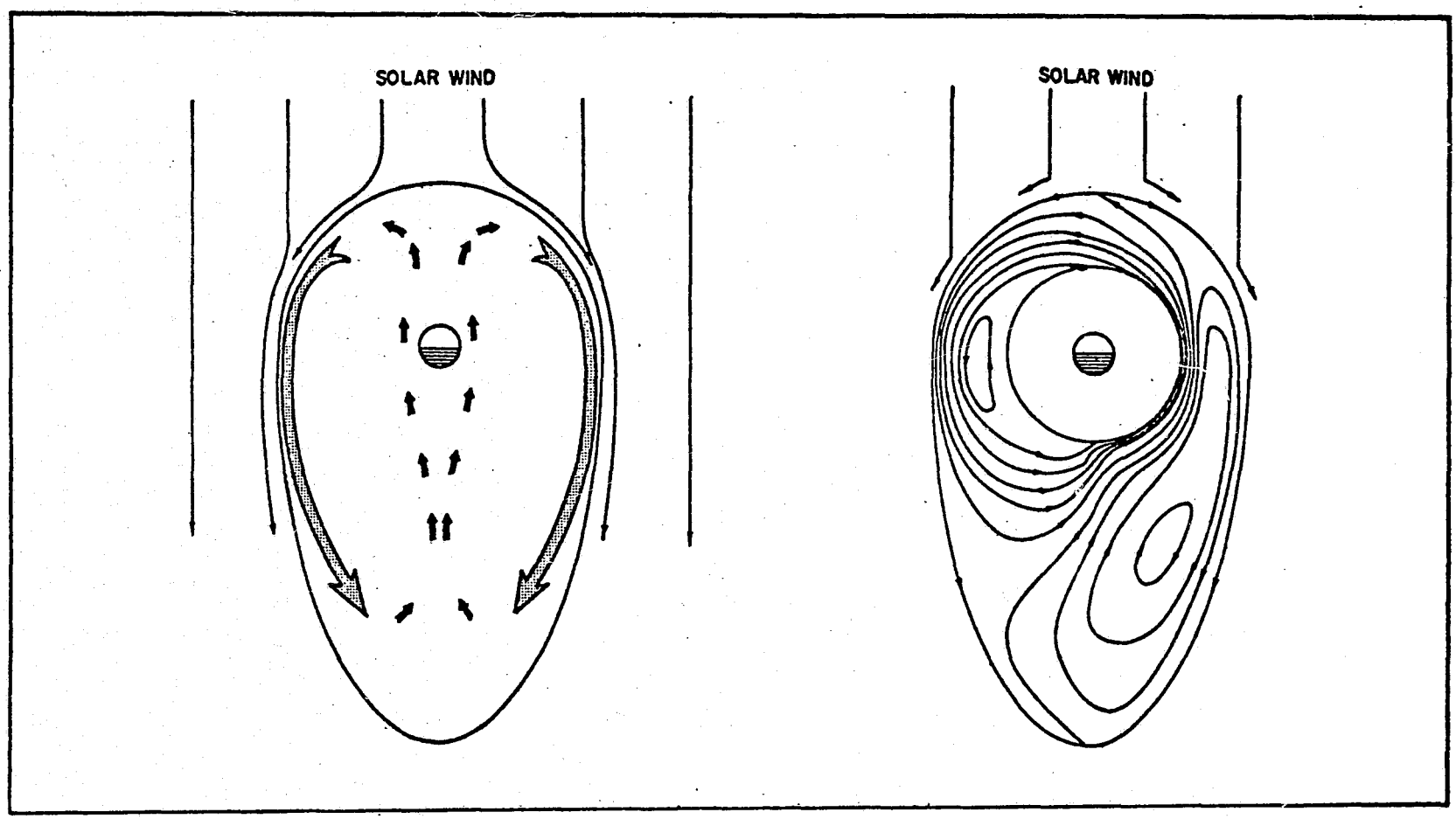

Figure 1.2.5 Convective motions in the equatorial cross-section of the magnetosphere

Figure 1.2.6 Convective motions in the equatorial cross-section of the magnetosphere with rotation included

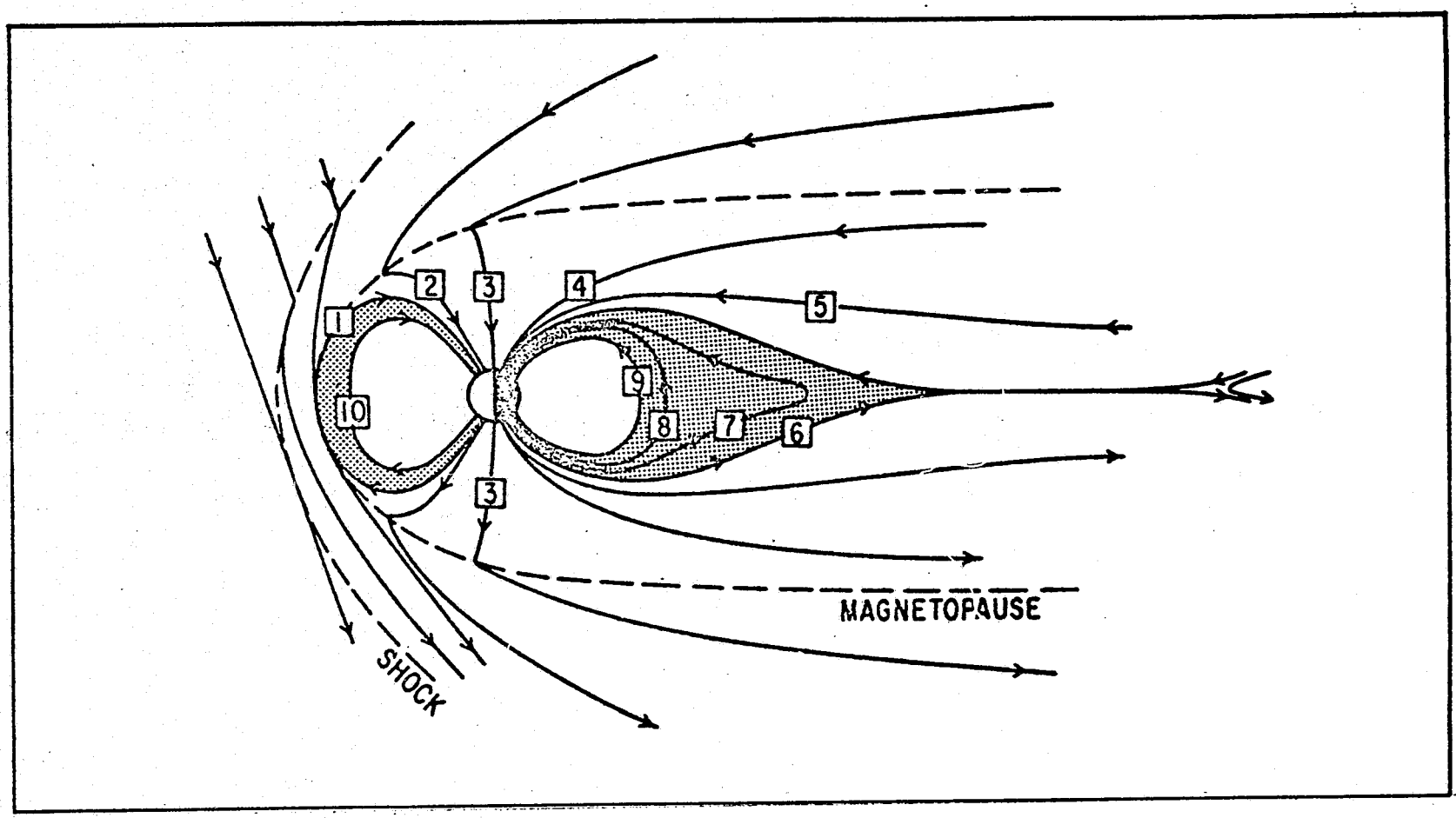

Figure 1.2.7 Dungey's model of reconnection of magnetic field lines

magnetosphere, the gas and field lines are locked to each other, and motions can exist which are not impeded by the magnetic field.

The solar wind in its passage past the earth will carry material in the outer regions of the magnetosphere away from the sun towards the geomagnetic tail. As we have seen, this material is linked to the geomagnetic field and therefore constrained to remain with the magnetosphere and so it builds up an excess concentration in the region of the tail. This build-up cannot persist in steady state, thus a return flow of ionization is set up in the interior of the magnetosphere, and circulatory loops will be established, like those depicted in Figure 1.2.5, in which the ionization convects continuously. The ionization being locked or "frozen" to the field lines will also convect down to lower heights in the ionosphere. Therefore, the pattern of motions of which only the equatorial section is shown in Figure 1.2.5 will be extended throughout the whole magnetosphere. Assuming that the geomagnetic field lines are equipotentials, implies that electric fields existing in one region must be mapped along field lines to other regions. This means that the whole magnetosphere is in a convection state.

A different way of interpreting the convective motion is to consider the forces acting on a ionized particle in a frame of reference fixed with respect to the earth where a particle is subject to both electric and magnetic forces. No net force exists in a steady state with low collision frequency, so that

$$q\vec{E} + q\vec{V} \times \vec{B} = 0 \qquad (1.2.8)$$

where the electric field $\vec{E}$ is mainly perpendicular to the magnetic field $\vec{B}$, q is the particle's charge and $\vec{V}$ its velocity; thus, the concept of velocity and electric field are interchangeable and related through the relation

$$\vec{V} = \frac{\vec{E} \times \vec{B}}{B^2} \qquad (1.2.9)$$

Thus, interpretation of Equation (1.2.9) generates an alternative way of defining convection simply by postulating the existence of electric fields in the magnetosphere which drive the ionization at a velocity V given by Equation (1.2.9).

The derivation of Equation (1.2.9) is valid only for low energy particles, because as the particle energy increases, additional "drifts" are imposed by the gradient of the magnetic field and its curvature. For the low energy plasma (1 eV) these additional drift motions are negligible and therefore it follows the convection pattern very closely.

Particles convecting from the tail of the magnetosphere to the inner boundary are energized while de-energization occurs in the opposite sense. To show this we follow Gold (1959).

Let us consider an expansion of a magnetic flux tube from an L value of L_A to L_B. Since the magnetic field strength varies as $1/L^3$ the cross sectional area will be, after expansion, $(L_B/L_A)^3$ greater than it was at L_A. Since the length of the tube is proportional to L, the volume of the flux tube has changed in proportion to $(L_B/L_A)^4$. Taking the pressure as a measure of the energy density, we have for an adiabatic expansion, and a monatomic gas,

$$pV^{5/3} = \text{const. or } p = \text{const. } x\ R^{-20/3}$$

and for an isothermal expansion, with R being the distance from the center of the earth,

$$pV = \text{const. or } p = \text{const. } x\ R^{-4}.$$

It has been noted by Axford and Hines (1961) that the energization of particles during the inward convection will to some extent be self-stabilizing. This is because as a particle increases its energy, the longitudinal drift motions introduced by the inhomogeneity of the geomagnetic field are enhanced, thus tending to carry the convecting particles around in longitude, out of the zone of inward convection.

Because the magnetosphere as a whole does not rotate with the earth, a convenient coordinate system to study the convection is an inertial frame of reference, fixed for example with the sun-earth's line in the magnetosphere. If the earth's rotation is not taken into account, then the convection pattern is like the one shown in Figure 1.2.5. With rotation included the pattern assumes the form of Figure 1.2.6. When studying the effects of convection on the earth's ionosphere, an observer will not see the effect of rotation because he rotates with the frame of reference fixed with the earth. The convection pattern at ionospheric heights is thus obtained by mapping patterns like Figure 1.2.5 along magnetic field lines. Each velocity vector then represents the velocity of convecting plasma as seen by an observer on the earth directly under that point.

As we have seen, the solar wind is the primary energy source for convective motions. The dissipation of this energy occurs in the

ionosphere where current flows can easily be established. It can be shown that joule dissipation is always dominant over viscous dissipation and that the height limits of this dissipation lie primarily between 100 and 300 km (Walbridge, 1967).

1.2.5 Penetration to Low Latitudes

A distinction should be made between electric fields inside the region of closed field lines and outside it, even though both sides may be in the magnetosphere. The reason for this distinction, not always observed by different workers, is that within the region of closed field lines the electric field may be at times of ionospheric origin, mapped from the ionosphere along the high conducting magnetic field lines. We will use the term magnetospheric electric fields intended to represent phenomena characteristic of the region of open field lines like aurora and convection.

The plasmapause is generally defined as the region that separates the inner magnetosphere, or roughly the region of closed magnetic field lines, from the region of open field lines, or outer magnetosphere. The plasmapause is also the limit within which the plasma essentially corotates with the earth whereas outside it the plasma follows the convection circulation. Stated in other words, the plasmapause is the region where the force of gravity equals the centrifugal force. For neutral particles this limiting region would be located at 6.6 earth radii (i.e. the same location at which geostationary satellites are placed). Charged particles, however, in addition, are subject to the co-rotational electric field which pushes the limit closer to the earth, at 5.8 earth radii (Lemaire, 1974) and convection

electric fields distort the otherwise circular shape of the plasmapause to the well known more elongated shape in the dusk sector (Carpenter, 1966). The high density gradient present at the plasmapause results from plasma escape to the interplanetary medium along open magnetic field lines.

In theoretical calculations and magnetospheric modeling, it has been suggested that under steady-state conditions, the plasmapause must be an equi-potential surface (e.g. Block, 1966) such that there will be no drift across it. This implies that magnetospheric electric fields do not penetrate the plasmapause and are therefore confined to the high latitude regions. This view was shared by many workers for some time until it became evident, through a variety of measurement techniques, that the plasmapause is by no means a steady-state boundary but instead is constantly expanding or contracting, probably under the influence of an east-west convection electric field. More detailed investigations based on power spectrum analyses of electric field data collected by probes on balloons (Mozer, 1973) show that electric field variations of scales less than one day can effectively penetrate to lower latitudes.

Several years ago, when electric field measurements were not yet available, all the information on magnetospheric electric fields had to be deduced from high latitude equivalent currents deduced from magnetograms. We will first review the findings of this type of study and then analyze the electric field data.

Simultaneous magnetogram records from widely distributed stations were analyzed by Nishida et al. (1966), who identified a new

type of geomagnetic variation that extends all the way from the polar regions to the equator. The equivalent current system deduced from these fluctuations, DP2 variations, is similar to the high latitude convection pattern and the authors concluded that these fluctuations result from the electric field of magnetospheric origin. Thus the electric field of magnetospheric origin is seen to have influence down to equatorial latitudes.

Sarabhai and Nair (1969) and Nair et al. (1970) also based on magnetic variations at equatorial latitudes attribute part of the variation to magnetospheric processes, even on days which are not magnetically disturbed. We may conclude, therefore, that magnetospheric-ionospheric coupling, based on the analysis of geomagnetic variations alone, is important at all latitude regions.

For the interpretation of electric field data, we show in Figure 1.2.8 the magnetospheric equatorial cross section. The dotted curve A represents the average location of maximum electric fields as measured by OGO-6 (Heppner, 1973) while curve B represents the limit of ± 5 mV/m electric fields. Also shown are the L shells of Millstone Hill (3.2), Chatanika (5.8) and balloon measurements (6.9). The OGO-6 results show that the latitudinal variation in electric fields is not uniform over different local time sectors. The steepest gradient occurs close to the midnight sector, where the maximum electric fields reach their lowest point in latitude at about 22:00 L.T. The day side has no well defined maximum probably because of the then high conductivities. These general characteristics are in excellent agreement with the Chatanika data (i.e. Brekke et al., 1974). The balloon data,

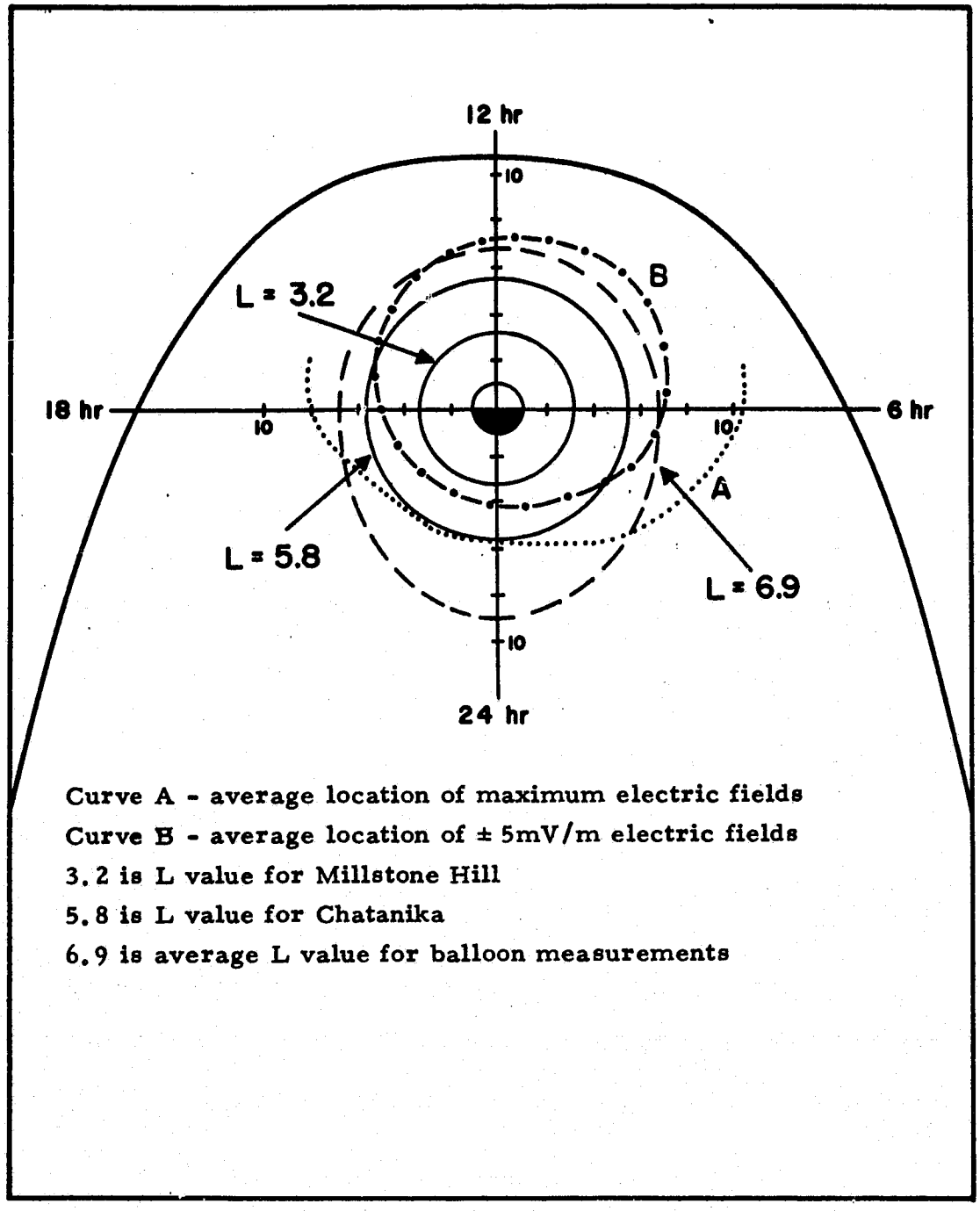

Figure 1.2.8 Magnetospheric equatorial cross-section indicating high latitude variation of electric fields

gathered at an average L = 6.9 shell, show a maximum between 18 - 19 L.T. (Figure 1.3.7) as can be predicted from Figure 1.2.8. These high latitude electric field measurements have thus a number of characteristics in common. It is more difficult however to predict variations for Millstone Hill, from the previous measurements, since it is located within the lower limit of 5 mV/m and therefore convection electric fields at Millstone may be of the same order of magnitude as dynamo generated electric fields and the contribution of each one is difficult to distinguish. Consequently, an experiment was conducted at Chatanika and Millstone Hill simultaneously to determine the similarity in the electric fields at each station. It was found (Carpenter and Kirchhoff, 1975) that both stations have the same electric field variation in local time (Figures 1.3.2 and 1.3.3) which led the authors to conclude that convection electric fields extend to lower latitudes at least down to L = 3.2.

The mechanisms by which the electric fields in the outer magnetosphere penetrate to lower latitudes are still under extensive investigation. In a simplified picture, the presence of the electric fields imply in a potential difference across the high latitude ionosphere thus producing currents that can flow in the whole E-region shell, indirectly producing an electric field. Another possibility appropriate for time varying conditions is a transformer-like action between the outer and inner magnetosphere.

Further measurements at Millstone during more active magnetic periods, when convection electric fields are expected to be stronger, show a behavior that differs from the quiet day average in the sense that the convection pattern (Mendillo, 1973) is reproduced in

the data, giving a peak in the northward velocity component at about 13 L. T. and a peak in the westward velocity at about 18 L. T. (Figure 2.4.1). This leads us to the conclusion that electric fields of magnetospheric origin can penetrate to lower latitudes. At Millstone Hill their effect is small when $\Sigma K_p < 24$ but can dominate the dynamo fields for $\Sigma K_p > 24$.

1.3 Electric Field Observation Methods

1.3.1 Incoherent Scatter

The incoherent or Thomson scatter technique is an effective ground based radar technique that measures ionospheric parameters such as electron densities, electron and ion temperatures and drift velocities, and all of these can be determined simultaneously. Essentially this technique utilizes a high power radar coupled to a high sensitive detection system. The frequency of operation is higher than foF2, the plasma frequency at the peak of the F-layer, and the scattered power arises from the existence of density fluctuations in the ionospheric medium. Power returns are essentially proportional to electron density, whereas the drift velocities are determined from doppler shifts in the frequency spectrum. A thorough review on incoherent scatter is given by Evans (1969). The incoherent scatter technique has made many valuable contributions to the understanding of ionospheric physics.

In the area of plasma drift velocities, the earlier works were related to vertical drifts only. Evans et al. (1970) describe the system at Millstone Hill and the accuracy of the technique and present measurements between 450 and 900 km altitude. More data was analyzed by Carpenter and Bowhill (1971), and Evans (1971). Woodman

(1970) describes the system at Jicamarca and presents results for several days. The Arecibo Observatory is described by Behnke (1970) and the polar facility at Chatanika by Doupnik et al. (1972). All the foregoing represent monostatic, pulsed radars. Two additional facilities using CW bistatic facilities are available in England (Taylor et al., 1973) and France (Carru et al., 1967).

At Millstone Hill the first study on drift velocities perpendicular to the magnetic field was presented by Evans (1972). The steerable radar antenna was pointed toward magnetic north and west respectively, at an elevation angle of 15^{o}. Measurements were taken at different height levels with the conclusion that in the F-region the drift velocity is reasonably constant with height and that E-region drifts lag behind F-region drifts. This last characteristic led the author to conclude that the magnetosphere could be ruled out as a source for the drift motion. The measurements were however taken only in the daytime, and the data could be fit with a harmonic variation of period 12 hours. His average results are shown in Figure 1.3.1.

Kirchhoff and Carpenter (1975) extended the measurements through nighttime periods. It was found that the magnitudes are greater at night, and that, for the data set studied, the diurnal harmonic component was in fact the dominant one. One should not therefore rule out the magnetosphere as a possible source for the electric field at night. This conclusion was later substantiated by Carpenter and Kirchhoff (1975), through simultaneous measurements of drift velocities at Chatanika and Millstone Hill.

Watt (1973), Brekke et al. (1974) have discussed a number of characteristics pertinent to higher latitudes. Among these are the

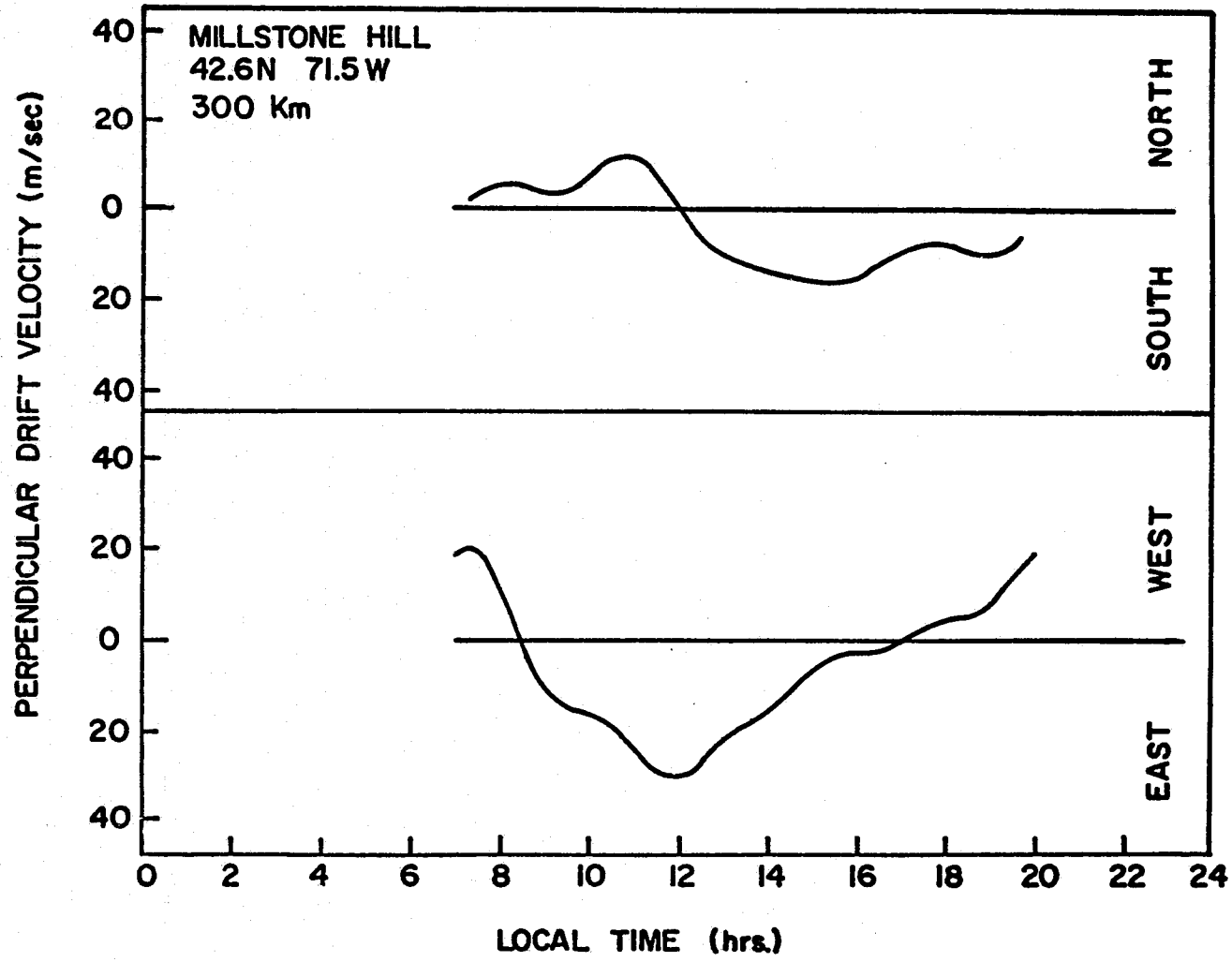

Figure 1.3.1 Daytime drift velocities from Evans (1972)

very high values of electric fields, and the variability of E-region conductivities and currents.

Behnke and Kohl (1974) studied the effect of neutral winds and electric fields from measurements taken at Arecibo and general characteristics of drift velocities were treated by Behnke and Harper (1973).

In Table 1.3 the incoherent scatter stations and their coordinates are listed. A study on the accuracy of the measurements and elevation angle optimization is included in Appendix B.

Chatanika Measurements

The Chatanika incoherent scatter radar (65.1N, 147.5W) operates an L-band steerable antenna. Due to its high latitude location the majority of ionospheric studies are related to magnetic perturbation effects and aurora.

The Chatanika radar has been described by Doupnik et al. (1972) and Banks et al. (1974), and electric fields in the auroral zone have been studied by Doupnik et al. (1972) and Banks et al. (1973, 1974).

In order to study latitudinal variations in drift velocities, Carpenter and Kirchhoff (1975) made simultaneous measurements at Chatanika and Millstone Hill. The results have shown that the shape of the local time variations are similar for the two stations, and for both components of drift velocity perpendicular to the magnetic field lines (Figure 1.3.2 and Figure 1.3.3).

Table 1.3 Coordinates for Incoherent Scatter Stations

		Millstone Hill	Chatanika	Arecibo	Malvern	Jicamarca	St. Santin
Geographic	latitude	42.6 N	65.1 N	18.3 N	52.1 N	11.9 S	44.6 N
	longitude	71.5 W	147.5 W	66.7 W	2.3 W	76.9 W	2.2 E
L value*		3.2	5.8	1.4	2.6	~1	1.8
Inclination or dip angle I		72	77	50	68	2	61
Geomagnetic** or dipole latitude		54.1 N	65.1 N	29.8 N	55.1 N	0.5 S	47.0 N
	longitude	1.9 W	77.5 W	3.6 E	83.4 E	6.7 W	83.7 E
Invariant latitude (Λ) defined from $\cos^2 \Lambda = 1/L$		56.0 N	65.5 N	32.3 N	51.7 N	~1 N	41.8 N
Dip latitude (θ) defined from $\tan I = 2 \tan \theta$		57.0 N	65.2 N	30.8 N	51.1 N	1.0 N	42.0 N

* From map in Matsushita and Campbell (1967)

** Calculated from geographic coordinates, assuming geomagnetic north pole tilted by 11.5°, at 70°W

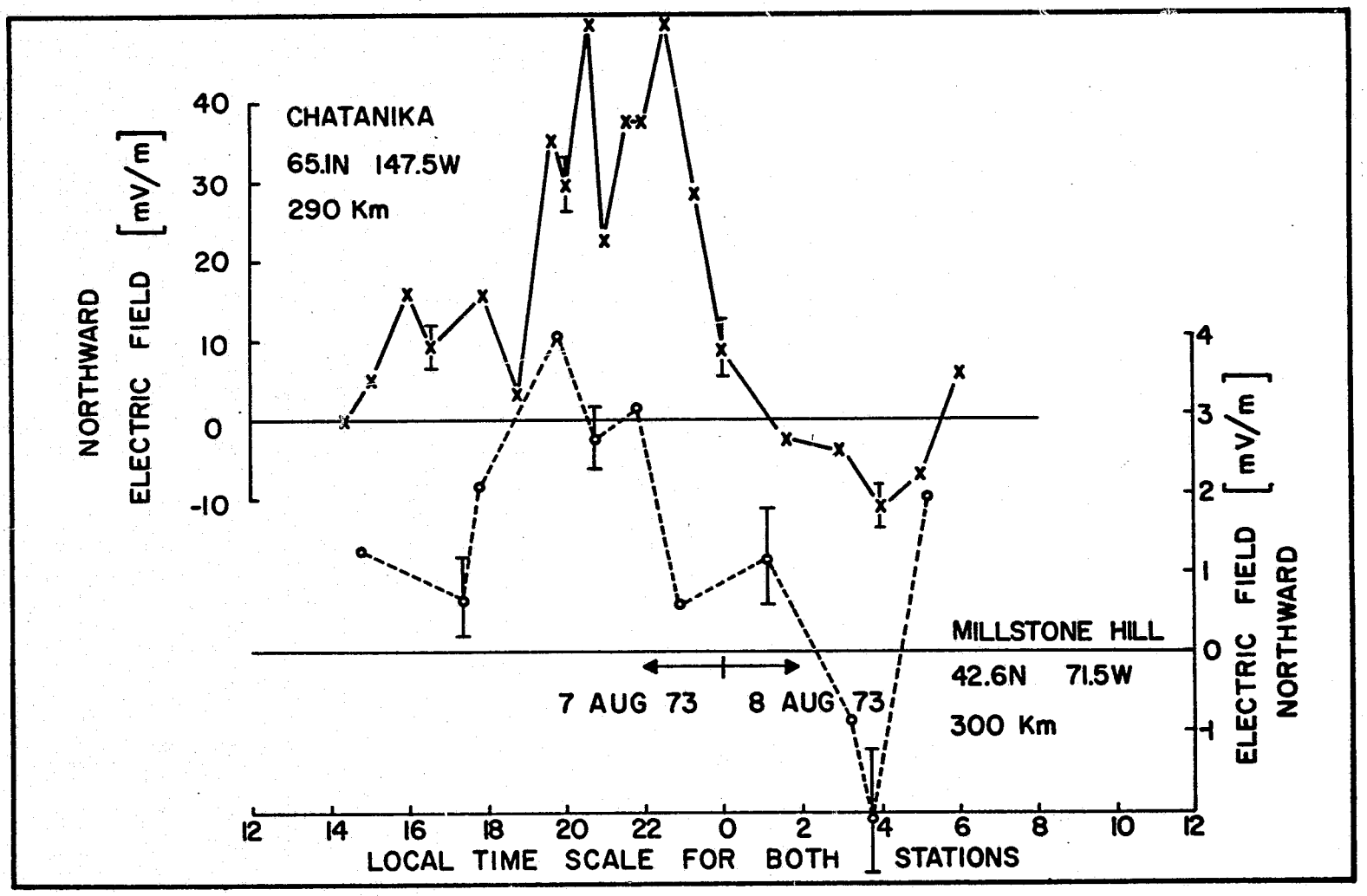

Figure 1.3.2 Comparison of northward electric fields from Carpenter and Kirchhoff (1975)

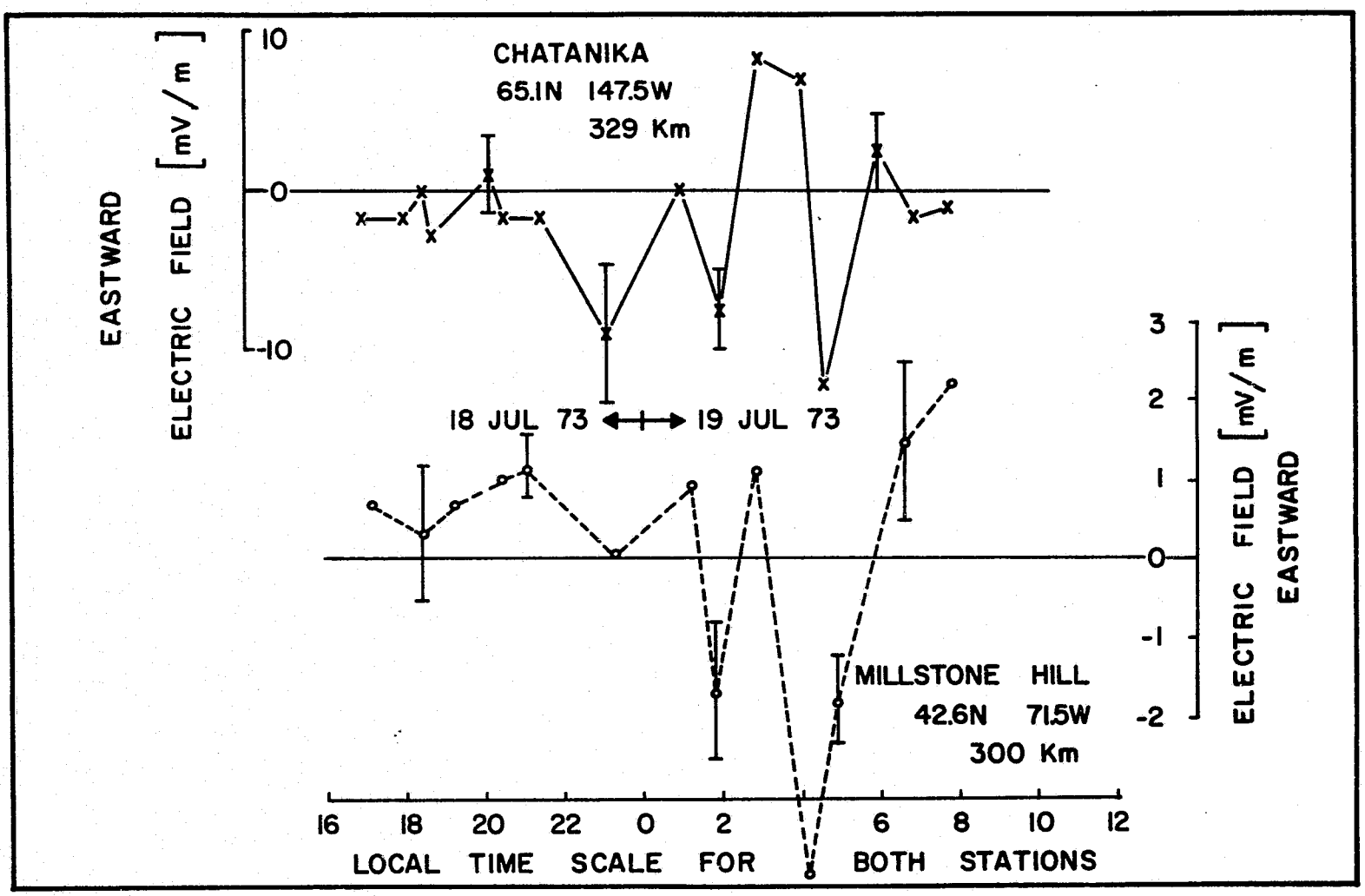

Figure 1.3.3 Comparison of eastward electric fields from Carpenter and Kirchhoff (1975)

Arecibo Measurements

The Arecibo ionospheric observatory in Puerto Rico (18.3N, 66.7W) operates a large antenna of spherical shape with a diameter of 305 meters. Although the antenna is fixed, the antenna beam can be scanned up to about 15 degrees from the vertical for all azimuths.

Studies on plasma drift velocities have been published by Behnke (1970), Behnke and Harper (1973), Behnke and Kohl (1974) and Behnke and Hagfors (1974). An average drift velocity variation with time (local standard) for northward and westward components perpendicular to the magnetic field lines is shown in Figure 1.3.4.

1.3.2 Whistlers

A whistler is originated from a lightning discharge (Storey, 1953). The audio frequency portion of this broadband electromagnetic energy pulse is capable of propagating along the earth's magnetic field lines and can be detected on the ground by appropriate transducing equipment such as an amplifier and a loudspeaker (Helliwell, 1965); earlier studies used whistler data mostly to infer electron densities in the plasmasphere and to study the plasmapause (Carpenter, 1970). More recently whistler audiograms have also been used to study the motion of whistler ducts in the plasmasphere (Carpenter et al., 1972; Park, 1972). In this way the radial convection velocities at about $L = 4$ have been deduced, and these in turn can be mapped to ionospheric heights.

From the nose frequency of recorded whistlers, it is possible to calculate the equatorial electron gyro frequency (Park, 1972) and thus assuming a magnetic field model it is possible to calculate the

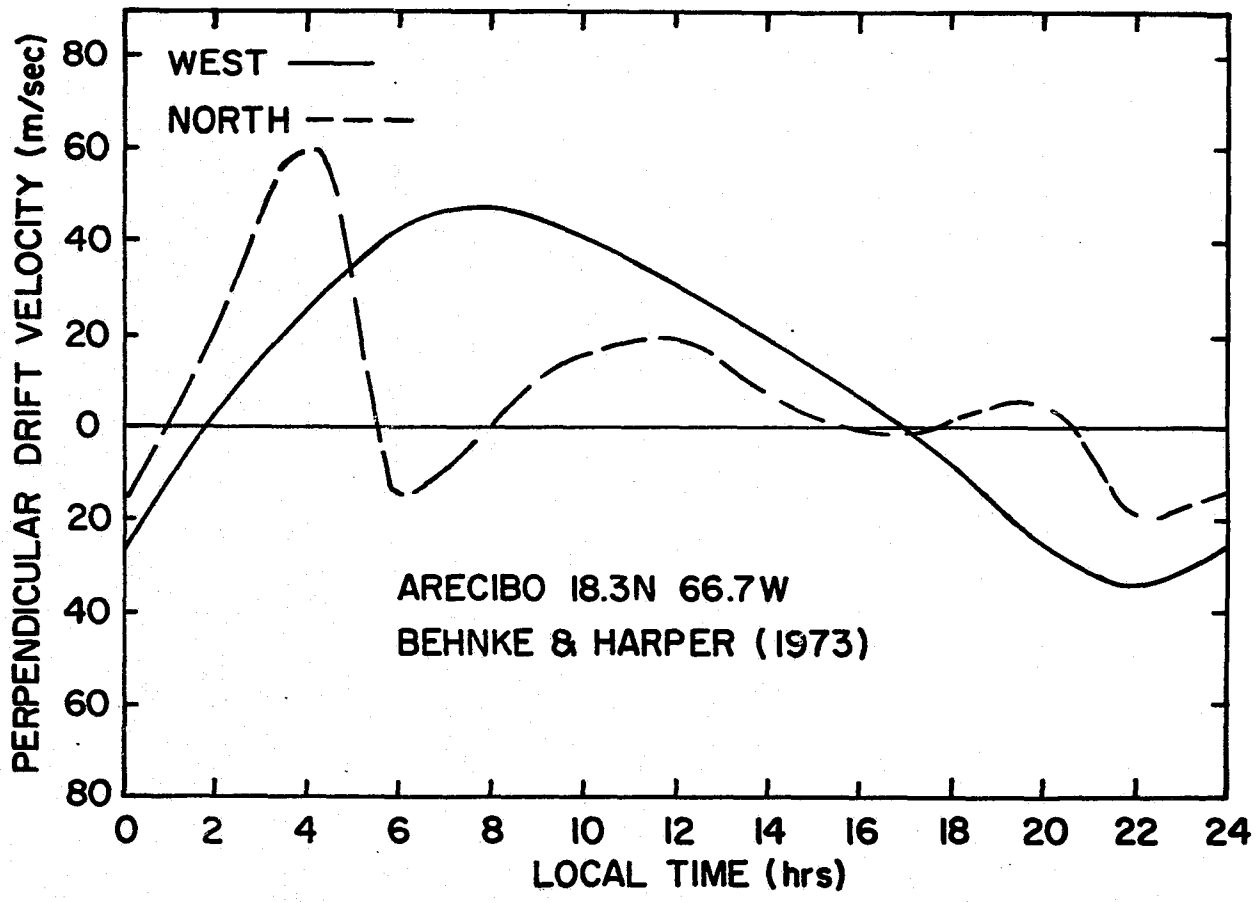

Figure 1.3.4 Average drift velocities for Arecibo at 300 km

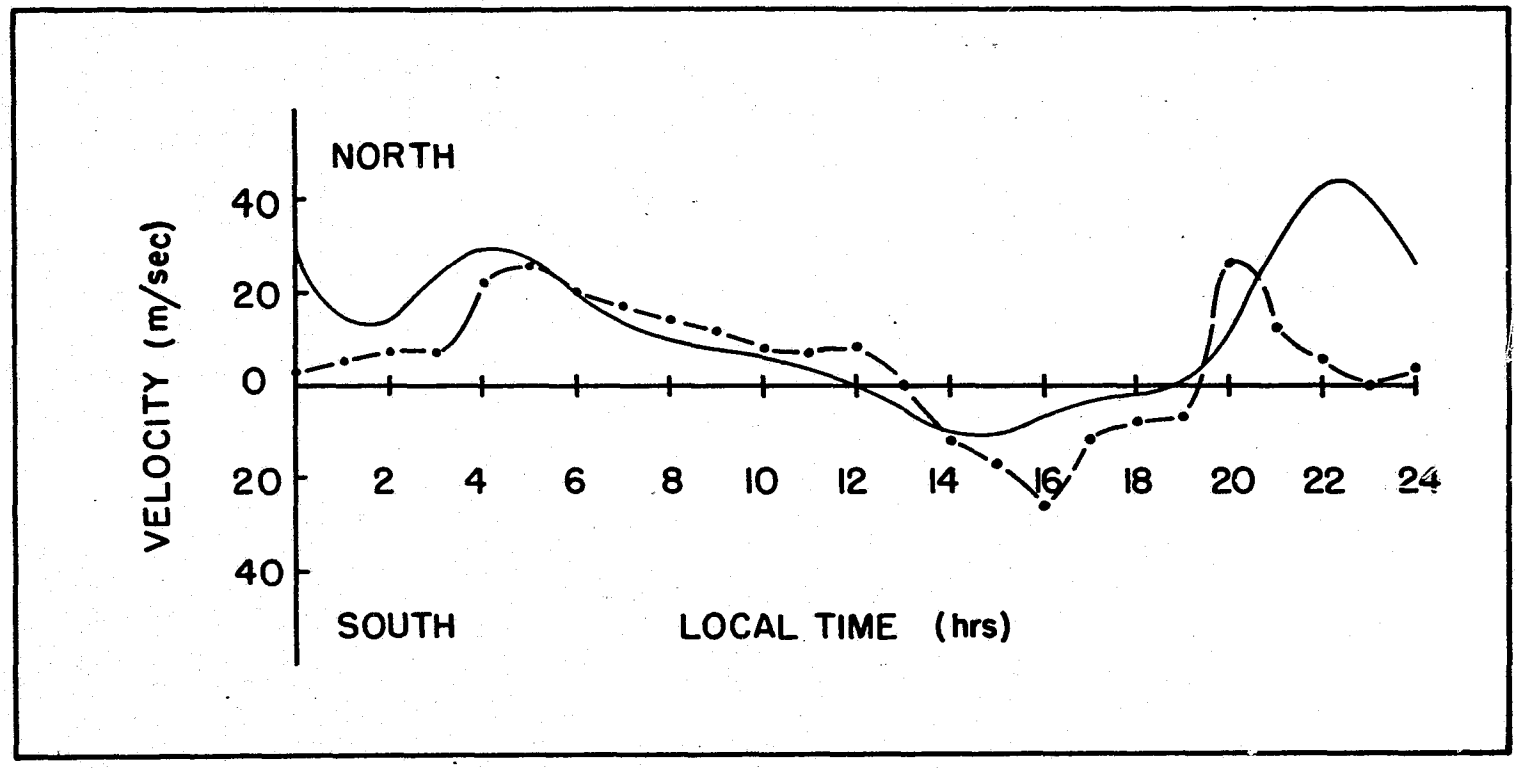

Figure 1.3.5 Average northward drift velocities from whistler measurements (— ∘ —) and incoherent scatter (—)

equatorial radius of the whistler duct. This position tracking is then used to infer the cross L drifts in the plasmasphere. Most of the measurements correspond to regions of $3.5 < L < 5.5$. To compare the whistler measurements with those of Millstone, a mapping along magnetic field lines has to be performed (Mozer, 1970; Matsushita, 1971). Whistler measured east-west electric fields in the equatorial plane multiplied by a factor of 8 correspond to ionospheric electric fields at $L = 4$. Only east-west components of electric fields can be deduced from the whistler measurements.

Recent analysis of whistler measured plasmaspheric electric fields have been published by Carpenter and Seely (1975) and an average drift velocity variation with time has been reproduced from their results in Figure 1.3.5, for 7 days. To compare these results with the incoherent scatter measurements, the northward drift velocity of Kirchhoff and Carpenter (1975) is also shown in that figure.

1.3.3 Balloon Measurements

Measurement of electric fields by probes carried on balloons has largely been the work of Mozer and associates. Published results appear in Mozer and Serlin (1969), Mozer (1971), Mozer (1972) and Mozer and Lucht (1974). This last paper presents a comprehensive analysis on several hours of balloon measurements and these average results are reproduced in Figures 1.3.6 and 1.3.7. The average L value for these measurements is $L = 6.9$ and the amplitude scale is divided by a factor of 4. Also shown for comparison are drift velocities measured by incoherent scatter radar (Kirchhoff and Carpenter, 1975).

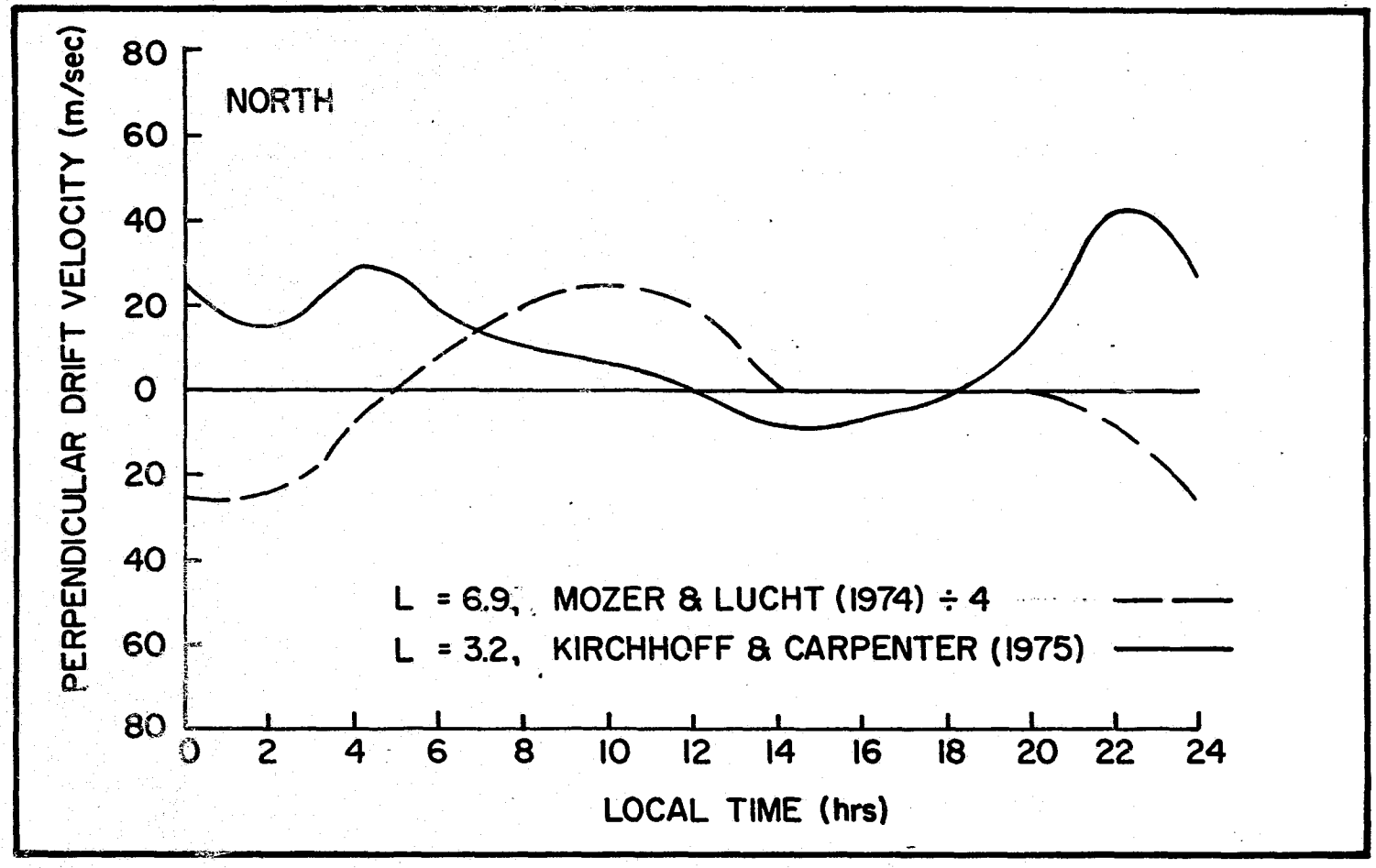

Figure 1.3.6 Average northward drift velocities at L = 3.2 and L = 6.9

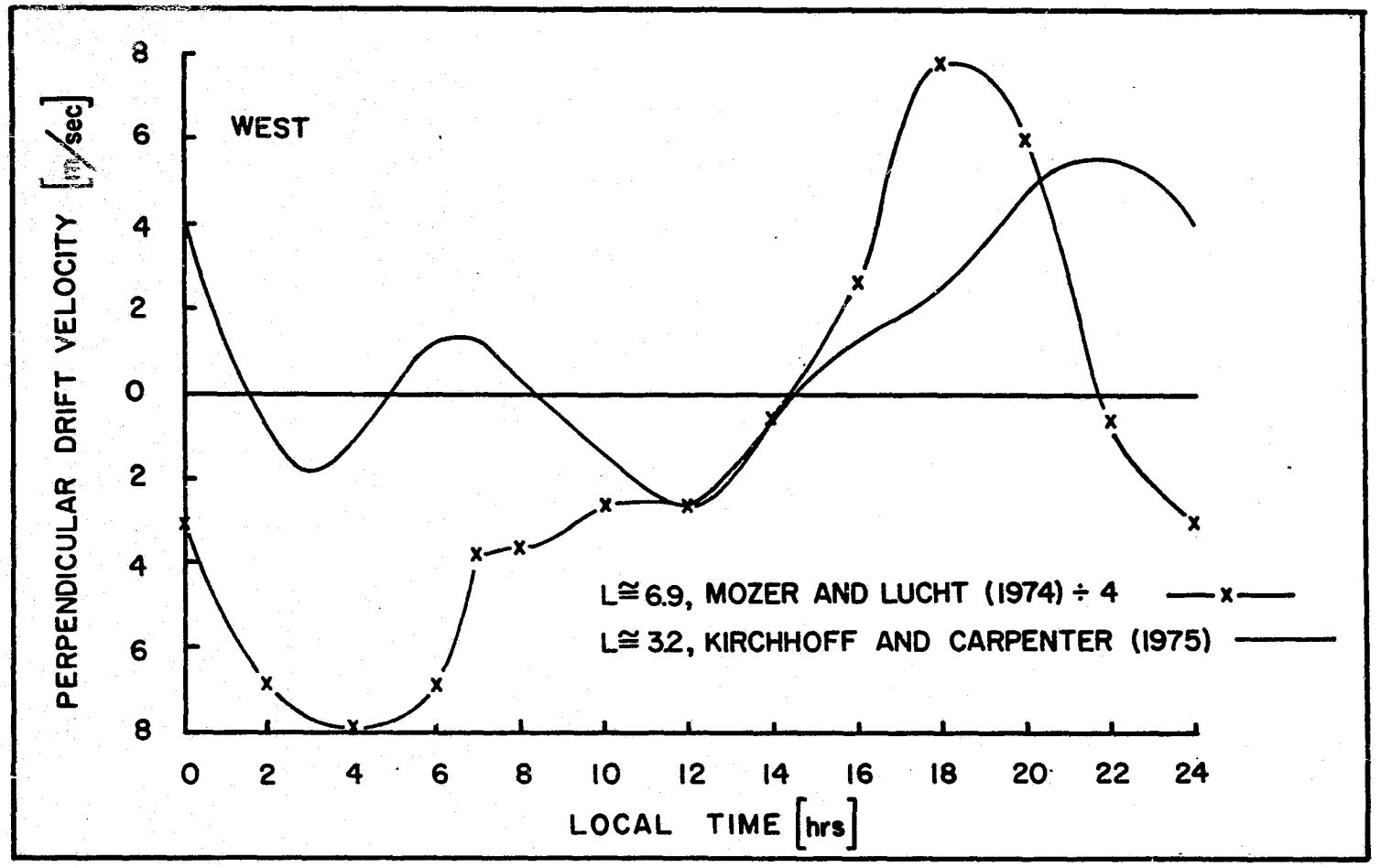

Figure 1.3.7 Average westward drift velocities at L = 3.2 and L = 6.9

1.3.4 OGO-6 Measurements

The double probe floating potential equipment on OGO-6 provided a number of electric field measurements published in Heppner (1972), Heppner (1972a), Heppner (1973) and Maynard (1974). For the purpose of inferring latitude variations of electric fields we have mostly made use of Heppner (1973) and Mozer and Lucht (1974). The OGO-6 results are depicted in a somewhat different form in Figure 1.2.8 and have been discussed in Section 1.2.5.

1.4 Mechanisms and Variables Controlling Observations

1.4.1 Ionospheric Conductivities

The formulas for the ionospheric conductivities were originally derived for the study of ionospheric current flows (Baker and Martyn, 1953; Maeda, 1953). Maeda (1955) used this theory to deduce a horizontal wind system in the E-region of the ionosphere, and Maeda (1956) extended the calculations to include effects of daily variations.

The concept of the layer conductivities has also been used in magnetospheric problems. By making numerical calculations, Swift (1972) shows that the formulas derived for $J_z = 0$ are still valid when vertical currents are present and concluded therefore that the height integrated conductivities are generally applicable in the magnetosphere as well.

The formulation of the conductivity expressions is reviewed in detail in Appendix A.

1.4.2 E-Region Tidal Winds

The nature of the wind field responsible for the Sq variations is still one of the major problems of the ionospheric dynamo theory.

Theory and observations agree, however, on the fact that in the dynamo region the amplitude and direction of the wind change rapidly with height. On one hand theory favors dominance of the solar diurnal tide (Tarpley, 1970) whereas experimenters tend to favor dominance of semidiurnal modes in the E-region (Evans, 1972; Salah et al., 1975).

The important sources of energy for the diurnal tide are water vapor and ozone absorption. Neutral wind observations between 80 and 100 km rely on the tracking of meteor trails. Above this region, neutral winds are studied by chemical vapor trails released from rockets. Hines (1966) analyzes a number of wind profiles, reporting significant diurnal winds with 20 ± 3 km vertical wavelength which is very close to the theoretical value of the (1, 1) tidal mode. Woodrum and Justus (1968) included some nighttime data and the results confirmed those of Hines.

The semidiurnal tide is basically excited by ozone absorption in the stratosphere and lower mesosphere, according to the studies of Butler and Small (1963). Most of the energy of the semidiurnal tide is contained in the fundamental semidiurnal mode, the (2, 2) mode. This however is an evanescent wave in the mesosphere, a large fraction of its energy being trapped below the mesopause. Therefore it seems that in the dynamo-region the (2, 4) mode prevails among the semidiurnal modes. Salah et al. (1975) deduce a neutral wind model for the E-region consisting only of the (2, 4) mode and solve the dynamo equation to find the electric fields. Calculated amplitudes are found to agree rather well with daytime measurements but the phase

of the southward component lags the observations by about four hours. This discrepancy is attributed to additional sources for the daytime electric fields.

1.4.3 Thermospheric Winds

In Section 1.2.2 it was seen that at night thermospheric winds may have a direct effect on F-region drift velocity measurements. The global neutral wind system above about 120 km is produced by pressure gradients originated from the daily heat input from the sun. The daily temperature variations lead to a daytime expansion of the atmosphere, the diurnal bulge, located in the lower latitudes at about 14:00 local time. The horizontal pressure gradients around the bulge provide the driving force for the thermospheric wind system. This wind system is dominated by ion drag and it blows outwards from the bulge, across isobars, from the dayside to the nightside of the earth.

With the formulation of more accurate upper atmospheric models, based on the results of the drag experienced by satellites, more accurate determinations of the pressure gradients became available, and a number of calculations on the wind system followed. Geisler (1966) assumes that ion drag forces balance the pressure gradient driving forces, Lindzen (1967) and Kohl and King (1967) also include viscosity and inertia, and Cho and Yeh (1970) calculate the winds by solving the continuity and equation of motion simultaneously.

More recently, the meridional component of the wind has been deduced from incoherent-scatter measurements. Thus Amayenc and Vasseur (1972) present meridional wind components for various F-region altitudes and compare these with calculated neutral wind

profiles, showing that an accurate neutral atmospheric model is very important for the calculation of neutral winds. Rishbeth (1972) reviews the major works in the area.

1.5 Specific Statement of Problems

The purpose of this work is to make ionospheric electric field measurements using the incoherent scatter facility at Millstone Hill and organize the available data in such a way that the following specific problems may be answered:

1) What is the daily variation of the electric field at midlatitudes?

2) What are the variations in the fields caused by seasonal, magnetic activity and solar cycle effects?

3) What is the relative contribution of each source to the total observed fields?

CHAPTER II

ANALYSIS OF MEASUREMENTS

2.1 Introduction

The Millstone Hill incoherent scatter radar is located in Westford, Massachusetts (42.6N, 71.5W). Relevant coordinate parameters are listed in Table 1.3 for Millstone Hill and other stations.

At Millstone Hill, one fixed vertically pointing antenna with a parabolic reflector of diameter 67.5 m is available for operation at UHF (λ = 68 cm), and one steerable antenna, 25.6 m in diameter operates at L band (λ = 23.2 cm). Further details on the equipment are given by Evans (1967) and Evans et al. (1970a).

Basically four different geometries have been used at Millstone Hill for the measurements of ionospheric plasma drift velocities and these are briefly described below.

Geometry I. This was the first procedure followed to measure ionospheric drifts. It uses only the UHF vertical antenna and therefore measures only vertical drifts (see Evans et al., 1970).

Geometry II. This antenna positioning procedure was used by Evans (1972) and uses only the L band steerable antenna at small elevation angles to measure nearly horizontal drift velocity components.

Geometry III. This uses both L band and UHF antennas combining geometries I and II (Carpenter and Kirchhoff, 1974). Vertical drift velocities, as well as electron density, electron and ion

temperatures, are measured with the vertically pointing fixed antenna. The steerable antenna is then used to measure the horizontal components of drift velocity. In this way three dimensional drift vectors can be deduced, and diffusion velocities and meridional neutral winds can be calculated. Because of these features this is the most versatile geometry for drift velocity measurements. However, since the radar is monostatic, the measurements in different directions do not apply to the same volume of ionospheric plasma.

Geometry IV. In a proposal for upgrading the Millstone Hill radar for the International Magnetosphere Studies (IMS), Evans (1974) proposes to use the L band antenna alone, pointing sequentially east and west of magnetic north at elevation and azimuth angles such that two drift velocities perpendicular to the magnetic field can be measured at the same L value. Different azimuth and elevation angles allow these drifts to be measured at different L values.

The first measurement of drift velocities perpendicular to the magnetic field lines at Millstone Hill was made by Evans (1972), during the daytime, and his results for 9 days in 1968-69 will be included as part of the data base of this study. As mentioned earlier Geometry II was used for these measurements. The 1971-72 data consists of either northward or westward drifts only. For the period 1973-74 either Geometry III or IV was used, thus permitting the calculation of neutral winds.

Two basic difficulties complicate drift measurements at night. The electron densities are lower and the scattering volume is farther away from the radar. This leads to lower signal-to-noise ratios and

consequently, larger uncertainties in the measurements. This was the basic reason that measurements at Millstone Hill were first conducted in the daytime.

The drift velocities in the F-region have been shown to be approximately constant with height (Evans, 1972) so that measurements between about 200 and 400 km are in general averaged and referred to an average altitude of 300 km. Local standard time (GMT - 5 hrs.) is used in all figures and tables.

Since the conductivity along magnetic field lines is very large, the ionospheric electric field is practically perpendicular to the magnetic field lines and therefore the components of the drifts are separated into westward (horizontal) and northward (at 18^{o} elevation).

The Millstone Hill measurements used in this work are shown in Table 2.1 which specifies the day of the measurement, its duration, the ΣK_p index and the solar flux index. Also shown is a code designation which stands for the following:

Letter a, summer days for the north-south component
b, summer days for the east-west component
c, seasonal variations
d, high magnetic activity
e, low magnetic activity

The uncertainties of the measurements are studied in Appendix B. It is shown that the antenna positioning can be optimized, and that it is possible, by varying the elevation angle, to minimize the uncertainty and keep the signal-to-noise ratio above a threshold.

The individual days measurements, including the vertical velocity, are given by Carpenter and Kirchhoff (1975a).

Table 2.1 Millstone Hill Measurements

Date	Local Time	Code	ΣK_p	F 10.7
21 Nov. 68	09 - 19	c	12.33	137.1
10 Dec. 68	10 - 18	c	21.0	152.6
22 Jan. 69	10 - 20	c, e	7.0	138.2
17 Apr. 69	07 - 18	d	28.33	153.5
14 May 69	07 - 17	d	50.0	154.3
10 June 69	07 - 18	a, b, c, e	15.66	236.2
16 July 69	07 - 14	a, b, c	18.33	122.1
20 Aug. 69	07 - 18	a, b, c, e	6.0	106.9
19 Sept. 69	08 - 18	c, e	9.0	130.3
20 July 71	08 - 19	b, c, e	7.0	118.8
27 Jan. 72	11 - 15	d	24.0	118.9
24 Mar. 72	07 - 18	d	26.66	126.6
30 May 72	07 - 22	c	22.33	116.8
30 June 72	00 - 24	a, c, e	6.33	134.5
26 July 72	11 - 24	b, d	25.0	120.6
27 July 72	00 - 24	b, c, e	15.66	127.2
6 Sept. 72	08 - 21	c	18.66	119.2
15 Nov. 72	10 - 16	d	24.33	86.5
16 Nov. 72	08 - 16	d	33.33	89.6
6 Dec. 72	10 - 17	c, e	5.0	77.8
7 Dec. 72	08 - 16	c	18.0	87.1
2 Jan. 73	10 - 18	c, e	3.0	101.
27 Feb. 73	11 - 18	d	37.33	100.
28 Feb. 73	08 - 15	d	25.66	102.9
17 July 73	12 - 23	a, b, c, e	11.66	75.6
18 July 73	00 - 23	a, b, c, e	12.0	80.9
19 July 73	01 - 16	a, b, c	18.66	79.0
7 Aug. 73	12 - 24	a, b, c	16.66	88.3
8 Aug. 73	01 - 11	a, b, c	17.0	87.5
12 Feb. 74	07 - 21	d	35.66	78.5
16 Apr. 74	06 - 24	c, e	7.0	85.3
15 July 74	16 - 24	a, b, c	19.0	82.8
16 July 74	00 - 23	a, b, c	17.33	88.4
17 July 74	00 - 18	a, b, c	16.33	88.1

Code:

Daily variations Section 2.2	a
Daily variations (Westward) Section 2.2	b
Seasonal variations Section 2.3	c
Magnetic activity (high) Section 2.4	d
Magnetic activity (low) Section 2.4	e

2.2 Daily Variations

In this section the local time variation throughout a 24-hour period will be studied. Evans (1972) has previously discussed the daytime behavior and the major contribution of the present study will be in the inclusion of the nighttime measurements which were not previously available.

Table 2.1 shows the days included in our analysis, the times of observation and the solar and magnetic conditions. As can be seen only about eight of the days had usable nighttime observations; twelve had measurements of the north-south velocity and fourteen had measurements of the east-west component, for the summer season.

For each of the days the observations were interpolated to provide values on the hour local time and the hourly values were then averaged. Figures 2.2.1 and 2.2.2 show the results for the northward and westward components. The error bars shown at each time represent plus and minus the standard deviation from the mean value of the set of observations.

The average daily variations for summer days show a 24-hour periodicity with larger magnitudes at night, especially over the 22 L.T. period. This agrees with an earlier study (Kirchhoff and Carpenter, 1975) in which a Fourier analysis of the data indicated the dominance of the diurnal mode, found to be about twice as large as the semidiurnal one.

The pre-midnight period (18 - 24 hrs.) appears to be a continuation of the daytime variations reaching a north and westward peak at 22 L.T. The after midnight period (0 - 6 hrs.) shows a different

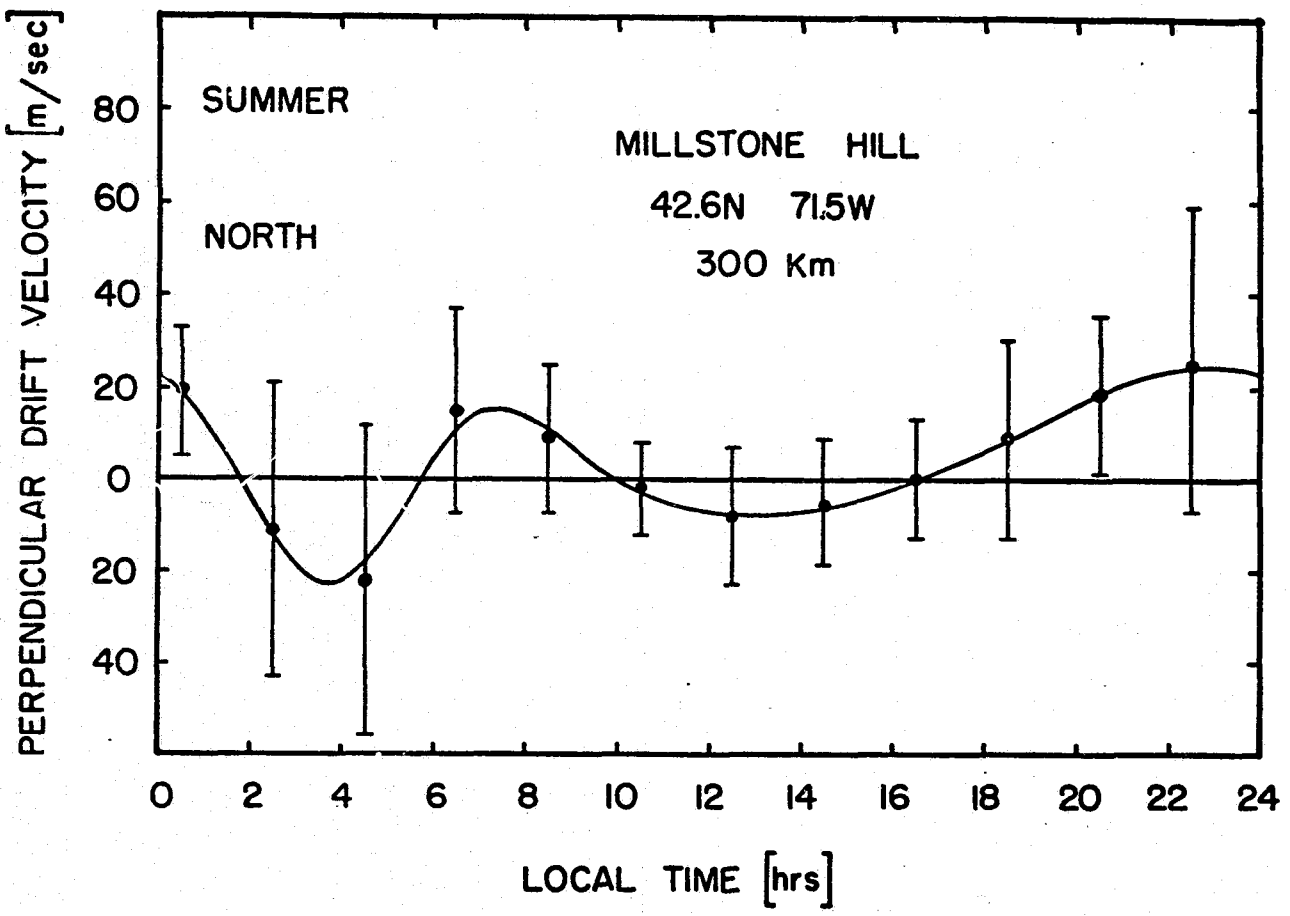

Figure 2.2.1 Average northward drift velocity for 12 summer days

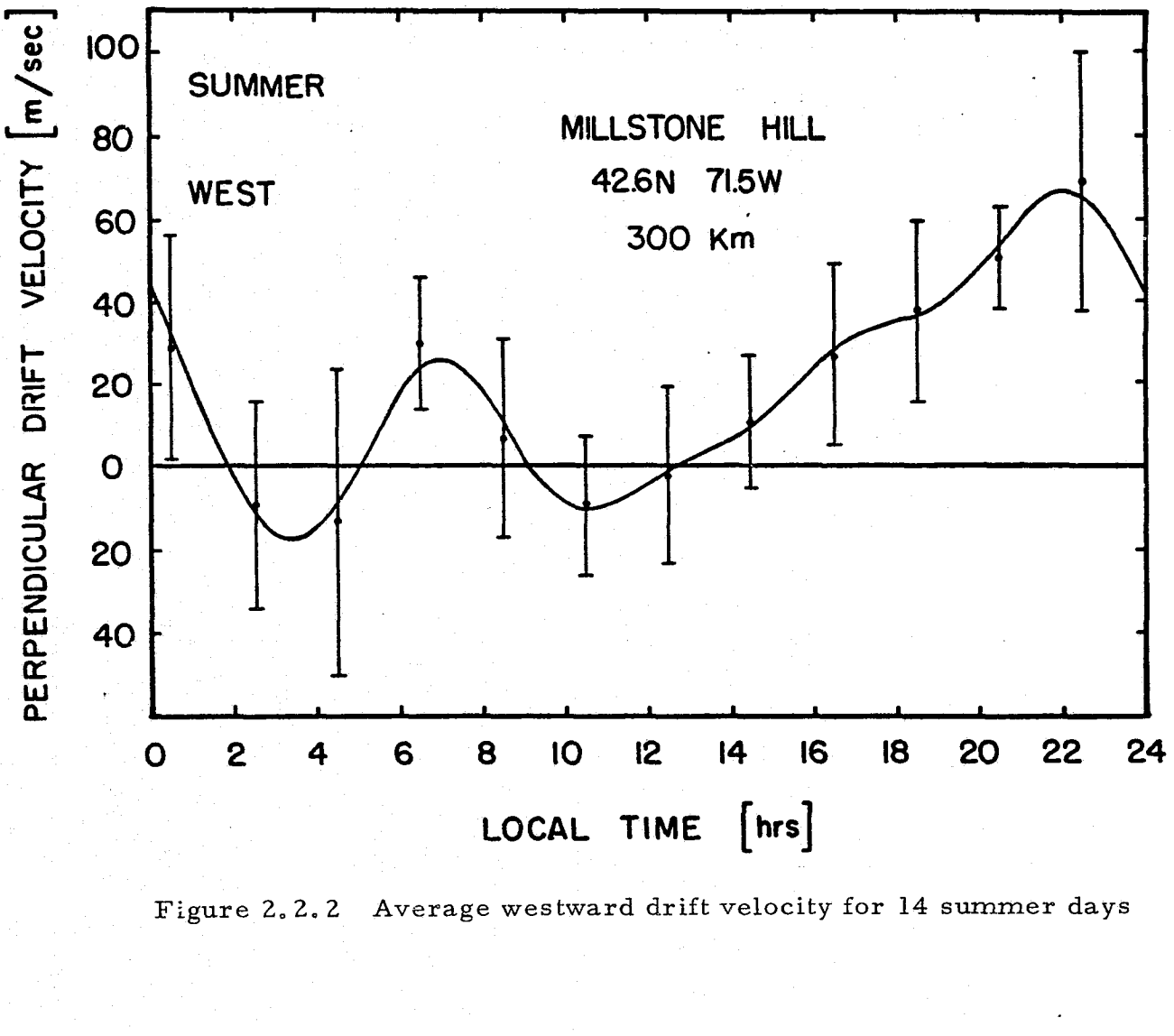

Figure 2.2.2 Average westward drift velocity for 14 summer days

behavior, in that the time variation is much faster. In this period the direction in both components reverses twice, both components having a peak (south and eastward) at about 4 L. T.

2.3 Seasonal Variations

To investigate the seasonal effect in the measured drift velocities the data coded by letter c in Table 2.1 was plotted as a function of solar zenith angle ($\chi = 0$ for overhead sun) and a running average performed for every 5° in χ. The result is shown in Figure 2.3.1. Only daytime values are shown ($25^{\circ} < \chi < 85^{\circ}$) because these are the most accurate. Sunrise sunset features are thus excluded.

The interesting feature in this figure is that in both components there is a peak in amplitude close to $\chi = 55^{\circ}$. This suggests that the amplitude peaks seen for summer days at about 8 L. T. and 22 L. T. (Figures 2.2.1 and 2.2.2) should be located much closer together for the winter months (see also the conjugate point effect) and at an intermediate location for equinox.

Solar zenith angles as a function of local standard time (L. T.) for Millstone are shown in Figure 2.3.2 for days in the middle of summer (day number D = 182), winter (D = 1), and equinox (D = 91 and D = 273), and indicate that seasonal variations have an appreciable effect on the overall variability of the drift velocities.

It will be seen in Section 2.6 that the analysis of magnetogram records for Weston, Massachusetts, in 1968 shows that higher amplitudes occur during summer and a delay in phase of two hours is present for winter compared to summer and one hour for equinox.

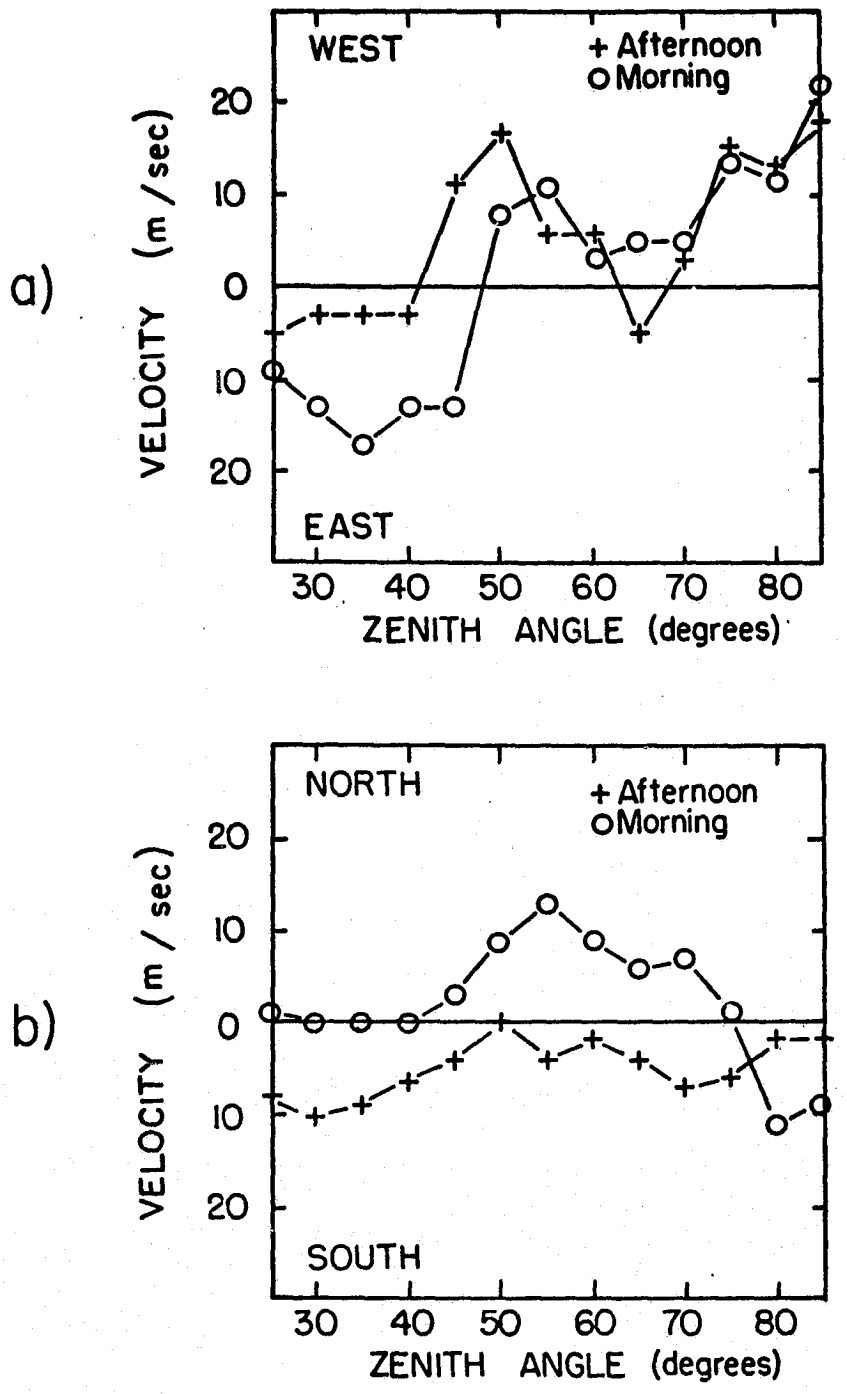

Figure 2.3.1 Drift velocity variation with solar zenith angle

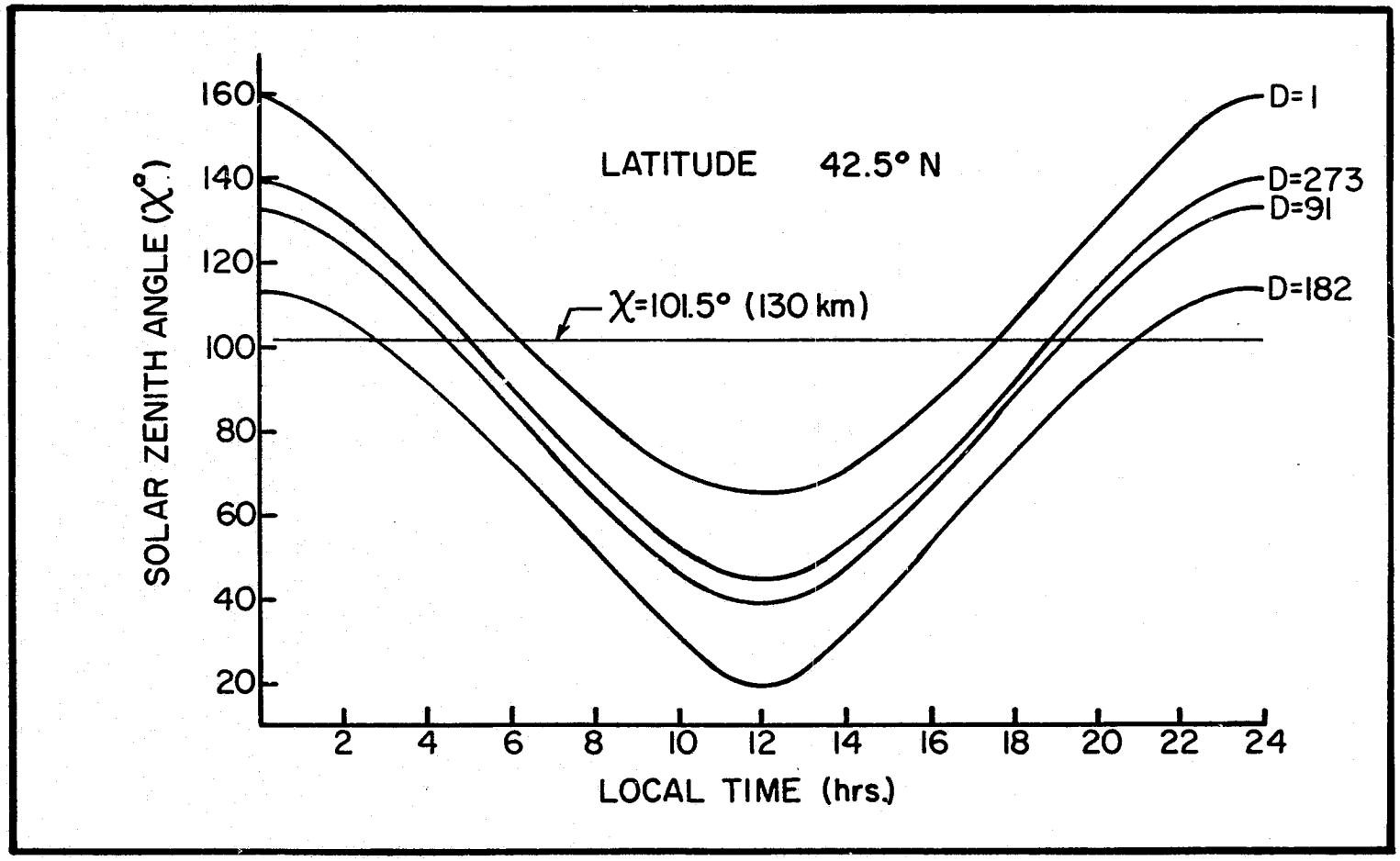

Figure 2.3.2 Solar zenith angles as a function of local time

2.4 Magnetic Activity Variations

The Millstone Hill data indicate that there are strong deviations in the drift velocities from the average on days for which ΣK_p is larger than 24. This is the basis for classifying the data into three groups: magnetically quiet periods with $\Sigma K_p < 16$; relatively quiet, with $\Sigma K_p < 24$; and perturbed with $\Sigma K_p > 24$.

In Figure 2.4.1 the perturbed north and westward average components of drift velocities are shown for the days coded d in Table 2.1, at the times (local standard) when the deviations from the average (dashed lines) are most evident. The characteristics shown agree with the peaks created by the convection electric fields (Mendillo, 1973).

Evans (1972) first noticed that on magnetic disturbed days, the westward component assumes larger amplitudes close to 18 L.T. This has been interpreted as being the result of a strong convection pattern in the magnetosphere. Since then it has been found (Carpenter and Kirchhoff, 1974) that the northward component is also affected showing a maximum amplitude at 13 L.T. So far there has been no detection of a systematic correlation between the K_p index and the drift velocity magnitudes directly. There is however a noticeable increase in the magnitudes, at the times indicated before, on days for which the ΣK_p index is greater than 24. Deviations from the average may be as high as 100 per cent or more. The error bars indicate the standard deviations from the mean, which are large compared to those for which ΣK_p is less than 24 (Figures 2.2.1 and 2.2.2) which is also an indication that they are due to the magnetospheric perturbation.

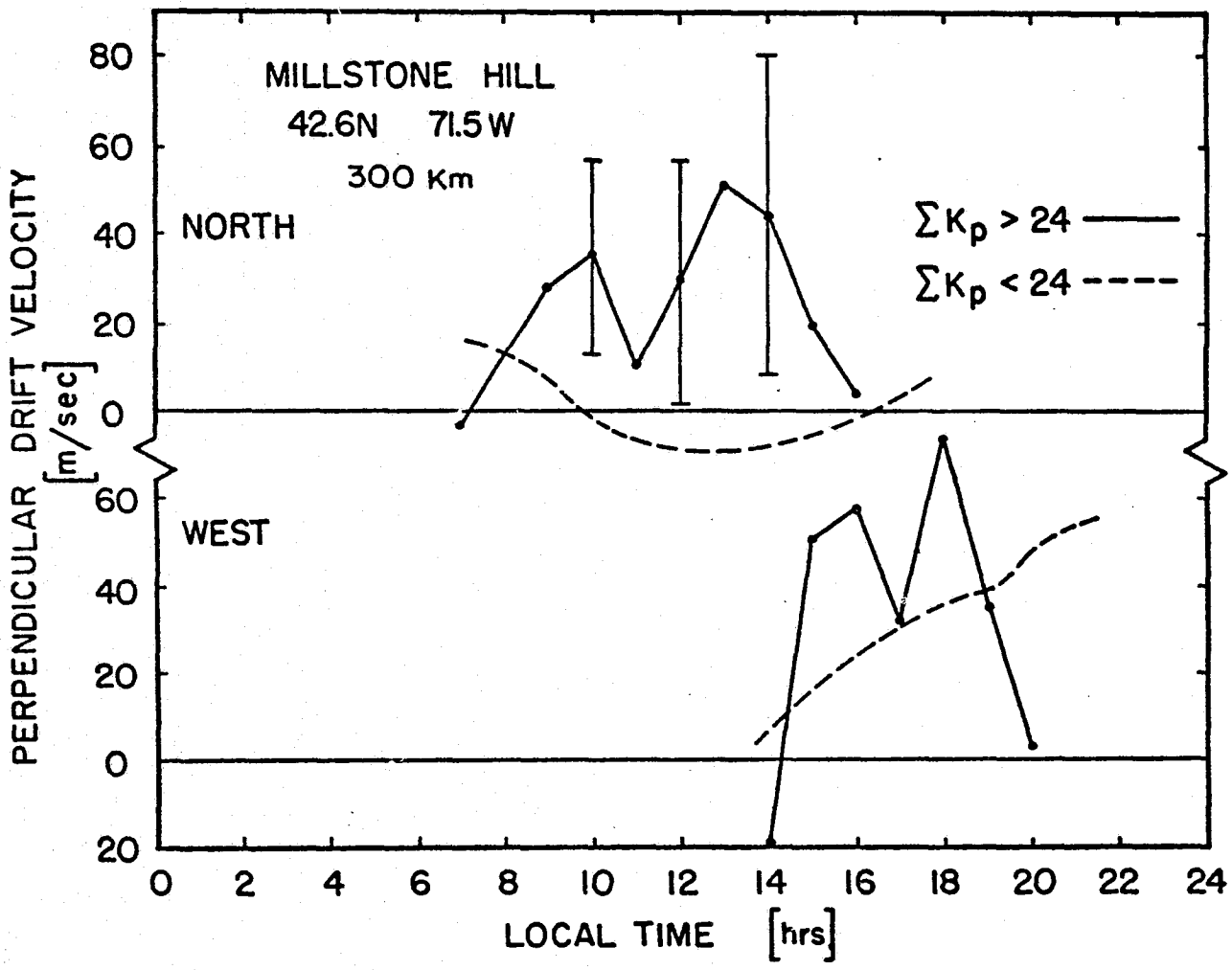

Figure 2.4.1 Drift velocities for magnetic active periods

For quiet periods the average variations are shown in Figure 2.4.2, for 12 days. They indicate smaller magnitudes but no significant deviations in the shape of the curves as compared to those of relative quiet periods.

2.5 Effects of Magnetic Conjugate Point and Solar Cycle

In this section the coupling between magnetic conjugate points is discussed, as are the solar cycle effects.

Besides magnetospheric effects, tidal neutral winds in the E-region and thermospheric winds in the F-region are the major sources that drive the ionospheric currents. Strong asymmetries in the neutral winds and the ionospheric conductivities due to seasonal as well as their different geographic location are communicated from one point to the other in the form of electric fields which are conducted along the high conducting magnetic field lines. Calculations in Section 3.4 include this conjugate coupling using an electric circuit connecting E and F regions of one hemisphere to their counterpart in the other hemisphere.

For Millstone Hill (42.6N, 71.5W) whose conjugate point is located at (71.9S, 80.7W) (Evans, 1968), sunrise occurs earlier at the conjugate point than local sunrise during winter. As seen in Figure 2.5.1, for an altitude of 130 km, the average height of the E-region layer, this effect occurs from mid September through March. This indicates that E-region dynamo generated electric fields at the conjugate point conducted along the magnetic field lines can be effective at Millstone Hill even before there is any appreciable amount of E-region ionization produced locally. Carlson and Walker (1972)

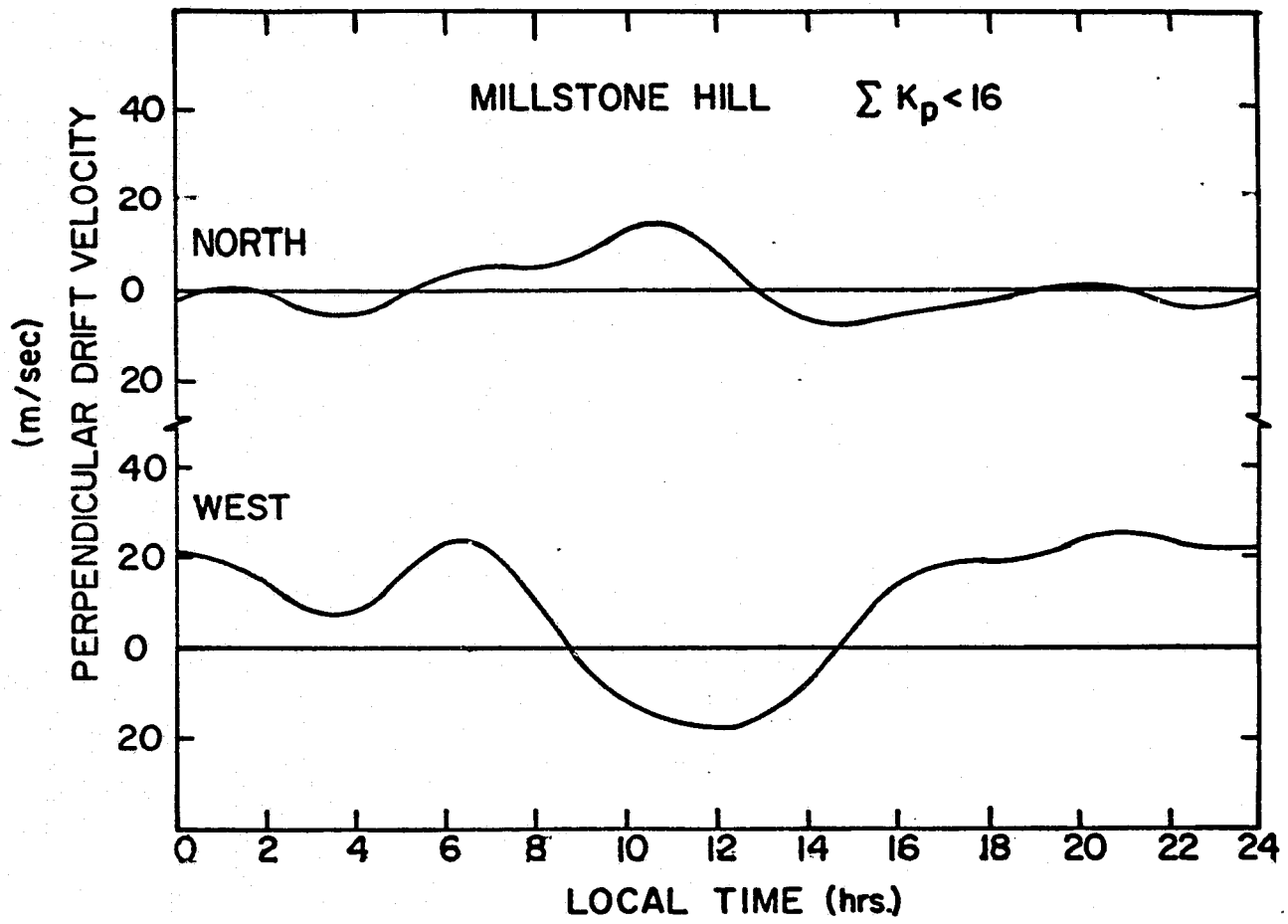

Figure 2.4.2 North and westward drift velocities for low magnetic activity

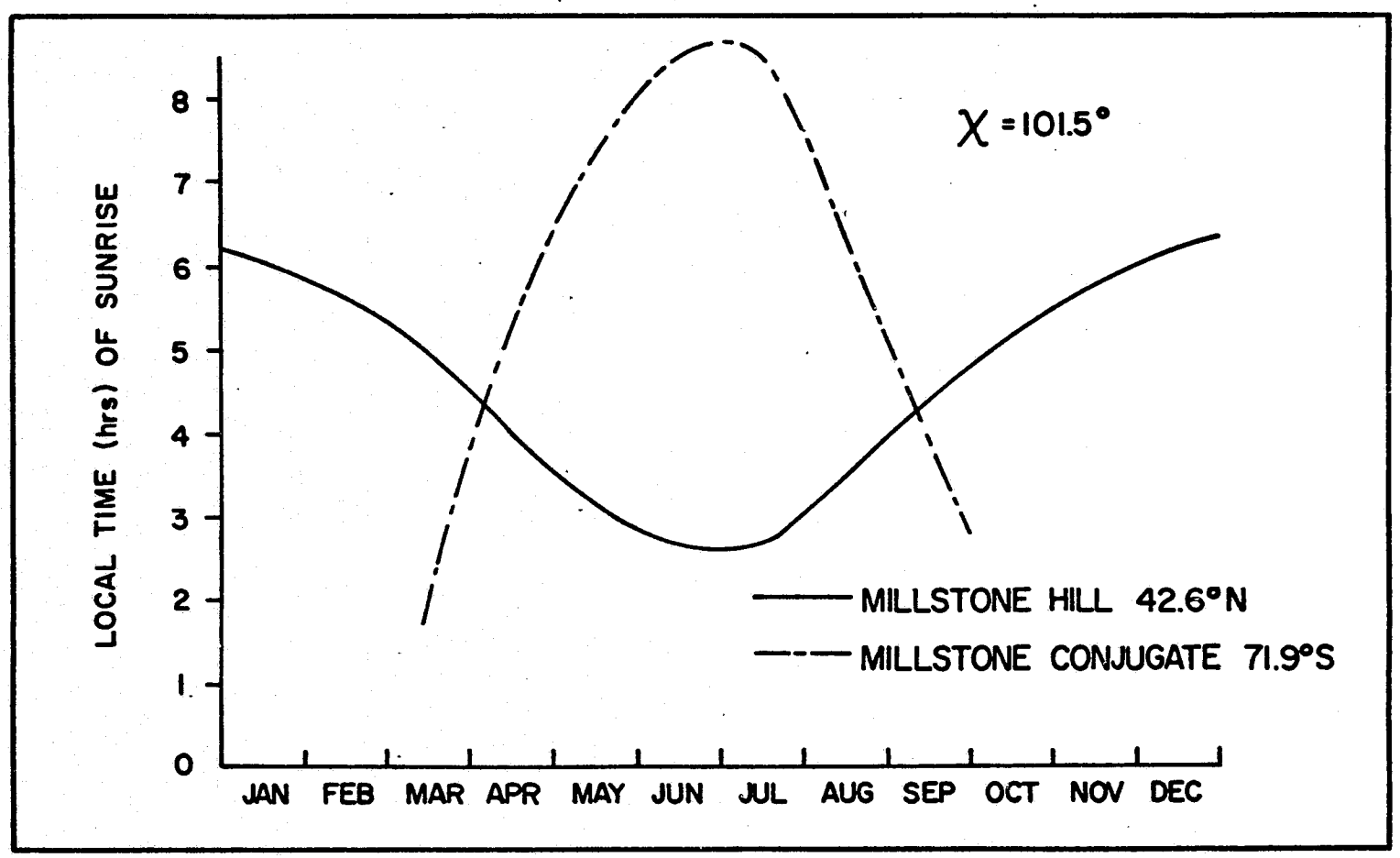

Figure 2.5.1 Local times of sunrise at 130 km

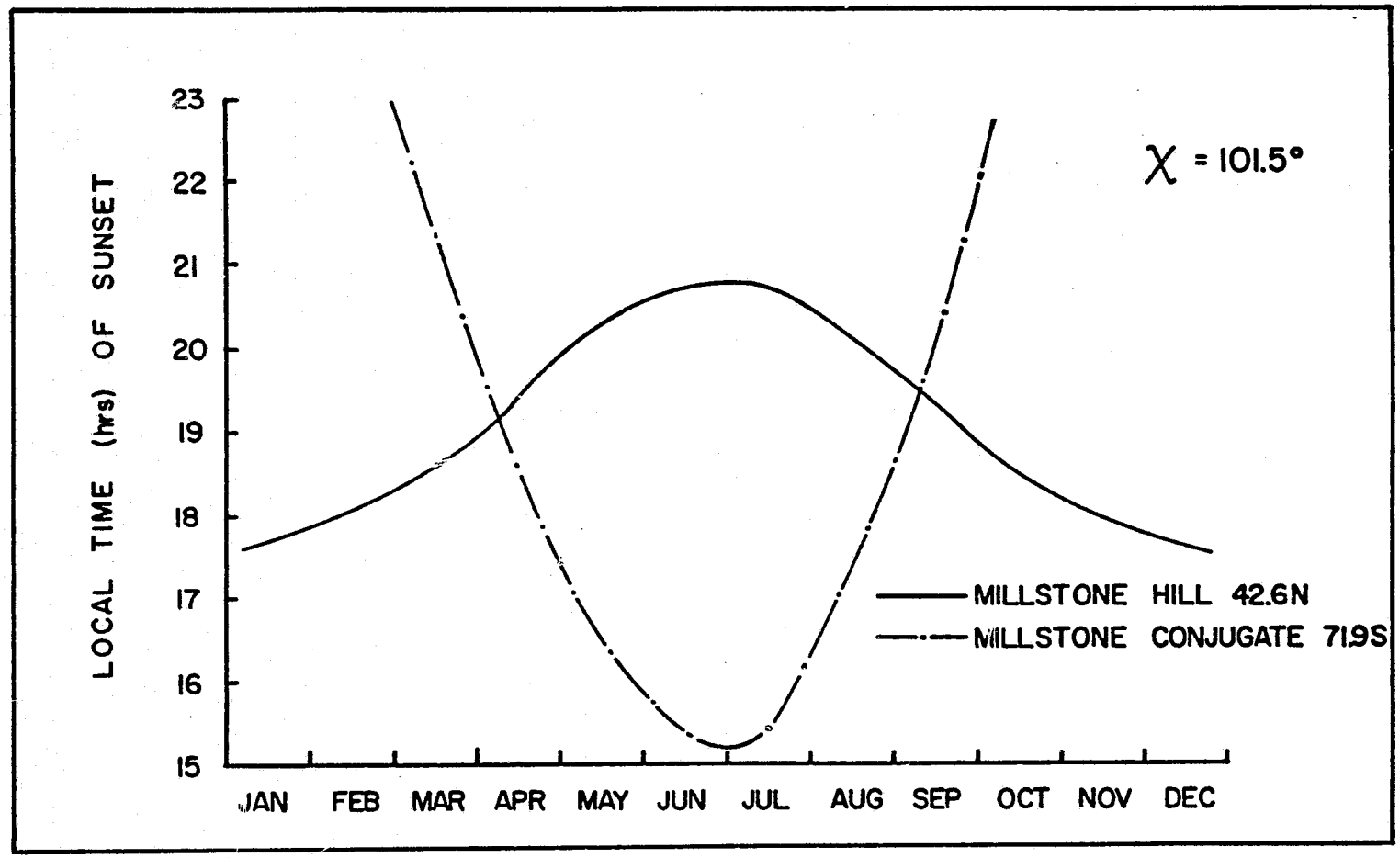

Figure 2.5.2 Local times of sunset at 130 km

predict ion drift velocity changes, due to conjugate sunrise, that are of the same order of magnitude as the dynamo region winds.

Currently available data for Millstone Hill do not have the necessary time resolution to investigate the effects of local and conjugate sunrise or sunset. It is suggested that this behavior be critically examined in an experiment with better time resolution. The calculations of local times of sunrise and sunset (Figures 2.5.1 and 2.5.2) indicate that the best time for such an experiment is 20 March or 20 September when local and conjugate sunrise are approximately two hour apart.

The identification of solar cycle effects from an analysis of the data is difficult at present because not much data is available over high and low solar cycle periods and because other variations are superimposed in the measurements.

The more recent Millstone Hill drift velocity data is representative of relatively low solar activity. The only data associated with higher solar fluxes are those from Evans (1972), for the daytime only. The average drift velocities for this period are shown in Figure 1.3.1 and although the shapes of the curves are similar to those of the more recent data (Figures 2.2.1 and 2.2.2) the maximum daytime values are somewhat larger.

2.6 Variation of Ionospheric Currents

Since ionospheric currents are closely related to the electric fields, some of their characteristics, as deduced from magnetograms, will be examined next. Magnetograms will be used from a station close to Millstone Hill, namely Weston, Massachusetts.

From the analysis of records from 1968, two outstanding variations are shown in Figures 2.6.1 and 2.6.2.

Figure 2.6.1 shows a variation that can only be caused by sporadic variations either in the conductivity or the electric field (see Equation (A. 10)) since seasonal and magnetic activity variations were eliminated by choosing days of the same month and the same ΣK_p. The horizontal magnetic field variation ΔH is shown for 1 March 1968 ($\Sigma K_p = 17^+$) and 2 March 1968 ($\Sigma K_p = 18$). Thus, although the ionospheric conditions appear to be the same for the two days, the westward current peak differs for the two days by a factor of two.

Seasonal variations, also much in evidence in the current variations, are shown in Figure 2.6.2. Monthly mean values of ΔH are plotted for January, April and June. For its analysis three time periods are defined, morning, (0-8, local standard time), day (8-16), and evening (16-24).

The morning period is influenced by sunrise (indicated by solid arrows for local, dashed arrows for magnetic conjugate) and low conductivities, the daytime by high conductivities, and the evening period again by low conductivities and sunset.

The morning period tends to show a different behavior in the summer months from winter and equinox. During summer the westward current tends to increase rather steadily toward the daytime maximum whereas during winter and equinox, the current is rather constant over the period having the tendency to show a small peak in the eastward direction close to sunrise. Since close to sunrise the

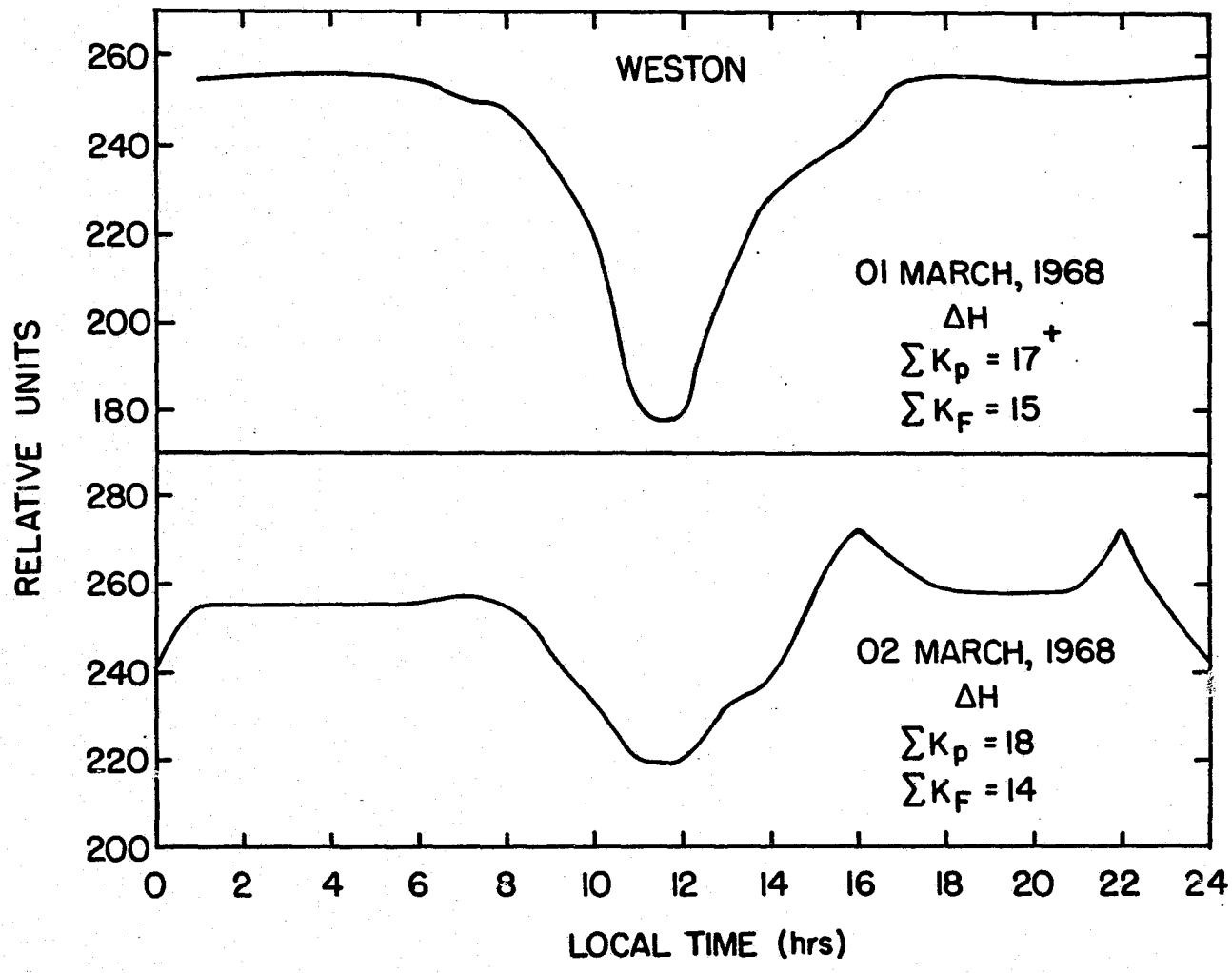

Figure 2.6.1 Current variations from magnetograms

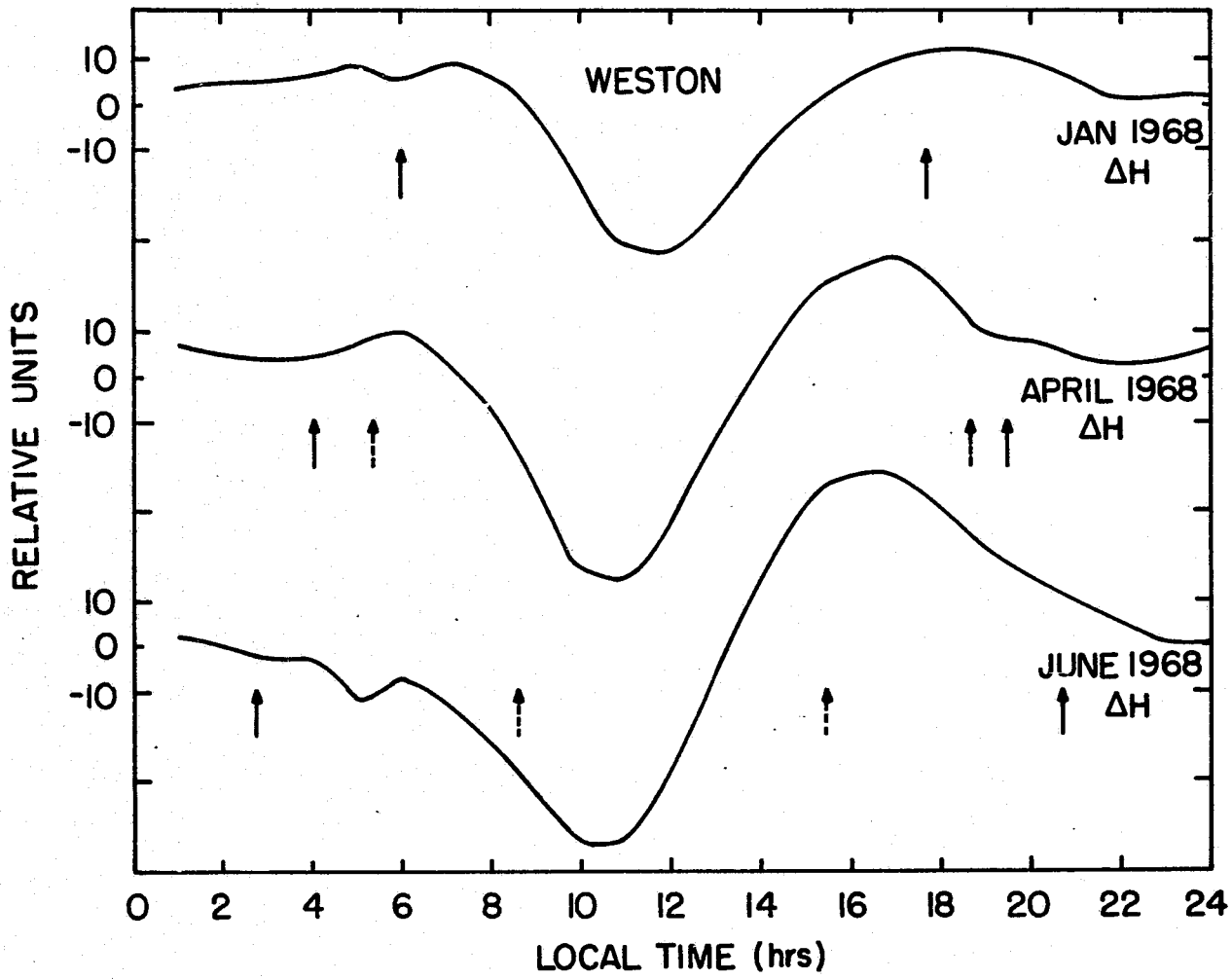

Figure 2.6.2. Seasonal current variations from magnetograms

conductivities are still very low, this must be caused by a change in the total electric field from summer to winter and equinox.

The daytime period peak changes position in time from 10 L. T. in summer to 12 L. T. in winter and 11 L. T. in equinox. Since the conductivity changes between 10 and 12 L. T. over the different seasons are only magnitude changes, it must again be the total electric field that has a phase change with season.

The evening period shows an eastward peak at 16-17 L. T. in summer and equinox but not in winter. This is probably caused by conductivity variations. During summer this peak occurs some 4-5 hrs. before sunset, at which time the conductivities are still 50% of their maximum value. In the winter, however, the peak should occur at the time of sunset, when the conductivities already have their low nighttime values, and therefore no current is produced.

CHAPTER III

DEVELOPMENT OF A MODEL

3.1 Introduction

In this chapter an electric field model will be developed. Three major sources of electric fields are included and the objective is to obtain calculated drift velocities that agree with the measurements of Chapter II. Calculations will be made of ionosphere currents, the convection electric field and F-region drift velocities. These will be used to relate the observations to the problems raised in Section 1.5.

3.2 Ionospheric Currents

The objective of this section is to test recently deduced models of neutral winds and electric fields by using them in the calculation of currents and comparing the results with magnetogram records.

The current expressions have been reviewed in Appendix A. For convenience, Equation (A.10) can be written in the form

$$I_E = [\Sigma_P/\sin^2 I\,(V_N + U_S \sin I) + \Sigma_H/\sin I\,(V_W + U_E)] \times B$$

$$I_N = [-\Sigma_H/\sin I\,(V_N + U_S \sin I) + \Sigma_P\,(V_W + U_E)] \times B$$

where

I_E, I_N are height integrated east and northward currents (A/m)

Σ_H, Σ_P are height integrated Hall and Pedersen conductivities $(\Omega)^{-1}$

V_N, V_W are north and westward drift velocities (m/sec)

U_E, U_S are east and southward neutral E-region winds (m/sec)

I is the inclination angle (72^o for Millstone)

B is the magnitude of B (for Millstone at 130 km height B = 5×10^{-5} T)

Using the incoherent-scatter technique it is possible to deduce simultaneously the electron densities, electric fields and neutral wind properties. For this case, however, only F-region properties were measured and therefore a model for the conductivities and a model for the neutral E-region winds has to be used to calculate the currents.

Using the current formulas above, results will be calculated for two days, a magnetic quiet day, 18 July 1973, with $\Sigma K_p = 12$, and a perturbed day, 27 February 1973, with $\Sigma K_p = 37^+$. The calculations are based on the following assumptions:

a) Drifts. The average drift velocities deduced for summer (Section 2.2) are used.

b) Winds. The average E-region neutral wind from Salah et al. (1975) is used. This semidiurnal tidal (2, 4) mode has been deduced from tidal theory using Millstone Hill incoherent-scatter measurements of temperature in the ionospheric E-region. It consists of a purely semidiurnal sinusoidal variation with an amplitude of 25 m/sec. The northward phase is maximum at 12 L. T. and the westward phase at 9 L. T.

c) Conductivities. These are calculated using the formulas of Appendix A. Neutral parameters are calculated using the CIRA (1972) model and height integration is performed in steps of 5 km for the E-region, defined to extend from 90 to 150 km. The electron densities are calculated using the Ching and Chiu (1973) model. This is a model based on average ionospheric sounding data which are reproduced by empirical mathematical formulas. The input parameters required are local time, day number, ΣK_p, geographic and geomagnetic latitudes, solar flux parameters and the monthly relative sunspot number. In this order, the parameters used for 18 July 1973 are respectively local time from 5 to 20 hours, D = 199, ΣK_p = 12, 42.6, 54, 80.9, 86.1, 43.3. For 27 February 1973 the input parameters are local time from 9 to 18, D = 58, $\Sigma K_p = 37^+$, 42.6, 54, 100.1, 100.5, 43.3.

As is well known the eastward ionospheric currents cause variations in the northward horizontal component of the magnetic field at the ground (ΔH), while the northward currents affect the declination (ΔD), and increases in currents correspond linearly to increases in the magnetic field components. We will compare the diurnal variations of the calculated currents with magnetogram records. The dynamo currents in the E-region flow primarily during the day so that the relatively constant magnetic field during the night can be used as a zero reference level. The results are shown in Figures 3.2.1 and 3.2.2. The eastward current reverses direction at about 13 L.T. which corresponds well to the zero level in ΔH (dotted vertical line)

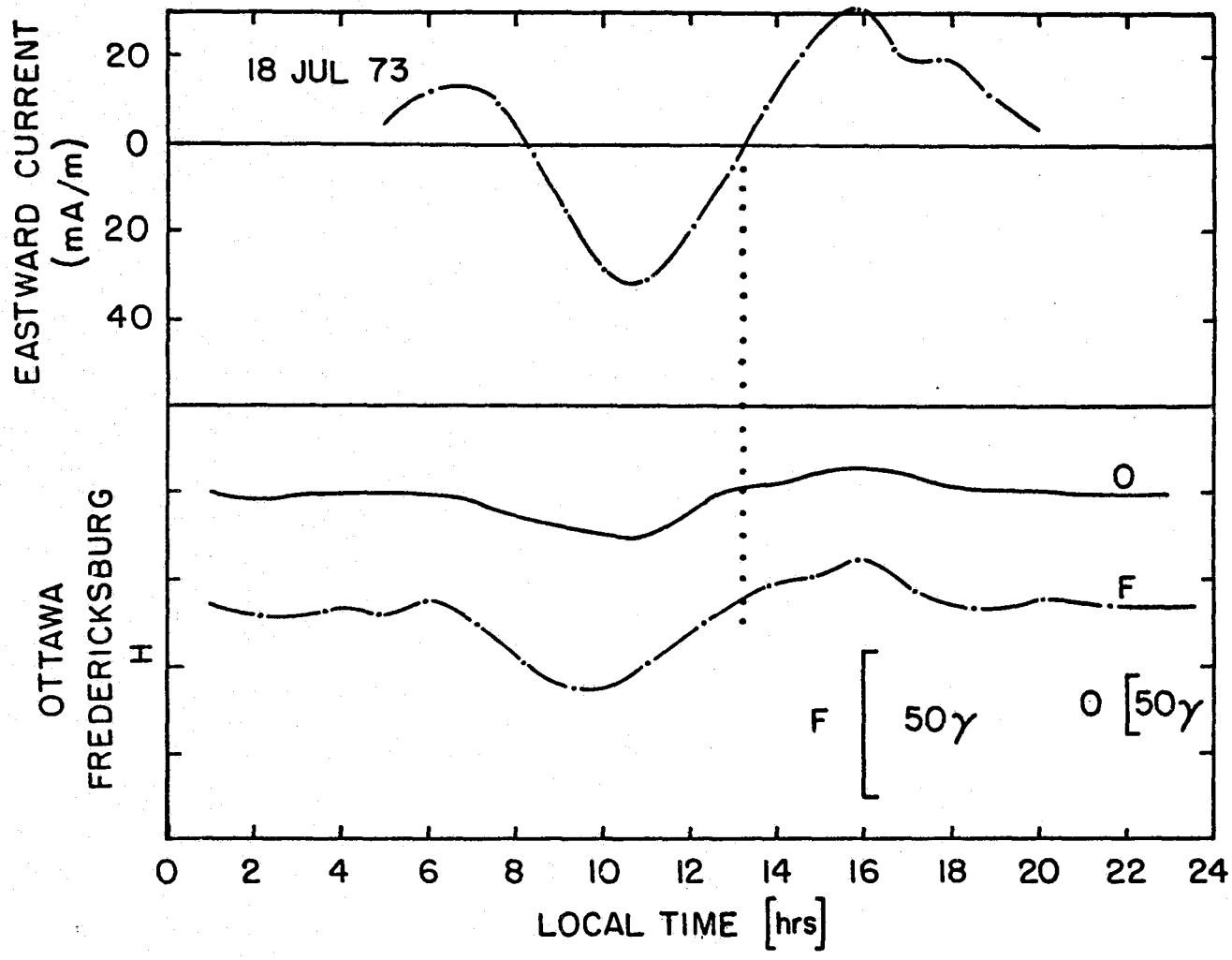

Figure 3.2.1 Height integrated E-region eastward current and magnetogram H traces

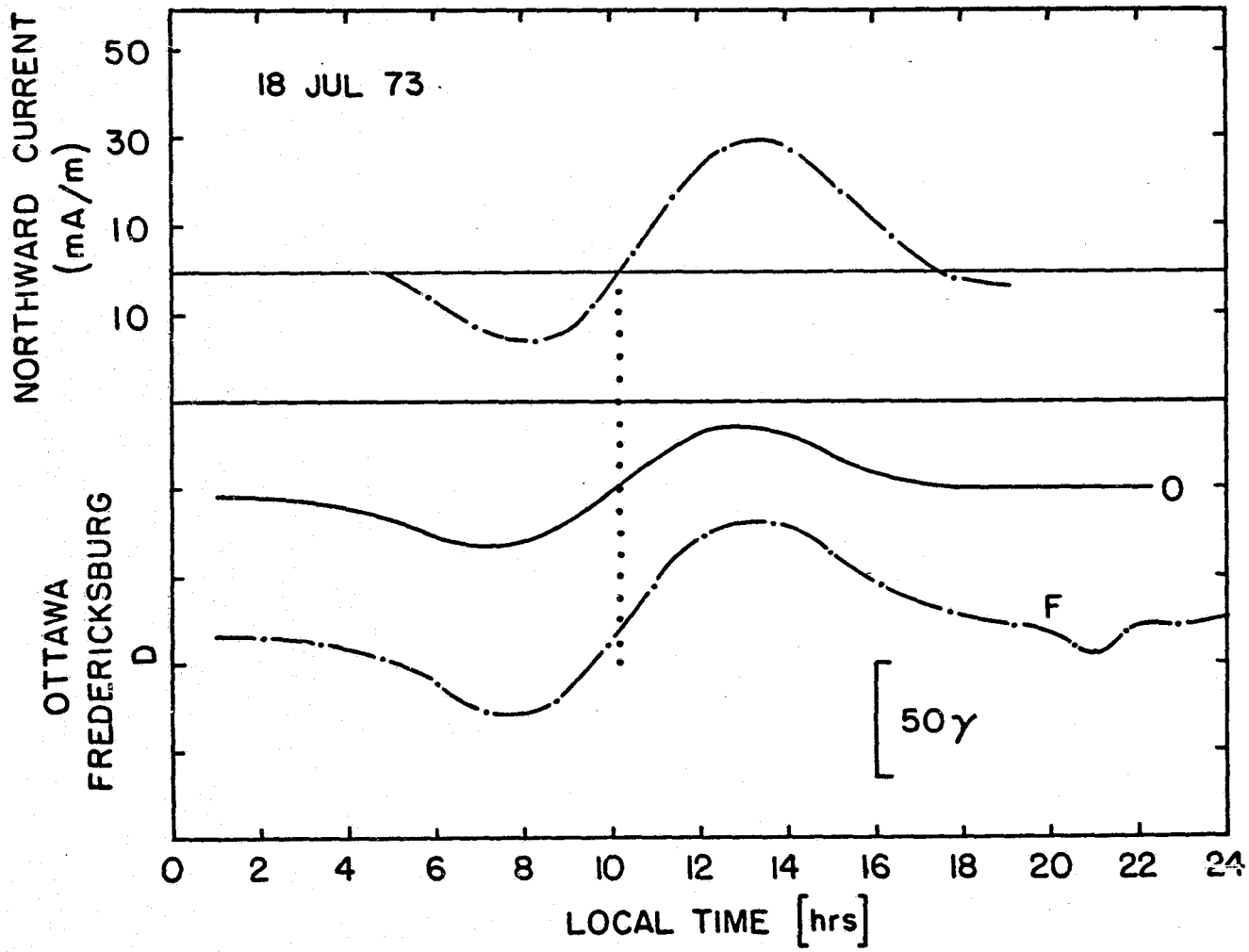

Figure 3.2.2 Height integrated E-region northward current and magnetogram D traces

for Ottawa (45.4N, 75.5W) and Fredericksburg (38.2N, 77.4W). Similarly for the northward current, in Figure 3.2.2, the reversal in direction occurs at about 10 L.T. which again agrees well with the D zero level for the same two stations. The same is seen to occur for the peaks in the currents, which are closely followed by peaks in ΔH and ΔD. For a disturbed day, however, on 27 February 1973, ($\Sigma K_p = 37^+$), Figures 3.2.3 and 3.2.4 show the currents and magnetogram traces with hardly any agreement, although electric field data were available for this day. The major cause for this is believed to be the neutral wind model used, not being adequate to represent magnetic disturbed periods. This is confirmed by the measurements of Forbes (1975), which show that E-region winds suffer drastic changes during magnetic disturbed periods.

In summary, on magnetic quiet days there is good agreement between calculated currents and magnetogram variations. This indicates that the independently derived electric field and tidal wind models are mutually consistent and substantiates the importance of the (2, 4) tidal mode in E-region dynamics.

3.3 Convection Electric Field

Instead of assuming an electric field in the magnetosphere, an alternate way of calculating the convection component of the electric field is to assume a current distribution in the ionosphere due solely to the convection electric field. As mentioned before, however, Nishida et al. (1966) actually deduced a number of equivalent current systems from the DP2 variations. Thus if the conductivities are known, the calculation of the convection electric field is

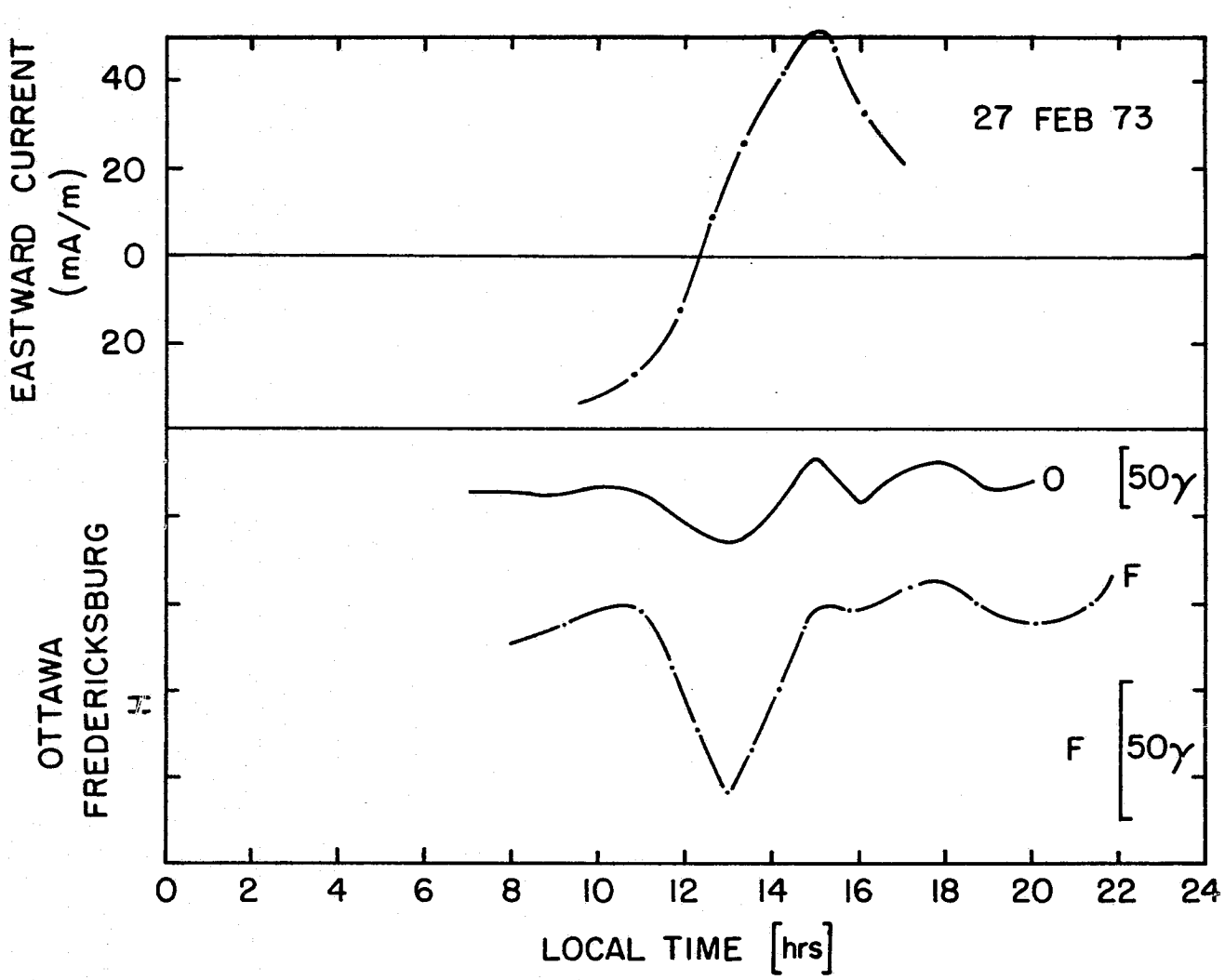

Figure 3.2.3 Height integrated E-region eastward current and magnetogram H traces

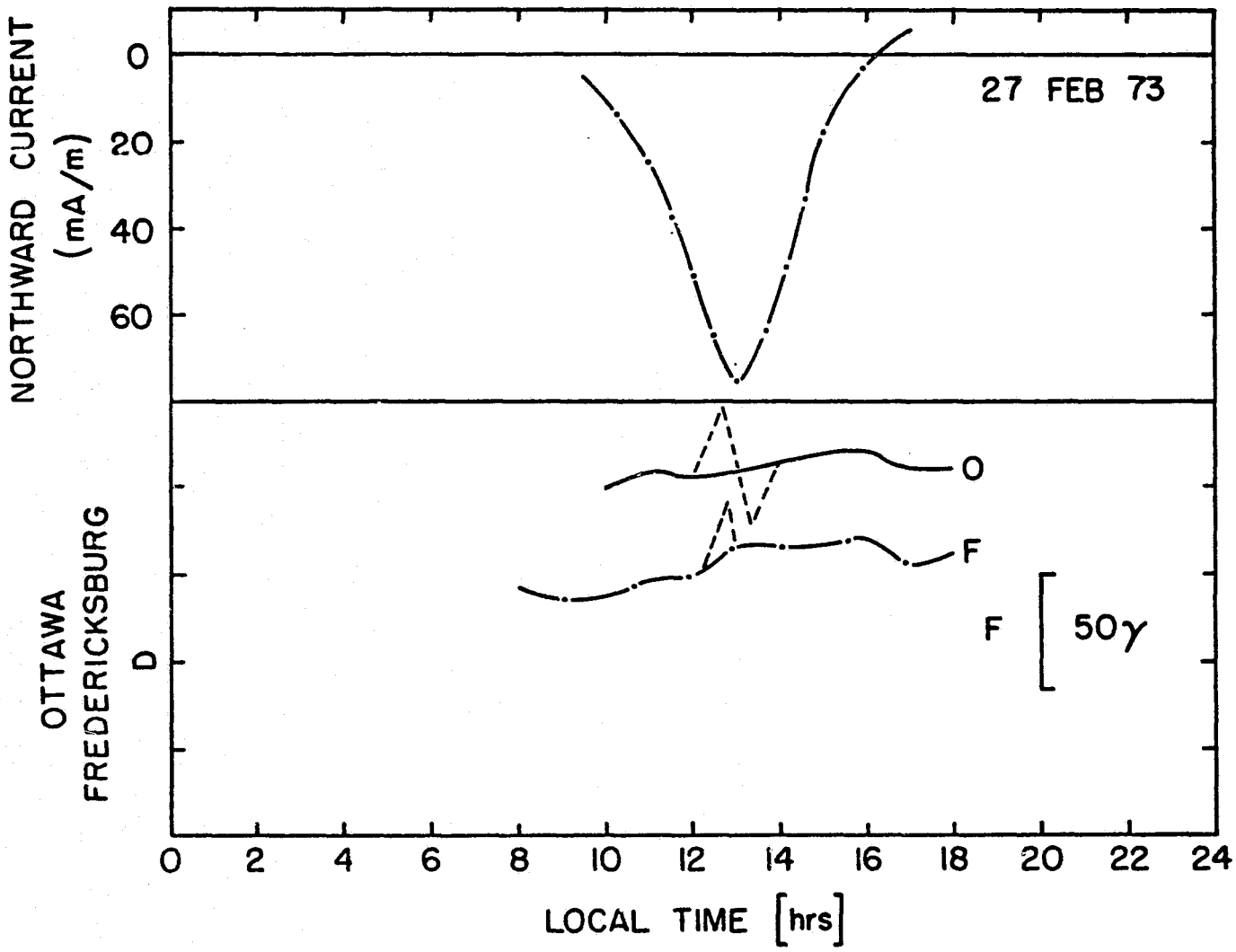

Figure 3.2.4 Height integrated E-region northward current and magnetogram D traces

straightforward by simply inverting the height integrated version of Equation (A. 10). The results of applying this method are shown in Figures 3.3.1 and 3.3.2 for Millstone Hill. Shown for comparison is the Mendillo (1973) model, which assumes a uniform east-to-west electric field exists in the magnetospheric tail, and this is then mapped along magnetic field lines to the ionosphere. The result in terms of ionospheric drift velocities as a function of local time is a simple sinusoidal diurnal variation, having a northward peak at 12 L. T. and westward maximum at 18 L. T.

Although the mapping procedure in Mendillo's derivation is correct, an implicit assumption is that the east-west electric field to be mapped is the same in the entire magnetospheric equatorial plane and therefore the model does not represent a true diurnal variation. The actual convection electric field in the ionosphere has an additional constraint, i.e. to satisfy Ohm's law, and therefore some degree of asymmetry is expected due to the diurnal variation of the ionospheric conductivity. In particular, the magnitude of the convection electric field should be small around noon because the conductivities are high. This is confirmed by these calculations, which show negligible electric field magnitudes over the daytime period (about 0.25 mV/m) but substantial contributions at night (about 2 mV/m).

3.4 Requirements for the Model

It has been shown in the literature review of Chapter I and the calculation of Section 3.3 that three independent sources contribute to the electric fields, namely the E-region dynamo where tidal winds dominate, the F-region dynamo where the thermospheric wind system

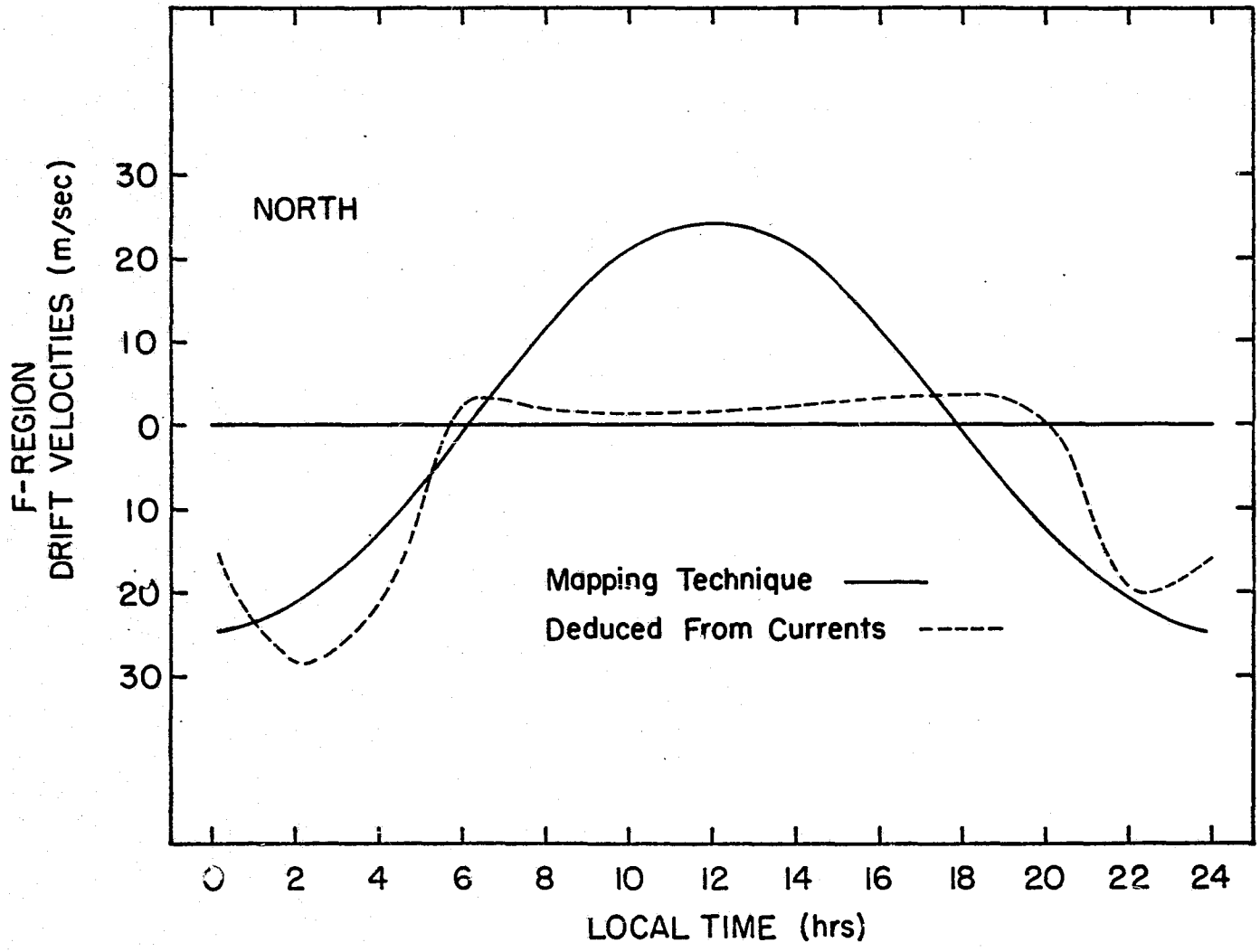

Figure 3.3.1 Northward convection drifts

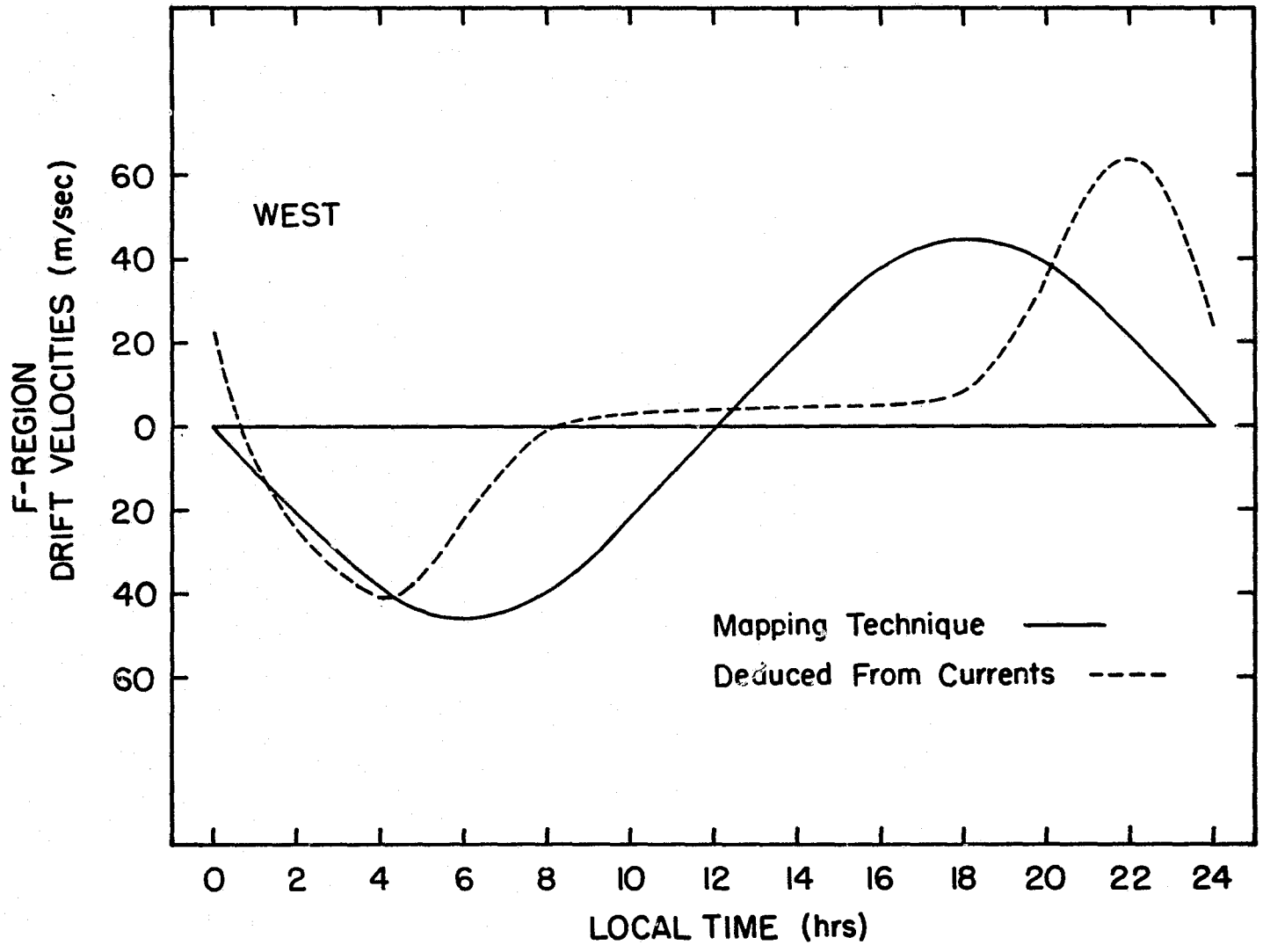

Figure 3.3.2 Westward convection drifts

drives the currents, and magnetospheric convection. The electric field models available previous to this work, however, are based on only one of the possible sources for the generation of electric fields, and are therefore incomplete.

One of the tasks in the development of a new model is to include all three sources of electric fields. An additional process that is likely to affect the electric field is the magnetic conjugate point effect discussed in Section 2.5. Although this is not actually an additional source, asymmetries between the southern and northern hemisphere, linked by the magnetic field lines, can alter the overall electric fields.

Based on the requirements above and using the height integration concept, an equivalent circuit for the new model can now be visualized in which E and F-region parameters are connected through the highly conducting magnetic field lines to their counterpart in the opposite hemisphere. We have thus combined two basic characteristics. First the ionospheric currents given for example by Equation (3.1) can be represented by an equivalent electric circuit (Stening, 1968) and secondly, any such circuit at a given point in the ionosphere is connected through the magnetic field lines to a similar circuit at the magnetic conjugate point. If an additional branch is then included to represent the F-region, the circuit is complete for the representation of E and F-region dynamos. The magnetospheric contribution is accounted for by an additional current driver connected across the previous two branches.

3.5 The Equivalent Circuit

The basic equivalent circuit is shown in Figure 3.5.1a. R_{FN} and R_{EN} are resistors representing the effect of the height integrated

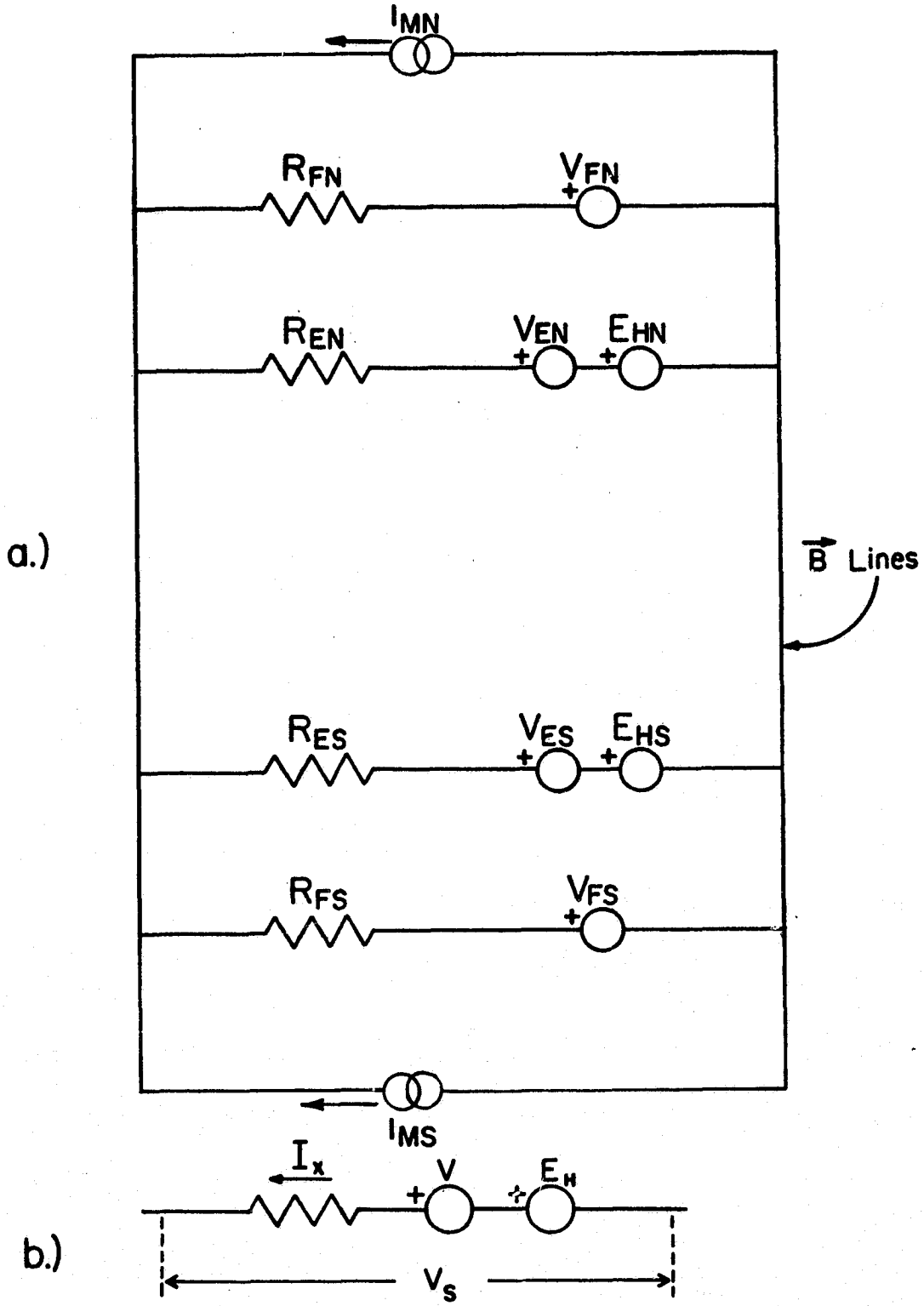

Figure 3.5.1a The equivalent circuit
b Detail of a branch of the circuit

Pedersen conductivity for the F and E-region of the northern hemisphere as are R_{FS} and R_{ES} for the southern hemisphere, and are calculated from the conductivities developed in Appendix A. $V_F = U \times B$ and $V_E = T \times B$ are F and E-region driving generators where U is the thermospheric neutral wind and T is the tidal E-region neutral wind. E_H is the Hall generator that accounts for the ionospheric Hall effect and which depends on the currents and conductivities of the circuit. The circuit shown, for example, is used for the north-south direction. A similar circuit is then used for the east-west direction.

The Hall generators are calculated as follows. Let x and y represent magnetic east and north directions. The currents are given by

$$\begin{aligned} I_x &= \Sigma_{xx} E_x + \Sigma_{xy} E_y \\ I_y &= -\Sigma_{xy} E_x + \Sigma_{yy} E_y \end{aligned} \qquad (3.1)$$

where I_x, I_y are current densities (A/m), the Σ's are the height integrated layer conductivities (ohms) and E_x, E_y are the total electric fields (V/m) $E_x = E_{sx} + (U \times B)_x$, where E_{sx} is the electrostatic field and U the neutral wind. This equation is valid for both hemispheres but Σ_{xy} is negative in the southern hemisphere. The current flow is generated by the action of U x B which has the dimensions of an electric field. Thus when U x B is positive toward the east it will move positive charges toward the east and thus is equivalent to a voltage generator producing eastward current.

Because of the Hall effect implicit in Equation (3.1) the currents I_x, I_y cannot be represented by a single generator in series

with a resistor. A circuit representation can however be done with the addition of another voltage generator E_H in the following way: referring to Figure 3.5.1b, the electrostatic field in the positive x direction corresponds to the total voltage V_S and one can write

$$E_{Sx} = I_x R - E_H - V$$

such that, with $(U \times B)_x = V$

$$E_x = E_{Sx} + V$$

and so

$$E_x = R I_x - E_H \tag{3.2}$$

If for the resistor R we use $1/\Sigma_{xx}$ for the x direction and $1/\Sigma_{yy}$ for the y direction, then with Equation (3.2) substituted into (3.1), the Hall generators become

$$E_{Hx} = (\Sigma_{xy}^2 I_x + \Sigma_{xx} \Sigma_{xy} I_y)/(\Sigma_{xx} \Sigma_{xy}^2 + \Sigma_{yy} \Sigma_{xx}^2)$$

$$E_{Hy} = (\Sigma_{xy}^2 I_y - \Sigma_{xy} \Sigma_{yy} I_x)/(\Sigma_{yy} \Sigma_{xy}^2 + \Sigma_{xx} \Sigma_{yy}^2) \tag{3.3}$$

Thus all elements are now available for the equivalent circuit representation. It is interesting to note that in the northern hemisphere a southward wind produces eastward current whereas in the southern hemisphere a northward wind does. Thus equatorward winds in both hemispheres produce currents in the eastward direction. An

eastward wind produces northward and southward current respectively in the northern and southern hemispheres.

3.6 Results for the Complete Model

The calculation of currents and electric fields using the equivalent circuit of the previous section will be called the E-F-M Model to emphasize the contribution of E, F and magnetospheric regions.

The results will be based on the following assumptions and input parameters:

a) Distributed ionospheric parameters are represented through lumped parameters in an equivalent circuit.

b) Solving for the loop currents of Figure 3.5.1a the electric field is calculated and results presented in terms of drift velocities.

c) The calculated electric fields are considered the same in E and F regions although a very small mapping factor is involved.

d) Neutral Winds. The average E-region neutral wind from Salah et al. (1975) is used. This semidiurnal tidal ($\tilde{2}$, 4) mode has been deduced from tidal theory using Millstone Hill incoherent-scatter measurements of temperature in the ionospheric E-region. It consists of a purely semidiurnal sinusoidal variation with an amplitude of 25 m/sec. The northward phase is maximum at 12 L.T. and the westward phase at 9 L.T. This same neutral wind has been used for the

calculation of currents in Section 3.2. The same mode is assumed to dominate at the southern hemisphere, scaled by a factor of 0.75 according to tidal theory (Chapman and Lindzen, 1970).

For the thermospheric winds the calculations of Cho and Yeh (1970) are used. These are based on the simultaneous solution of the equations of motion and continuity, and results are given for different seasons and solar activity. Results are used for 45N latitude taking into account the seasonal difference between northern and southern hemispheres.

e) Conductivities. These are calculated using the formulas of Appendix A. Neutral parameters are calculated using the CIRA (1972) model and height integration is performed in steps of 5 km. The E-region is defined to extend from 90 to 150 km. The electron densities are calculated using the Ching and Chiu (1973) model. This is a model based on average ionospheric sounding data which are reproduced by empirical mathematical formulas. The input parameters required are local time, day number, ΣK_p, geographic and geomagnetic latitudes solar flux parameters and the monthly relative sunspot number.

The results of the E-F-M Model calculations are shown in Figures 3.6.1 and 3.6.2. F-region drift velocities calculated for a summer day are shown for the north and westward directions. Common input parameters used are day number D = 180, $\Sigma K_p = 12$, $F_{10.7} = 80.9$ $\overline{F}_{10.7} = 86.1$, sunspot number = 43.3, Millstone Hill latitude and conjugate point. Also shown for comparison are the

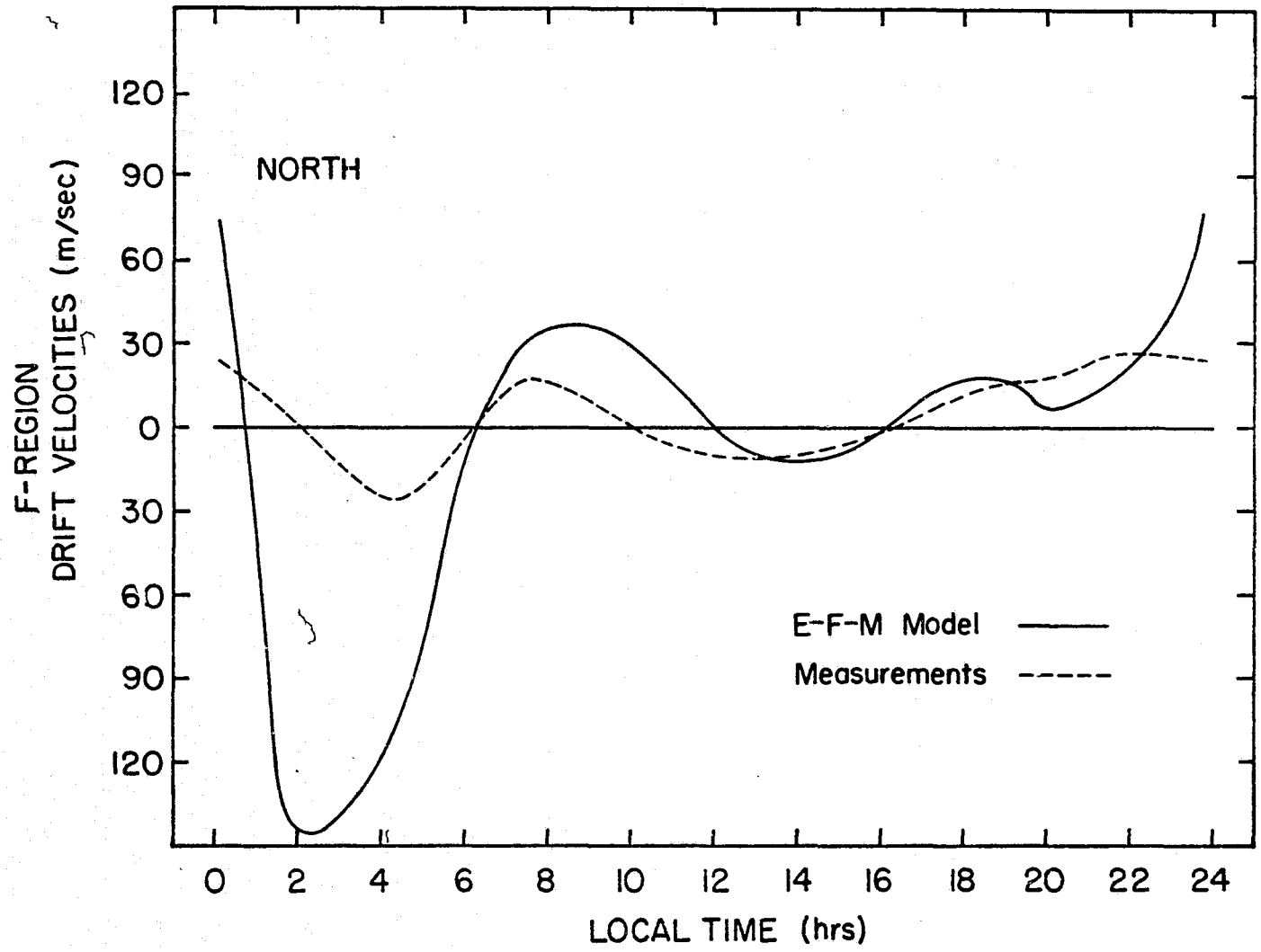

Figure 3.6.1 The model calculations compared with measurements. Northward drifts

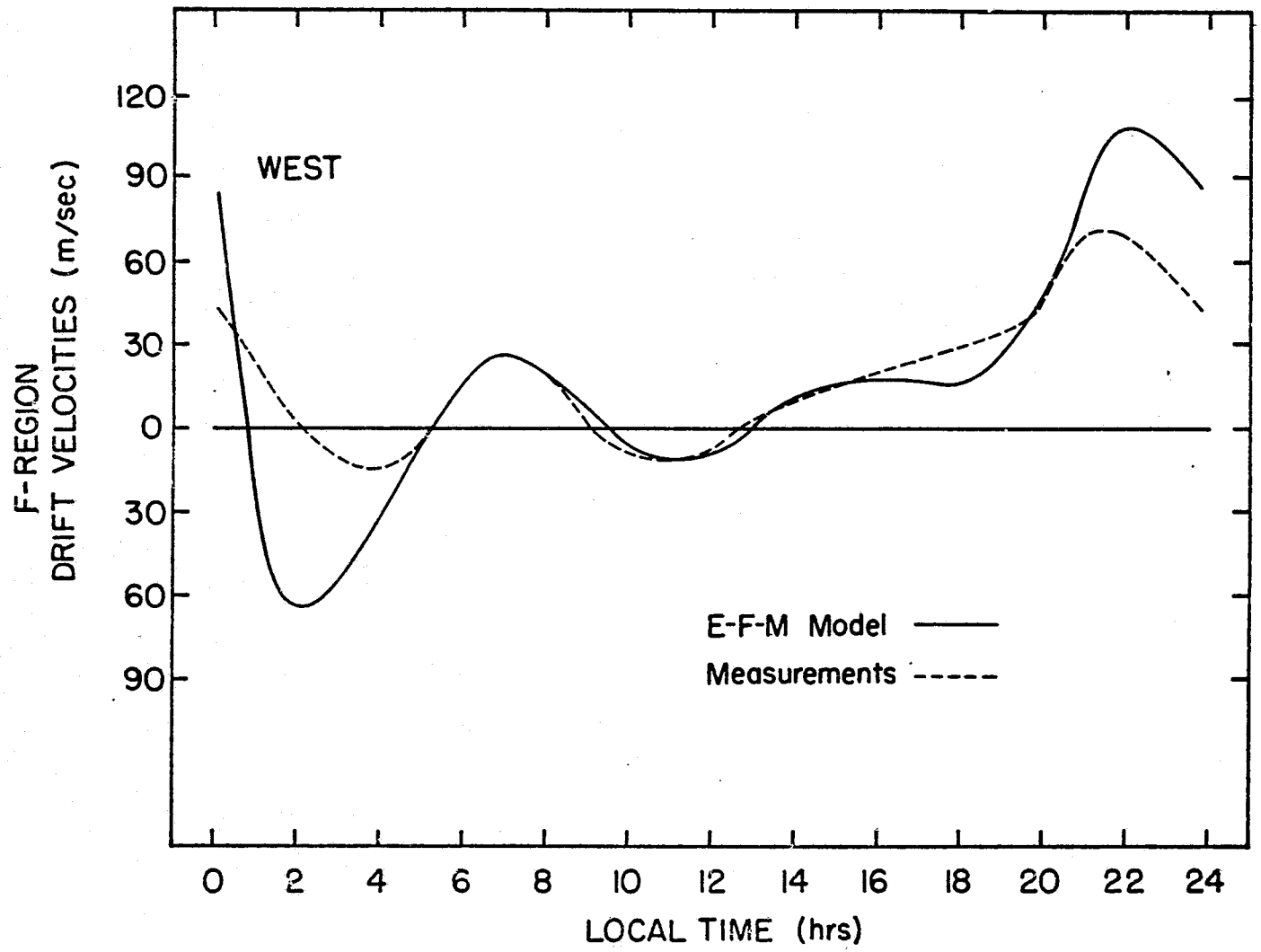

Figure 3.6.2 The model calculations compared with measurements. Westward drifts

average summer measurements for Millstone Hill discussed in Chapter II and shown separately in Figures 2.2.1 and 2.2.2.

It can be seen that during the daytime (6-18 hours) the calculations for both components reproduce the measurements to a good degree (i.e. within the standard deviations of about 20 m/sec). During the nighttime, particularly in the early morning period, the comparison is not so good. It must be remembered, however, that it is during this period that the measurements are subject to the largest uncertainties and that during this period the least number of measurements are available.

The large southward velocities in the early morning of Figure 3.6.1 must be primarily the effect of the F-region dynamo since at night the ratio of Pedersen E to F region conductivity is smaller and the thermospheric wind system drives the currents effectively.

Large southward drifts have been measured occasionally, and the rather fast reversal in direction that is shown by the calculations would contribute to the large standard deviations in the measurements.

3.7 Results Without Magnetospheric Contributions

The north and westward F-region drift velocities are shown in Figures 3.7.1 and 3.7.2, neglecting the effect of the magnetospheric electric field contribution. The same input parameters from the previous section are used.

As expected from a previous analysis the daytime results are practically unchanged. It was shown in Section 3.3 that the convection electric field is large primarily at night and therefore the daytime calculations should compare well with the measurements, which is the

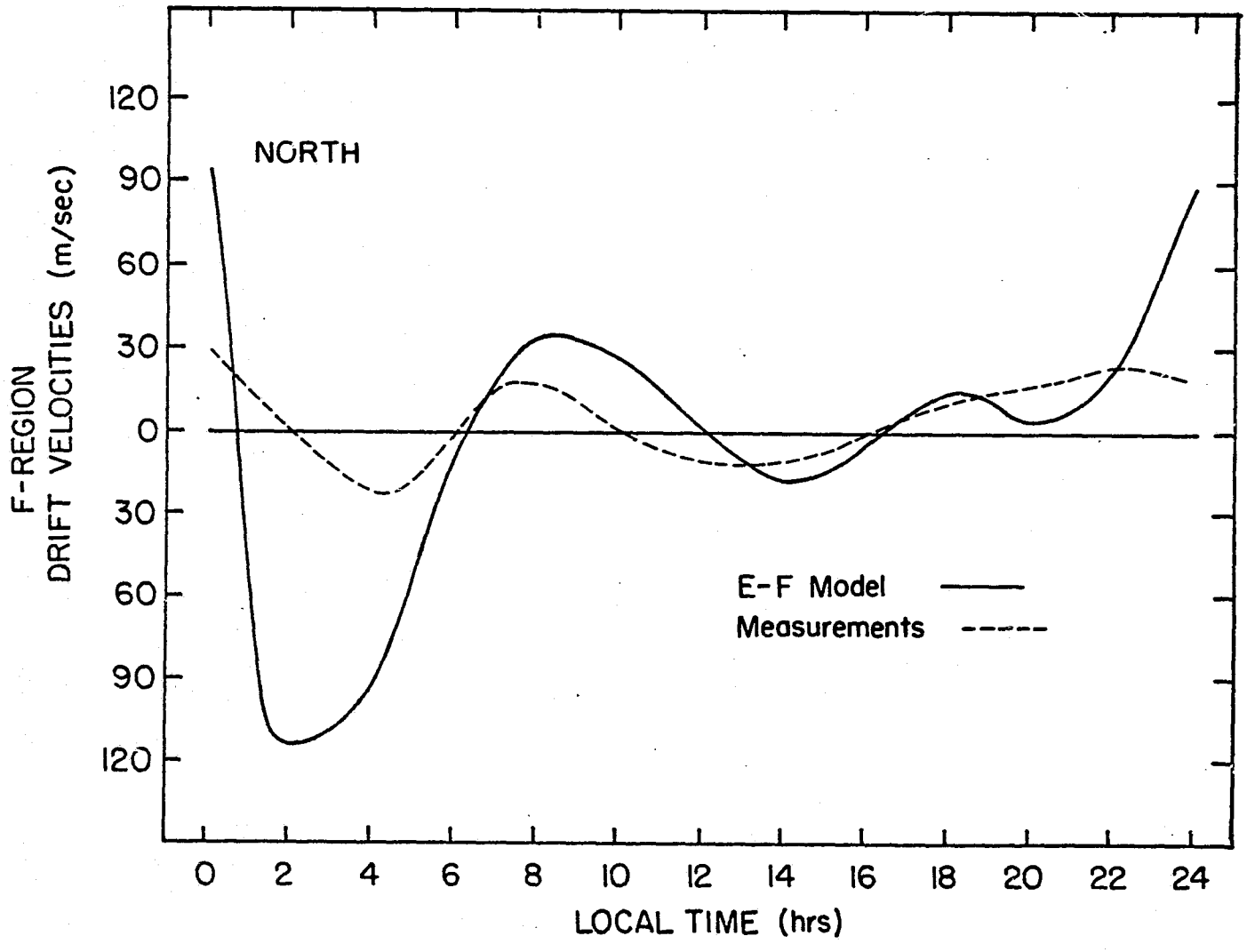

Figure 3.7.1 E and F dynamos compared with measurements. Northward drifts

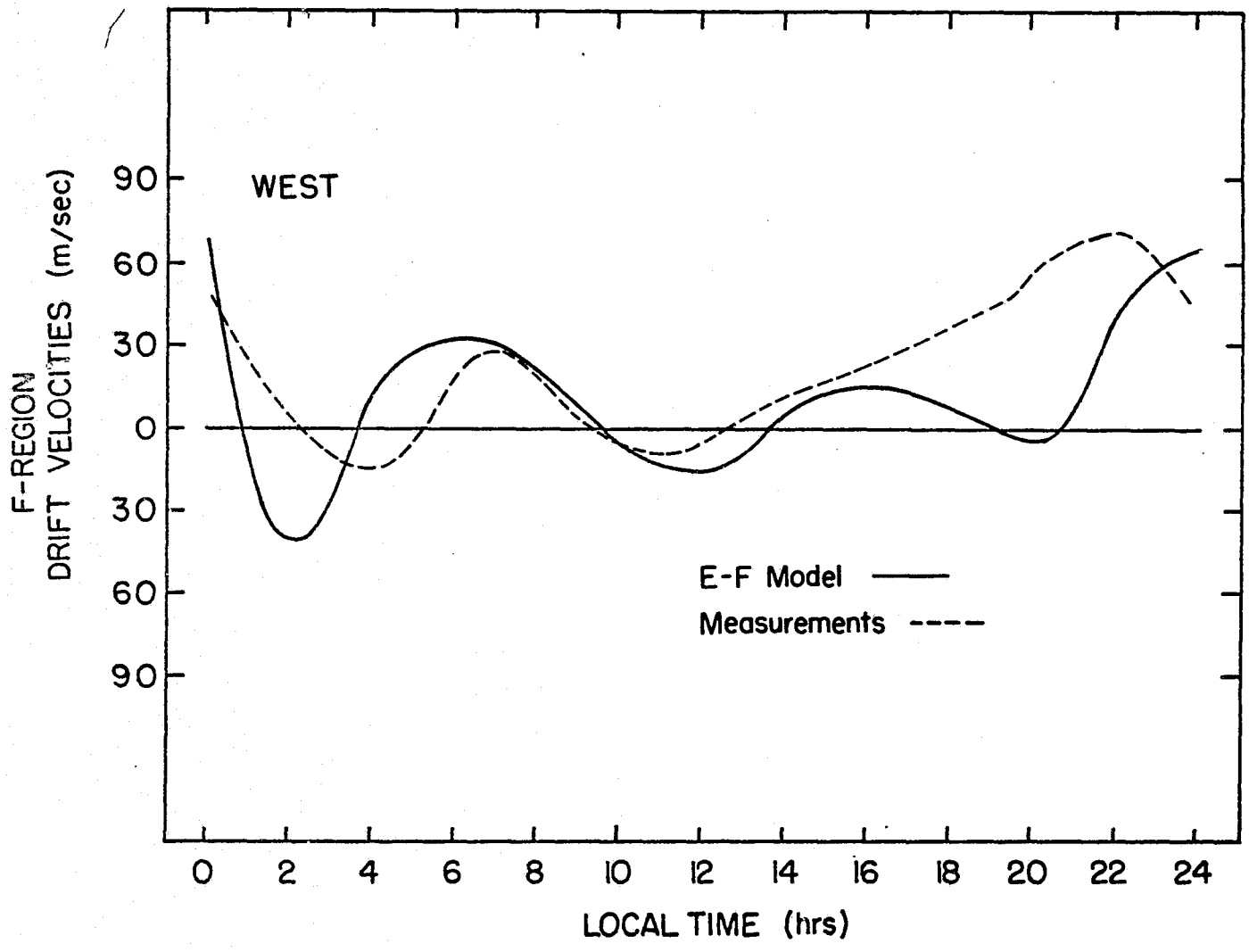

Figure 3.7.2 E and F dynamos compared with measurements. Westward drifts

case of Figures 3.7.1 and 3.7.2. The comparison is still within the standard deviation of the mean of the measurements. The largest discrepancy between calculations and measurements is seen now to occur for the westward component from 18 to 22 hours. Thus in the early evening the convection electric field represents a substantial contribution to the measured values.

3.8 The Effects of E-Region Tide Variations

In this section the effect of E-region tide variations in amplitude and phase will be evaluated, by comparing the results with those of the previous section.

The tidal E-region neutral wind from Salah et al. (1975) is an average result, not intended to represent any particular season. We will arbitrarily reduce amplitudes by a factor of two, and change phases by two hours in order to see how the calculated drifts respond to the E-region winds. Although arbitrary, these changes are believed to be reasonable, and might be expected to occur as a result of seasonal variations, for example.

The changes in the drift velocities due to the changes in the amplitudes of the E-region tides are shown in Figures 3.8.1 and 3.8.2. The continuous line is the result of Section 3.7 and is used for comparison. Results are calculated every two hours and shown by different symbols. The drift velocity that results when only the eastward tide is reduced by a factor of two is represented by (x); when only the equatorward amplitude is reduced by a factor of two, by (o) and when both components are reduced again by a factor of two the drifts are represented by (Δ).

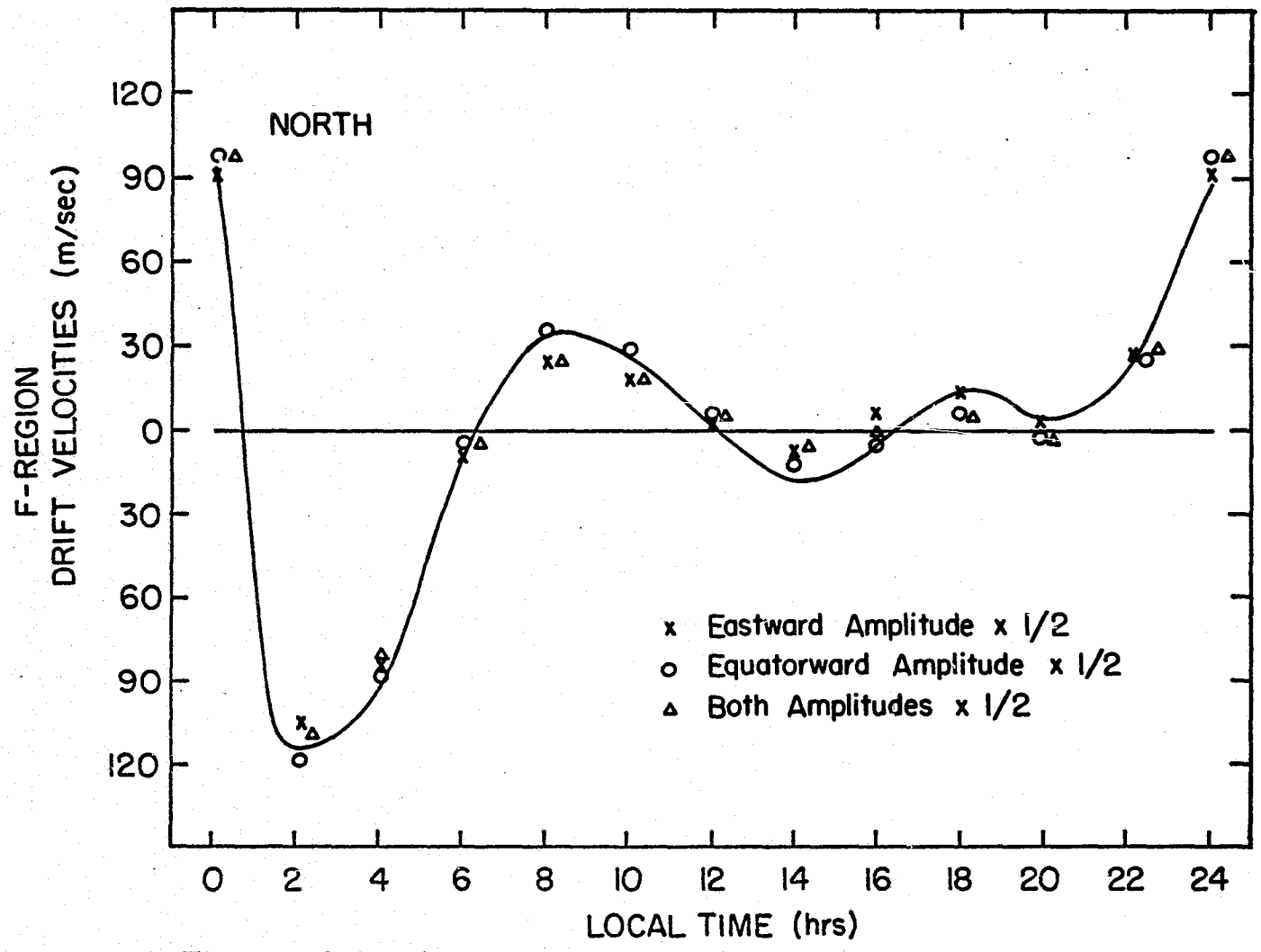

Figure 3.8.1 The effect of tidal magnitude changes. Northward drifts

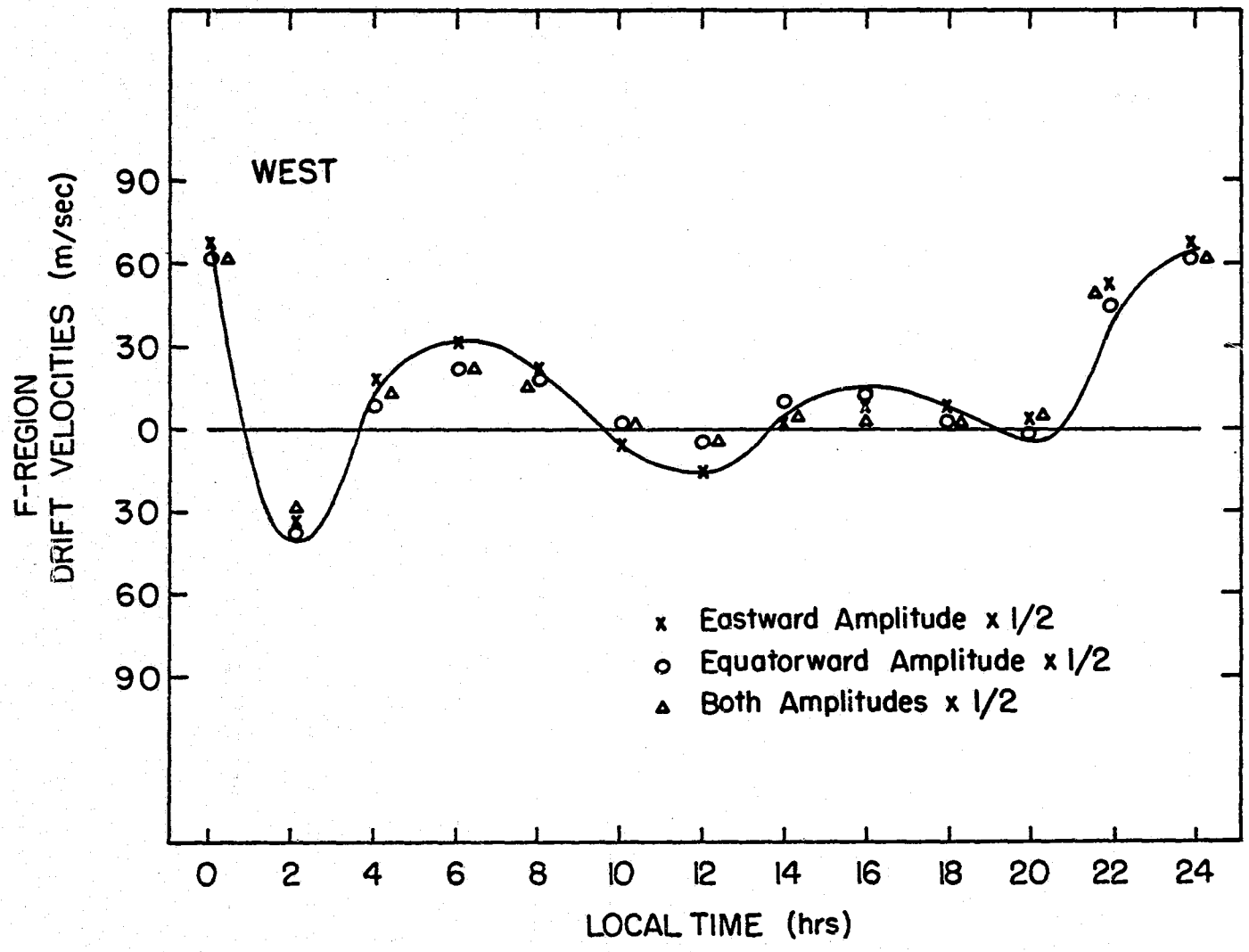

Figure 3.8.2 The effect of tidal magnitude changes. Westward drifts

It can be seen that in comparison with the results of the previous section, the relative magnitudes are changed little during the nighttime. During the day the relative changes are larger but not greater than 20 m/sec and the times of zero drift velocities are changed by no more than one-half hour.

The phases of the E-region neutral wind will be changed next. The times of maximum will be decreased by two hours, such that the north and westward components are maximum at 10 and 7 L.T., respectively.

The results expressing the changes in the drift velocities due to the changes in the phases of the E-region neutral wind are shown in Figures 3.8.3 and 3.8.4. The continuous line is the result of Section 3.7, and is used for comparison. Results are calculated every two hours and shown by different symbols. The drift velocity that results when only the eastward phase is changed is represented by (x); when only the equatorward phase is changed, by (o) and when both phases are changed the drifts are represented by (Δ). Again, relative changes are larger during the day but not larger than 20 m/sec. The times of zero drift velocities, however, can be changed by as much as two hours.

3.9 The Effects of F-Region Wind Variations

The extent to which the F-region contributes to the total electric field will be emphasized next. The only change in the model will be in the thermospheric wind system which will be reduced arbitrarily by a factor of 10.

The resulting drift velocities, calculated every two hours, are shown in Figures 3.9.1 and 3.9.2 by different symbols. The drifts

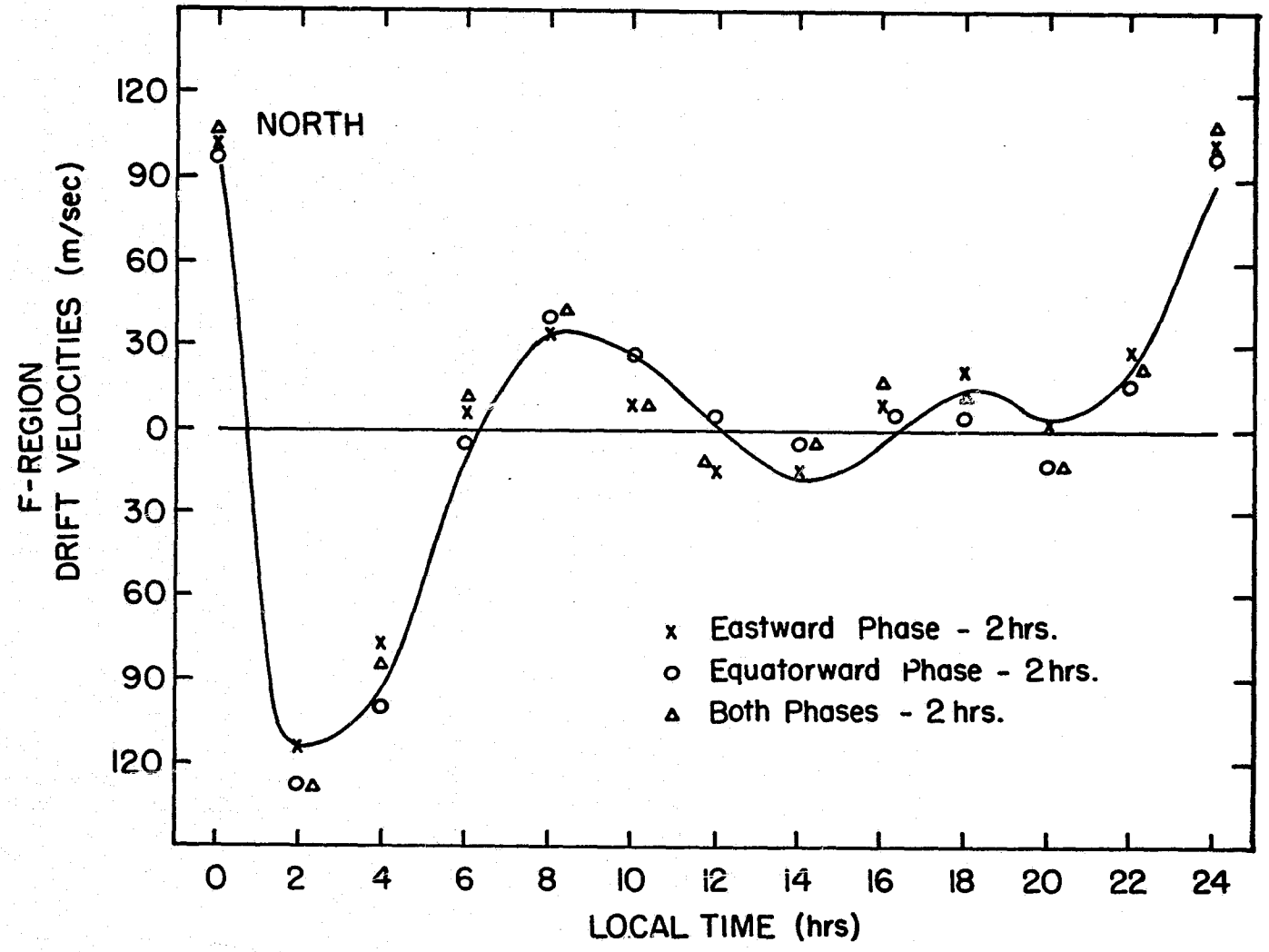

Figure 3.8.3 The effect of tidal phase changes. Northward drifts

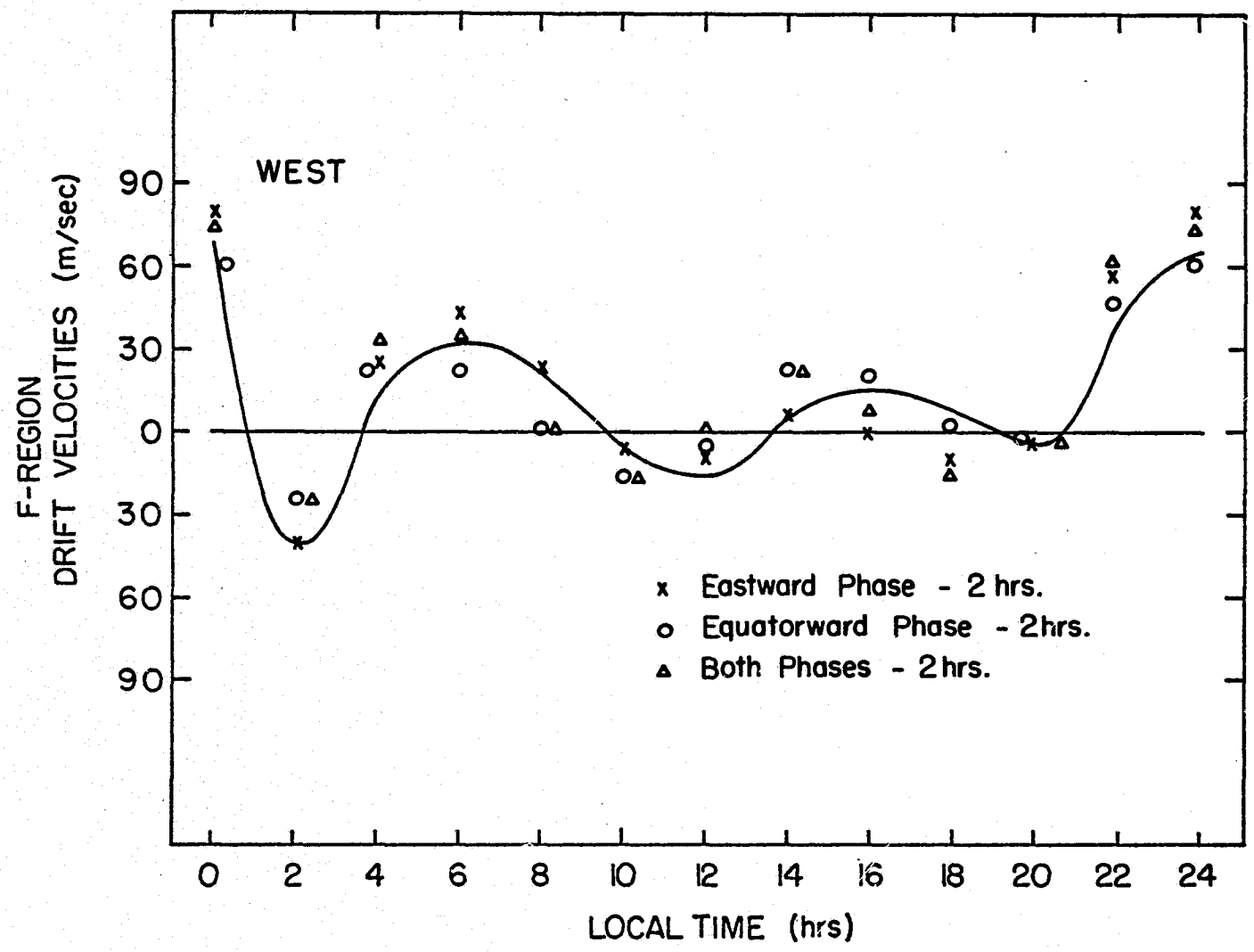

Figure 3.8.4 The effect of tidal phase changes. Westward drifts

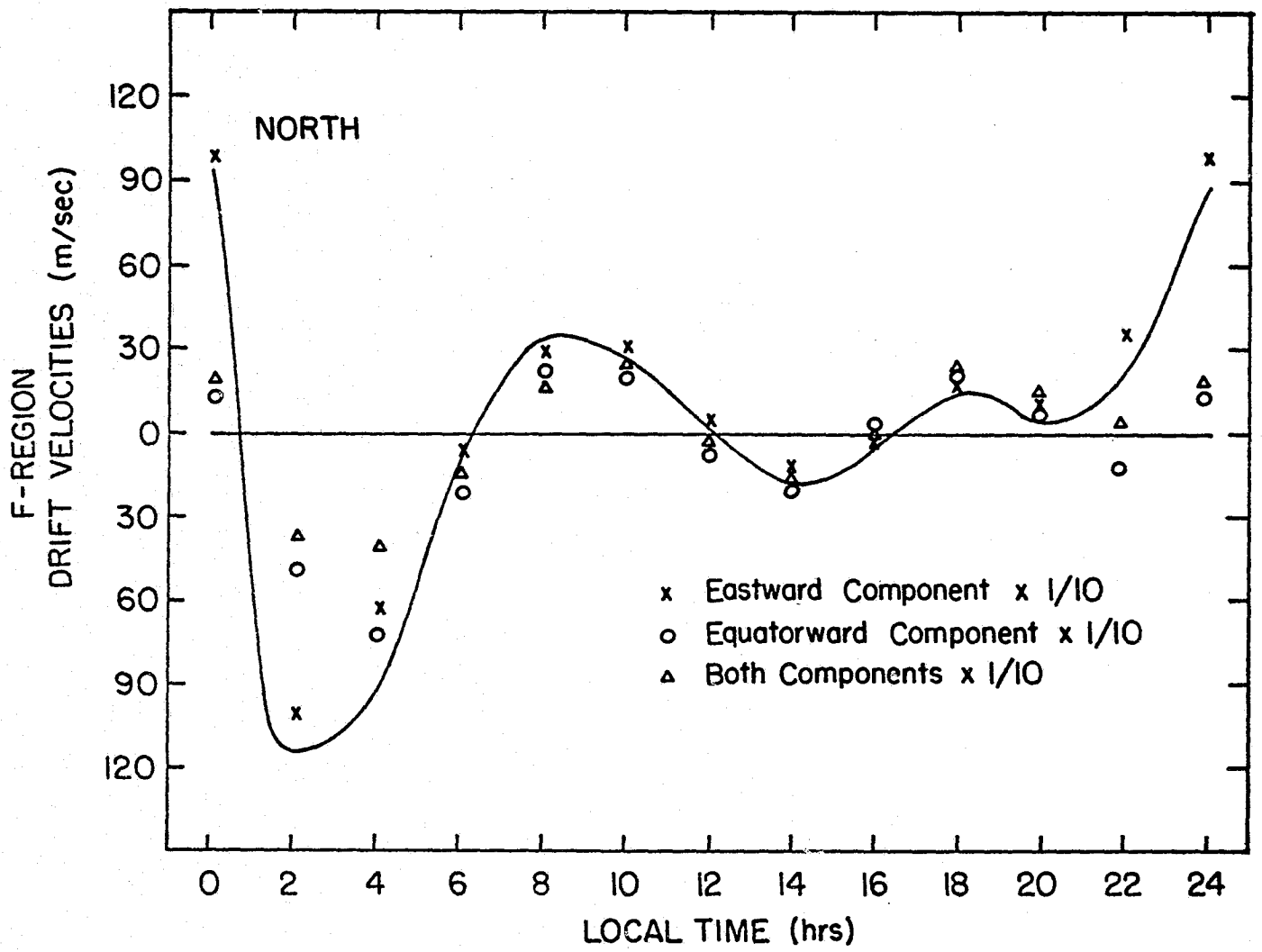

Figure 3.9.1 The effect of F-region wind changes. Northward drifts

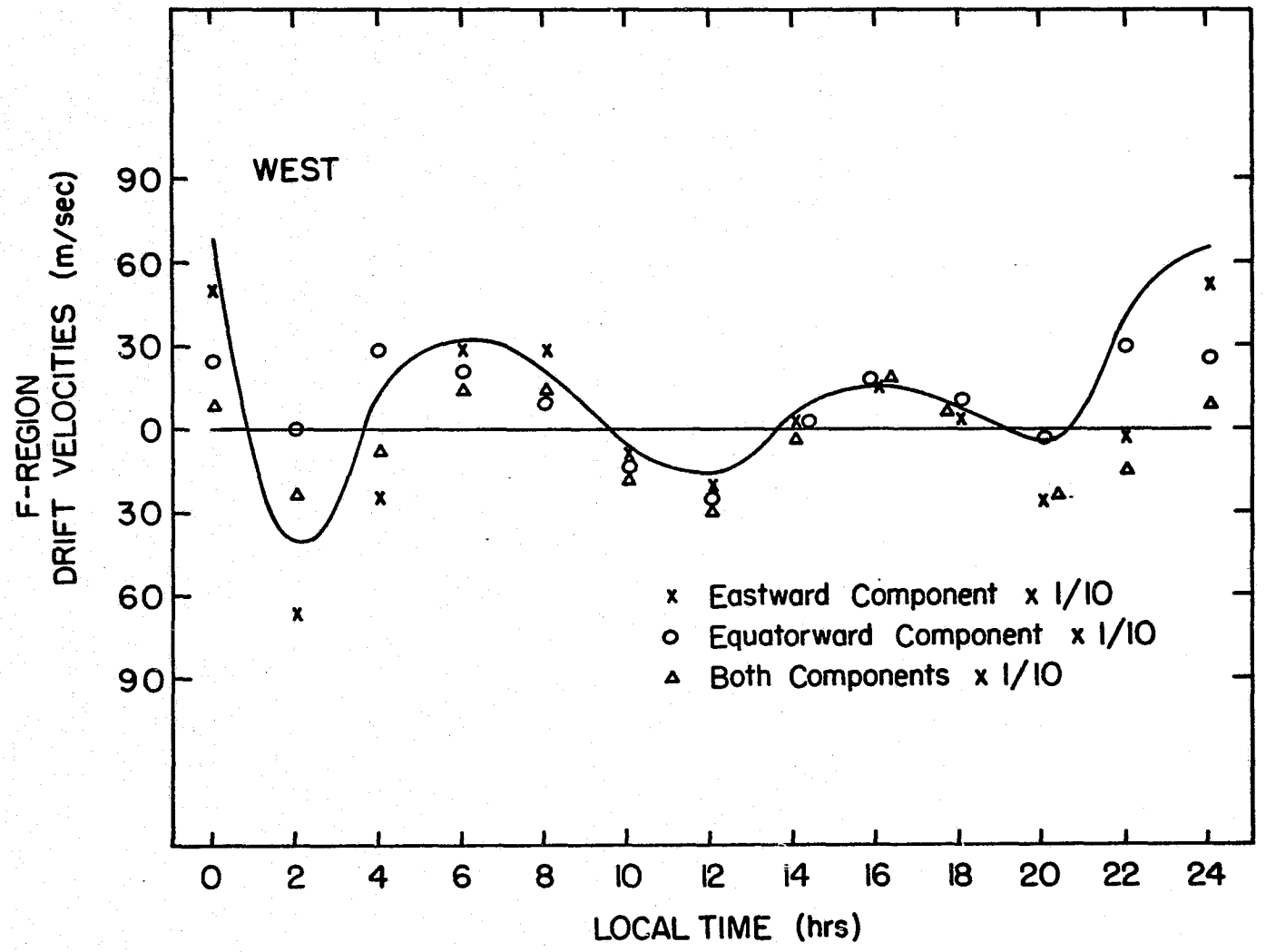

Figure 3.9.2 The effect of F-region wind changes. Westward drifts

that result when only the eastward component is reduced are represented by (x); when only the equatorward component is reduced, by (o) and when both components are reduced, the resulting drifts are represented by (Δ). The solid curve represents the results of Section 3.7 and is used for comparison.

The results show that during the daytime a large variation of the thermospheric winds causes only small variations in the drift velocities (not larger than 20 m/sec). During the night, however, particularly at 24, 2 and 4 L.T., when the wind magnitudes are normally large, the relative changes in the drifts, caused by the large reduction of the wind magnitudes, are also large. This shows that during the daytime the E-region dynamo is the dominant source for the electric field, as was deduced from measurements by Evans (1972), but that at night a large contribution comes from the F-region, as suggested by Rishbeth (1971).

3.10 Comparison with Other Models

The comparison of our calculations with the models of Stening and Matsushita, discussed in Chapter I, are shown in Figures 3.10.1 and 3.10.2, where the average Millstone Hill measurements are also shown.

It is apparent that over the whole 24-hour period the conjugate E-F Model compares better with the measurements than the other models. Essentially the Matsushita (1971) model fails to reproduce the southward drifts between 2 and 4 L.T. and the westward direction between 6 and 8 L.T. For the Stening model the overall comparison

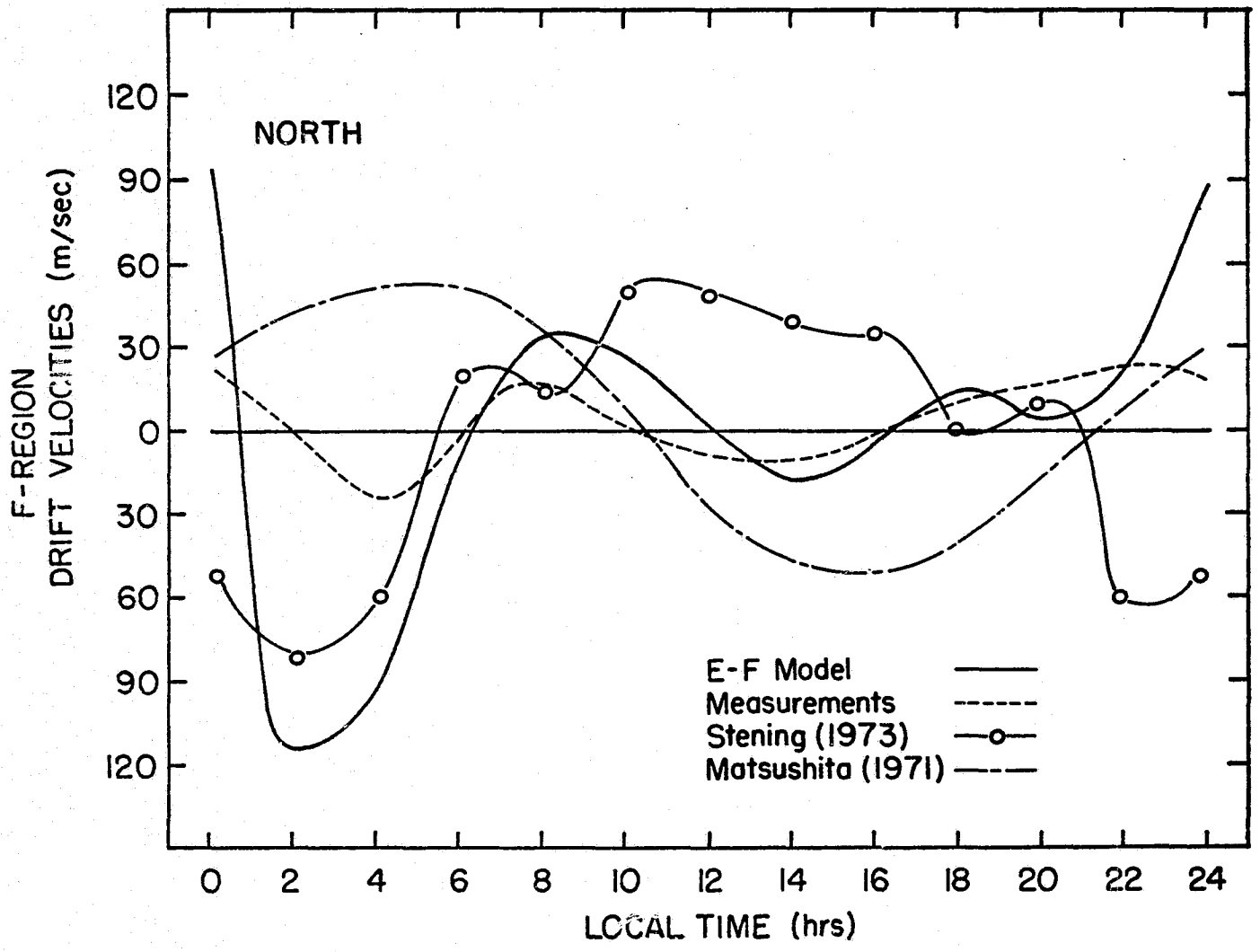

Figure 3.10.1 Comparison with other models. Northward drifts

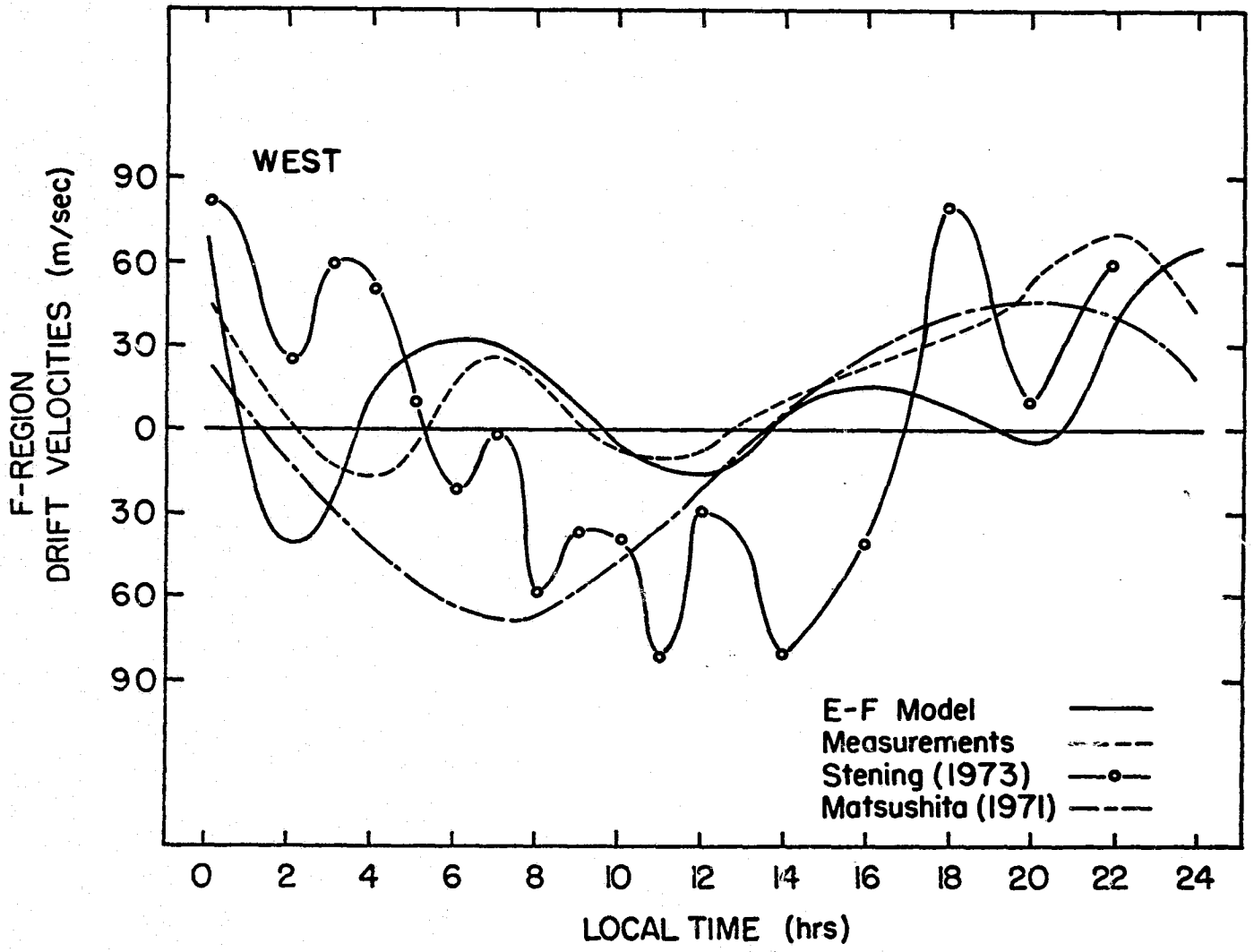

Figure 3.10.2 Comparison with other models. Westward drifts

with the measurements is not good for the westward component while the northward component is too large between 10 and 16 L. T.

3.11 Seasonal Variations

F-region drift velocities have been calculated for three days characteristic of different seasons, in order to predict seasonal variations. The only parameters changed are the day number, the conductivities and the thermospheric neutral winds. Day numbers used are D = 180 for summer, D = 1 for winter and D = 90 for equinox.

The results are shown in Figures 3.11.1 and 3.11.2. For the northward component, larger changes in magnitude and the first crossover occur during the early morning. This is also seen in the westward component although in this case the changes extend through the daytime period. For the northward drift component there is no appreciable difference in the zero velocity crossing times. The early morning southward magnitudes, however, show significant seasonal differences being largest in equinox and smallest in winter.

The westward component shows a reversal in direction between 2 and 4 L. T. In summer and equinox the westward magnitude increases in this time period but in winter it decreases. Between 10 and 14 L. T. the eastward drifts are larger in winter and equinox than in summer.

In summary, the seasonal variations predicted by these calculations are not simply increases or decreases in amplitude, or changes in phase but rather show complex variations that are different for both components and over different time periods.

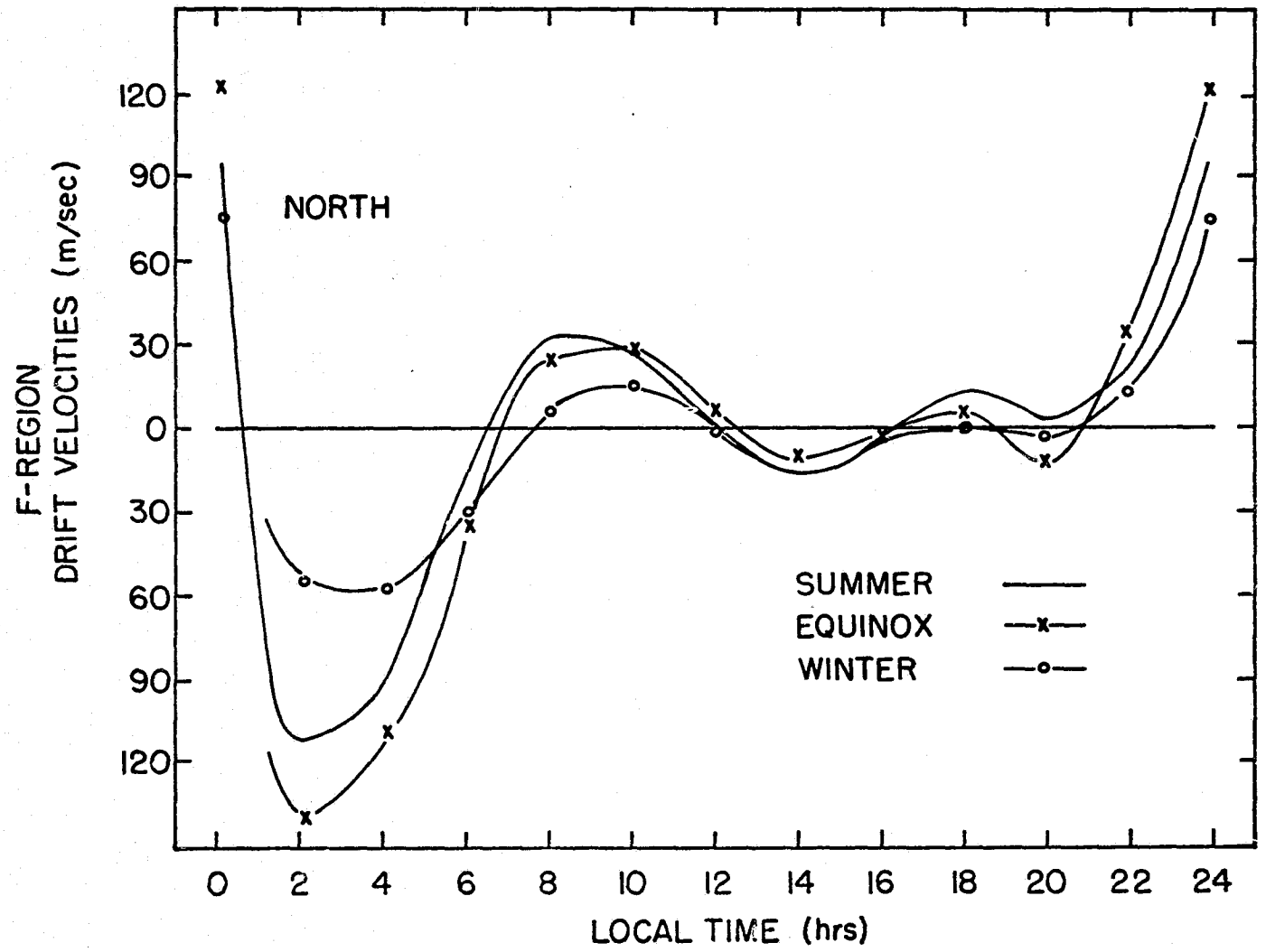

Figure 3.11.1 Seasonal variations for northward drifts

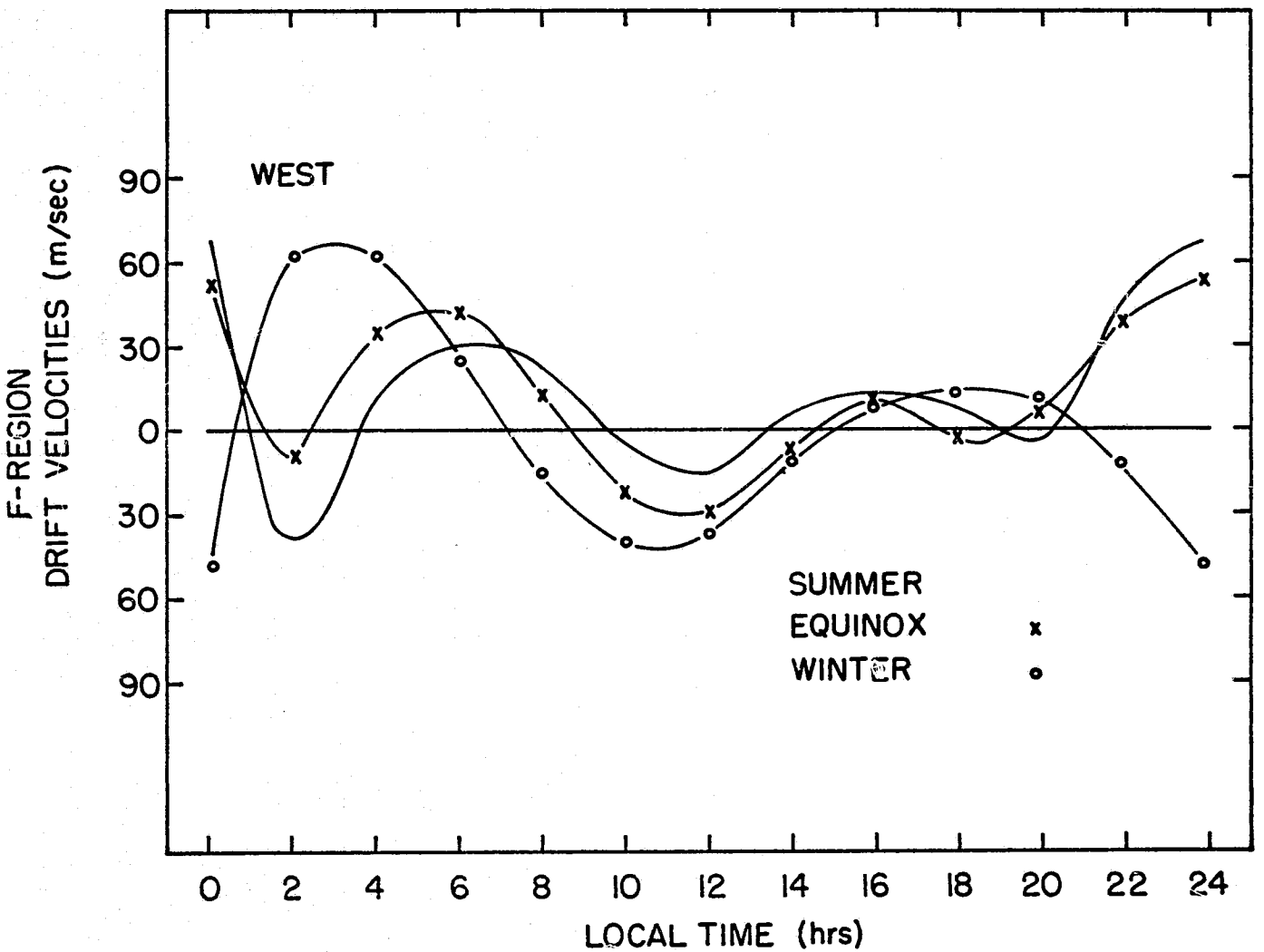

Figure 3.11.2 Seasonal variations for westward drifts

CHAPTER IV

CONCLUSIONS

4.1 The Daily Variation

Nighttime measurements of drift velocities perpendicular to the magnetic field lines have been made and incorporated with daytime results to study the daily variation. The velocity uncertainties are larger at night but can be minimized by choosing an adequate elevation angle.

A comprehensive electric field model has been developed that includes for both local and conjugate regions the effects of the E and F-region dynamos, magnetospheric sources and the ionospheric conductivities.

Calculations and measurements of the F-region drift velocities indicate that the dominance of the diurnal mode in the daily electric field variation is due to the combined effects of the much lower E-region conductivities at night and the larger thermospheric winds at that time. The importance of the semi-diurnal E-region neutral wind (2, 4) mode, determined by Salah et al. (1975) is confirmed for the daytime electric fields and the calculation of currents.

The average variation deduced from measurements and the calculations indicate larger magnitudes at night. From approximately 15 L. T. through midnight, the drift velocity is north and westward. It reverses to south and eastward at about 6 and 4 L. T. respectively, and then peaks at 8 and 7 L. T. The direction changes again at 12 L. T. for the northward component and at 9 L. T. for the westward, before reversing again around 15 L. T.

4.2 Seasonal, Magnetic Activity and Solar Cycle Variations

Seasonal variations are as follows: the northward drifts maximum seasonal changes occur between 2 and 4 L. T. in the early morning. Equinox magnitudes are the largest (140 m/sec), winter the smallest (60 m/sec), and summer in between (110 m/sec). The next largest change in the northward drifts occur between 8 and 10 L. T., again winter with the smallest magnitude, about half that of summer and equinox (30 m/sec).

For the westward drift component a direction reversal occurs in winter between 2 and 4 L. T. Between 10 and 12 L. T. the eastward peak is maximum in winter (40 m/sec), intermediate in equinox (30 m/sec) and minimum in summer (15 m/sec).

It is not known yet how the (2, 4) mode varies with season. It is likely, however, that a phase shift occurs as can be seen, for example, from the current variations. In the model calculations the (2, 4) mode was kept the same for different seasons and therefore the results probably underestimate seasonal effects. This is in agreement with the seasonal analysis of the measurements which suggest phase shifts of the order of two hours.

For the magnetic activity variations the data available can be divided into two major categories: days for which ΣK_p is less than 24 and those with ΣK_p larger than 24, corresponding respectively to relative quiet and perturbed conditions. On magnetic perturbed days the drifts deviate rather strongly from the quiet days average, especially around 13 L. T. for the northward and 18 L. T. for the westward component. The standard deviation from the mean under these conditions is larger by a factor of two to three.

If it is assumed that the tides amplitude decreases during higher solar fluxes, the calculations show that the northward peak around 8 L. T. shifts toward 10 L. T. and the westward peak from 6 L. T. to 5 L. T., while the daytime magnitudes decrease.

4.3 The Relative Contribution of Sources

The calculations confirm the earlier finding that the E-region dynamo dominates the daytime drifts. During the day and low magnetic activity it is practically the only process that contributes to the total observed field. Magnitudes of both north and west components are small compared to nighttime results (approximately 20 m/sec or 1 mV/m).

The F-region dynamo dominates during the night when the largest drift magnitudes occur. Its contribution for the south and westward components is largest between 0 and 2 L. T. (60 m/sec or 3 mV/m).

The convection electric field is also largest at night. The drifts add to the south and eastward components between 2 and 4 L. T. and to the westward component between 18 and 24 L. T. The convection component dominates the westward drifts between 18 and 22 L. T. (60 m/sec or 3 mV/m).

4.4 Contribution to Ionospheric Research

Some of the contributions of this work to ionospheric research are:

1) The extension of the electric field measurements at Millstone Hill to the nighttime periods to complete the study of the diurnal variation.

2) The confirmation of the importance of the semidiurnal E-region neutral wind (2, 4) mode, experimentally determined at Millstone Hill, for the calculation of currents and electric fields.

3) The use of independent measurements of currents to determine the convection electric field, for the study of magnetospheric-ionospheric coupling.

4) The development of an electric field model that includes for the first time in a consistent manner all of the geophysical processes affecting the midlatitude electric field and which allows quantitative predictions to be made. It has been shown that this model provides much better agreement with observations of the F-region drifts at Millstone Hill than previous models which did not include all of the mechanisms. This model is extremely useful in that it allows the relative importance of the various mechanisms to be studied under a variety of conditions.

4.5 Suggestions for Further Work

A comprehensive electric field model has been developed that depends on several input parameters. Further work is required to establish reliable values for the input parameters especially for the southern hemisphere. Some of the subjects that should be further investigated are:

1) The identification of the dominant E-region neutral wind tidal mode by Salah et al. (1975) has proven to be extremely

useful for the calculation of currents and drifts. It is therefore suggested that the same analysis including seasonal variations be made at the other incoherent-scatter facilities.

2) Thermospheric winds have recently been deduced from incoherent-scatter measurements at several locations. The results should be incorporated in model calculations using the more recent atmospheric models.

3) The calculation developed in Section 3.3 on the convection electric field should be extended to include magnetic activity, latitudinal and seasonal effects.

4) The data on drift velocity measurements presently available for Millstone Hill is unevenly distributed over local time and season. The number of measurements during winter and equinox should be increased and extended through the night.

The combined measurements of electric fields, electron densities, and currents are essential for the planned IMS studies. In this regard the installation at Millstone Hill of another steerable UHF antenna, as proposed by Evans, would be of considerable benefit to improve the nighttime and high L-value measurements.

For a comprehensive global analysis of electric fields it is essential to make simultaneous measurements at different locations through the coordination of incoherent-scatter stations with measurements of the neutral atmosphere and ionosphere over extended areas and of the magnetic fluctuations and measurements of the electric field using satellites.

APPENDIX A

CONDUCTIVITY FORMULAS

An electric field E_1 applied to a conductor of conductivity σ generates a current, whose density is given by

$$\vec{J} = \sigma \vec{E}_1 \qquad (A/m^2)$$

A current is also a charge in motion given by $\vec{J} = Nq \vec{V}$ such that

$$\vec{J} = \sigma \vec{E}_1 = Nq \vec{V} \qquad (A/m^2) \qquad (A.1)$$

where Nq is the density of free charges and $\vec{V}$ is the mean drift velocity of the free charge. Thus for the conductor, the conductivity relates the particle velocity $\vec{V}$ and the electrostatic field $\vec{E}_1$.

If the mean drift velocity is not changing with time, $\vec{E}_1$ and $\vec{V}$ are related by

$$q\vec{E}_1 - m\nu\vec{V} = 0 \qquad (A.2)$$

where ν is the mean collision frequency and ν^{-1} is short compared to the time interval involved.

Now let us consider the motion of charged particles in the ionosphere in order to obtain a conductivity term similar to Equation (A. 1). In the ionosphere we have a magnetic force acting on the particle and collisions with neutral particles which may also be moving. Equation (A. 2) is then modified to become

$$q\vec{E}_1 + q\vec{V} \times \vec{B} - m\nu (\vec{V} - \vec{U}) = 0 \qquad (A.3)$$

where $q\vec{E}_1$ is the force acting on the particle due to the presence of an electrostatic field $\vec{E}_1$, $q\vec{V} \times \vec{B}$ is the Lorentz force acting on the particle due to the motion of the particle with velocity $\vec{V}$ in a magnetic field $\vec{B}$ and $m\nu\ (\vec{V} - \vec{U})$ is a resisting force due to the collisions (at frequency ν) with neutral particles.

Our aim is to obtain a conductivity term for the ionosphere similar to the definition given in (A. 1) and then verify what $\vec{V}$ and $\vec{E}$ are. To do this let us rearrange (A. 3).

Eliminating the velocity $\vec{U}$ from Equation (A. 3) by substituting $\vec{v} = \vec{V} - \vec{U}$ which is the relative velocity of the charged particle with respect to the neutral particle velocity $\vec{U}$, we have

$$q\vec{E}_1 + q\vec{U} \times \vec{B} + q\vec{v} \times \vec{B} - m\nu\vec{v} = 0$$

but if $\vec{E} = \vec{E}_1 + \vec{U} \times \vec{B}$, called the total electric field, we have

$$q\vec{E} + q\vec{v} \times \vec{B} - m\nu\vec{v} = 0 \qquad \text{(A. 4)}$$

Thus Equation (A. 4) is similar to Equation (A. 2) and a σ can be defined as in Equation (A. 1) with the difference that in the relation for the ionosphere

$$\vec{J} = \sigma\vec{E} = Nq\vec{v} \qquad (A/m^2)$$

$\vec{v}$ is now a relative velocity and $\vec{E}$ is the summation of an electrostatic field $\vec{E}_1$ and a dynamo field $\vec{U} \times \vec{B}$. Since the current results from flow of both electrons and ions, we have

$$\vec{J} = \sigma\vec{E} = Nq\,(\vec{v}_i - \vec{v}_e) \qquad (A/m^2) \qquad \text{(A. 5)}$$

In order to find σ, let us choose a coordinate axis to determine the components of the $\vec{v}$. To simplify the definition of the conductivity a system is chosen in which z is parallel to $\vec{B}$ and $\vec{E}$ is in the xz plane. By inverting Equation (A. 4), the velocities are

$$v_x = \frac{E_x}{B} \frac{\nu\omega}{\nu^2 + \omega^2} \qquad v_y = - \frac{E_x}{B} \frac{\omega^2}{\nu^2 + \omega^2}$$

$$v_z = \frac{E_z}{B} \frac{\omega}{\nu} \tag{A. 6}$$

where $\omega = Bq/m$, is the gyro frequency.

Interpretation of Equation (A. 6) indicates that ionospheric currents are more prominent in the E-region. From Equation (A. 5) we know that the current is proportional to electron density N and to the difference in velocity between ions and electrons. Below the height $Z_e \simeq 80$ km where $\nu_e = |\omega_e|$, electrons and ions move with velocities $qE/m\nu$ in opposite directions but the electron density is very low suggesting a low current. Above a height $Z_i \simeq 140$ km where $\nu_i = \omega_i$ both particles move in the same direction perpendicular to $\vec{B}$, thus constituting no current. In the intermediate height range between Z_e and Z_i, only the electrons move with $\vec{E} \times \vec{B}/B^2$ whereas the ions remain almost stationary in comparison. In this height range the electron density is already appreciable and thus it is in this height interval that the currents are most prominent.

A remark about the velocities parallel to $\vec{B}$ must be made, because according to Equation (A. 6) electrons and ions move in

opposite directions along the magnetic field. However in writing Equation (A. 3) from which Equation (A. 6) was obtained gravity and pressure gradient were neglected and these terms play an important part at higher altitudes. Their effect is such that ions and electrons move together constituting plasma diffusion.

The velocities in Equation (A. 6) are substituted in Equation (A. 5) to give for the conductivities in $(\Omega m)^{-1}$

$$\sigma_1 = \frac{Nq}{B}\left(\frac{\nu_i \omega_i}{\nu_i^2 + \omega_i^2} + \frac{\nu_e \omega_e}{\nu_e^2 + \omega_e^2}\right)$$

$$\sigma_2 = \frac{Nq}{B}\left(\frac{\omega_e^2}{\nu_e^2 + \omega_e^2} - \frac{\omega_i^2}{\nu_i^2 + \omega_i^2}\right) \qquad \text{(A. 7)}$$

$$\sigma_o = \frac{Nq}{B}\left(\frac{\omega_i}{\nu_i} + \frac{\omega_e}{\nu_e}\right)$$

We have thus defined three conductivities: σ_o is in the direction of the component of the electric field parallel to B, σ_1 is in the direction of the component of the electric field perpendicular to B and σ_2 is in the direction perpendicular to both the electric and magnetic fields.

Each of the conductivities is directly proportional to the particle concentration and to mobility. The direct or longitudinal conductivity σ_o always exceeds σ_1 and σ_2, and is inversely proportional to the collision frequency. The Pedersen conductivity σ_1 depends on the ratio collision to gyro frequency, vanishing for very

small and very large collision frequencies and reaching a maximum when both frequencies are equal. The Hall conductivity σ_2 is directly related to the difference in mobilities of the positive and negative ions.

A combination of the conductivities σ_1 and σ_2 gives the Cowling conductivity σ_3, which is

$$\sigma_3 = (\sigma_1^2 + \sigma_2^2)/\sigma_1$$

The conductivities are all positive quantities; σ_1 and σ_o are the result of the sum of two positive numbers, and σ_2 is the difference between two positive numbers.

Generalizing the coordinate system to permit the inclusion of an E_y component the current densities will be related to the electric field by

$$\begin{bmatrix} J_x \\ J_y \\ J_z \end{bmatrix} = \begin{bmatrix} \sigma_1 & -\sigma_2 & 0 \\ \sigma_2 & \sigma_1 & 0 \\ 0 & 0 & \sigma_o \end{bmatrix} \begin{bmatrix} E_x \\ E_y \\ E_z \end{bmatrix} \qquad (A.8)$$

The Layer Conductivities

Due to the limited vertical extent of the conducting layer in the E-region, vertical currents are inhibited because the current cannot flow into the region of low conductivity. If the current has a vertical component, the electric charges will be stopped at the boundaries of the layer constituting polarization charges which act until the current flow is horizontal. We thus feel it necessary to change again the

coordinate axis such that z points vertically (x is in the magnetic south and y in the magnetic east direction). The dip angle I is the angle between B and the horizontal plane, positive in the northern hemisphere. The transformation of axes then leads to the tensor conductivity

$$\sigma = \begin{bmatrix} \sigma_1 \sin^2 I + \sigma_o \cos^2 I & \sigma_2 \sin I & (\sigma_o - \sigma_1) \sin I \cos I \\ -\sigma_2 \sin I & \sigma_1 & \sigma_2 \cos I \\ (\sigma_o - \sigma_1) \sin I \cos I & -\sigma_2 \cos I & \sigma_1 \cos^2 I + \sigma_o \sin^2 I \end{bmatrix} \tag{A.9}$$

Imposing the condition of zero vertical current in Equation (A.9), the vertical electric field can be eliminated and σ can be replaced by a 2 x 2 tensor, and for right handed x, y axes,

$$\begin{bmatrix} J_x \\ J_y \end{bmatrix} = \begin{bmatrix} \sigma_{xx} & \sigma_{xy} \\ \sigma_{yx} & \sigma_{yy} \end{bmatrix} \begin{bmatrix} E_x \\ E_y \end{bmatrix} \tag{A.10}$$

and where the layer conductivities are given by

$$\sigma_{xx} = \frac{\sigma_o \sigma_1}{\sigma_1 \cos^2 I + \sigma_o \sin^2 I}$$

$$\sigma_{xy} = -\sigma_{yx} = \frac{\sigma_o \sigma_2 \sin I}{\sigma_1 \cos^2 I + \sigma_o \sin^2 I} \qquad \text{(A.11)}$$

$$\sigma_{yy} = \frac{\sigma_1 \sigma_o \sin^2 I + (\sigma_1^2 + \sigma_2^2) \cos^2 I}{\sigma_1 \cos^2 I + \sigma_o \sin^2 I}$$

The last parameters may be simplified in two regions of the ionosphere namely in the middle ionosphere where we already have $\sigma_o >> \sigma_1$ and near the magnetic equator where $I = 0$. Thus, at high and middle latitudes

$$\sigma_{xx} \simeq \frac{\sigma_1}{\sin^2 I}$$

$$\sigma_{xy} \simeq \frac{\sigma_2}{\sin I}$$

$$\sigma_{yy} \simeq \sigma_1$$

and at the equator

$$\sigma_{xx} = \sigma_o$$

$$\sigma_{xy} = 0$$

$$\sigma_{yy} = (\sigma_1^2 + \sigma_2^2)\,\sigma_1 = \sigma_3$$

where

$$\sin I = \frac{2 \cos \theta}{(1 + 3 \cos^2 \theta)^{1/2}}$$

and θ is the colatitude.

Height Integrated Conductivities

The magnetic variations ΔB associated with the ionospheric current density J are proportional to the integral with respect to height of the current density. In other words the magnetic variations are proportional to the horizontal linear current densities I. Integrating Equation (A.9), assuming E_x and E_y do not vary with height, we thus have

$$\begin{bmatrix} I_x \\ \\ I_y \end{bmatrix} = \begin{bmatrix} \Sigma_{xx} & \Sigma_{xy} \\ \\ \Sigma_{yx} & \Sigma_{yy} \end{bmatrix} \begin{bmatrix} E_x \\ \\ E_y \end{bmatrix} \quad \text{(A/m)}$$

The height integrated conductivities are found by integrating with height

$$\Sigma_{ij} = \int_{z_1}^{z_2} \sigma_{ij}\, dz$$

and can then be used in the current equation.

APPENDIX B

DRIFT VELOCITY UNCERTAINTIES AND ELEVATION ANGLE OPTIMIZATION

In general the east-west and north-south components of drift velocity are deduced from measurements made in different directions and at different elevation angles. Thus the velocity uncertainty in the resolved direction is in general a non-linear function of the radar line of sight velocity uncertainty and the elevation angle.

The statistical uncertainty in the line-of-sight measured velocity is given by:

$$\Delta v_m = \frac{v_{TH}}{\sqrt{2n}} \quad (S/N)^{-1} \qquad (B.1)$$

where v_{TH} is the thermal mean speed of the ions, n is the total number of pulses, and S/N is the signal-to-noise ratio. This expression is valid for S/N values less than unity.

The lowest S/N value which can still be used to evaluate the drift velocity from the doppler spectrum is 0.1, giving

$$\Delta v_{m\ max} = \frac{10^3 \times 10}{\sqrt{2n}}$$

For the D-mode operation, the integration time during the day is in general 16 minutes, and the pulse length is 1 msec with an interpulse period of 24 msec, implying a pulse repetition frequency of 40 pps. The total number of independent measurements in this case is $n = 3.84 \times 10^4$ which gives

D mode; τ = 1 msec; P.R.F. = 40 pps; S/N = 0.1

$$\Delta v_{m\ max} = \frac{10^4}{\sqrt{7.68 \times 10^2}} = 36 \text{ m/sec}$$

For the measurement of the vertical velocity of F-region heights the B and C modes are used through the UHF (λ = 68 cm) vertical antenna. The B mode uses, in general, a 0.5 msec pulse length, an interpulse period of 13 msec and an integration length of 4 minutes. This implies in a pulse repetition frequency (PRF) of 74 pps and a total number of pulses $n = 1.775 \times 10^4$. For low electron density (foF2 = 2 MHz) and at night, i.e. for the worst conditions, the signal-to-noise (S/N) ratio is about 1.0. The maximum uncertainty in the vertical measured velocity v_z is thus

B mode; τ = 0.5 msec; P.R.F. = 74 pps; S/N = 1.0
(night, low electron density)

$$\Delta v_{z\ max} = \frac{10^3 \times 1.0}{(35.5 \times 10^3)^{1/2}} = \frac{10}{1.8} = 5.3 \text{ m/sec}$$

The horizontal components of the drift velocity vector are deduced from the measured values v_m and v_z, where v_m is the measured velocity at elevation angle θ and v_z is the measured vertical velocity. The eastward velocity, v_E, for example, can be resolved according to Figure B.1

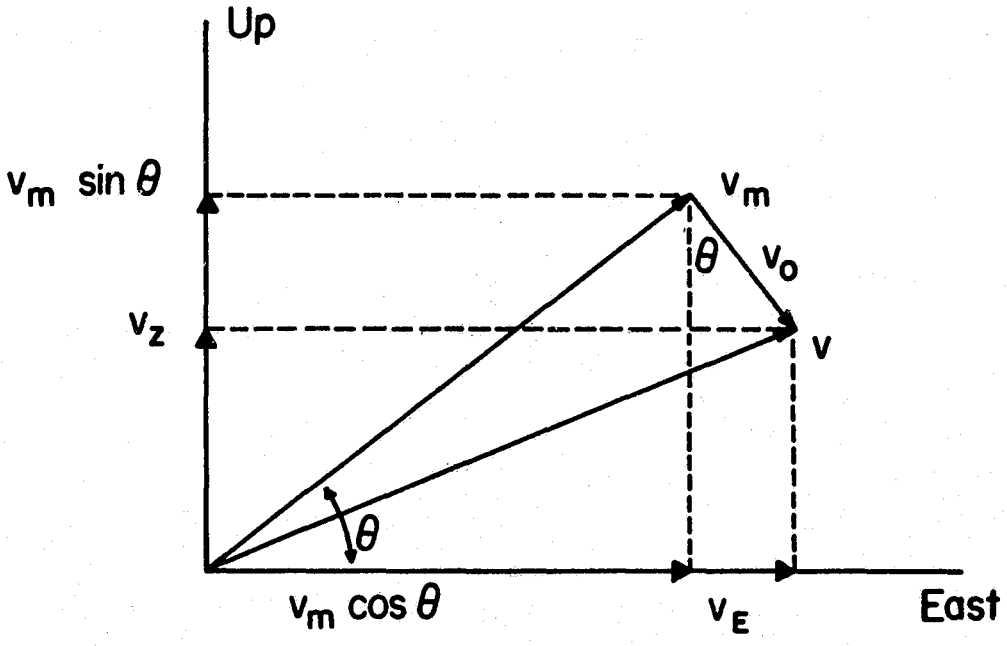

Figure B.1 Geometry for the calculation of uncertainties

$$v_E = v_m \cos\theta + v_o \sin\theta$$

$$= v_m \cos\theta + (v_m \sin\theta - v_z) \frac{\sin\theta}{\cos\theta}$$

$$= v_m \cos\theta + v_m \frac{\sin^2\theta}{\cos\theta} - \tan\theta\, v_z$$

$$= v_m/\cos\theta - v_z \tan\theta$$

The rms uncertainty in v_E, thus becomes

$$\Delta v_E = \sqrt{\left(\frac{\Delta v_m}{\cos\theta}\right)^2 + (\Delta v_z \tan\theta)^2} \qquad \text{(B. 2)}$$

The signal-to-noise ratio, S/N, is inversely proportional to the square of the range R, and with K_1 the radar constant,

$$S/N = \frac{K_1}{R^2} ,$$

and the height h of the scattering volume and elevation angle θ determine its range by

$$R \sin\theta = h .$$

If the other parameters remain constant, the S/N ratio varies with θ as

$$S/N = K_2 \sin^2\theta , \qquad K_2 = K_1/h^2$$

It was seen in Equation (B. 1) that

$$\Delta v_m = K_3 (S/N)^{-1}$$

with

$$K_3 = \frac{v_{TH}}{\sqrt{2n}} = 3.6$$

and thus

$$\Delta v_m = \frac{K}{\sin^2 \theta} \tag{B.3}$$

where $K = K_3/K_2$

and substituting K_3 and K_2

$$K = \frac{10^3}{\sqrt{2n}} \frac{h^2}{K_1} = \frac{3.6\, h^2}{K_1} \tag{B.4}$$

Substituting Equation (B.3) in (B.2) gives

$$\Delta v_E = \sqrt{\left(\frac{K}{\cos\theta \sin^2 \theta}\right)^2 + (\Delta v_z \tan \theta)^2} \tag{B.5}$$

This equation depends on the scattering height h, the number of total pulses n, and the radar parameters included in K_1, primarily the density but also the temperature which affects v_{TH}.

The uncertainty Δv_E can be analyzed as a function of θ, the elevation angle, and the parameters Δv_z and K. Considering the worst uncertainty in Δv_z previously calculated to be 5.3 m/sec, Equation (B.5) can be evaluated as a function of K for different θ but the extreme values are excluded because for $\theta = 0$, $v_E = v_m$ and for $\theta = 90^\circ$, the only velocity determined is v_z. These values are tabulated in Table B.1.

Table B.1 Calculation of Uncertainty Parameters

θ^o	$(\Delta v_E)^2$ in $(m/sec)^2$
15	$239K^2 + 2.0$
18	$123K^2 + 3.0$
25	$38K^2 + 6.0$
30	$21K^2 + 9.0$
35	$14K^2 + 14.0$
45	$8K^2 + 28.0$
60	$7K^2 + 84.0$
75	$17K^2 + 385.0$

In Table B. 1 it is seen that Δv_E is almost independent of the uncertainty in vertical velocity for large ranges, i. e. elevation angles below 35^o, and $K \geq 1$. As the elevation angle increases, however, the vertical velocity uncertainty component varying with tan θ becomes increasingly important. To keep Δv_E at a minimum, different values of K give different values of θ. To find the elevation angles θ at which a minimum in Δv_E is achieved, we have to consider the range over which K varies, according to Equation (B. 4), by using measured values in S/N, h_{max} and N_{max}.

Let us consider the data taken on 27 February 1973 and 30 June 1972 as reference, for the calculation of the radar constant K_1. The exact calculation of this constant (K_1) is somewhat difficult because it depends on the product of electron density and the overall radar efficiency, and the measured values of S/N do not, in general, correspond to the level where foF2 is given. However, we consider the mean S/N value to correspond to the peaks of the frequency spectrum at the delay times (ranges) closest to the peak of the layer.

For 27 February 1973, at 14:13, the peak of the layer was at 270 km, with foF2 = 6. 9 MHz (6×10^5 cm^{-3}); with an elevation angle of 18^o; this corresponds to a range of 875 km. The S/N value as defined above was 0. 235, thus

$$K_1 = 0.235 \times (875 \times 10^3)^2 = 18 \times 10^{10}$$

To confirm this value we check the data at 16:10, and at another day at different times referring to foF2 = 6. 9 MHz. The results are shown in Table B. 2.

Table B. 2 Calculation of Radar Constant

Date	Local Time	S/N	foF2 (MHz)	Range (km)	K_1
27 Feb 1973	14:13	0.235	6.9	875	18×10^{10}
27 Feb 1973	16:10	0.250	6.7	860	18×10^{10}
30 June 1972	17:35	0.150	7.7	985	11.7×10^{10}
30 June 1972	13:08	0.103	6.4	985	11.6×10^{10}
30 June 1972	15:01	0.110	6.45	985	12.3×10^{10}

We thus conclude that the radar constant K_1 varies from day to day but is relatively constant on a given day. To calculate the parameter K we use

$$K_1 = 15 \times 10^{10}, \text{ for foF2} = 6.9 \text{ MHz}$$

as a representative value. Thus limiting values for K with

$$N_{max} = 10^6 \text{ cm}^{-3} \text{ (foF2} = 9 \text{ MHz)}, \quad h_{max} = 220 \text{ km}$$

will be

$$K = \frac{3.6 \times (220\ 10^3)^2 \quad 6.9^2}{15 \times 10^{10} \times 9^2} = 0.7$$

and for typical night conditions where

$$h_{max} = 340 \text{ km}, \quad N_{max} = 10^5 \text{ cm}^{-3} \text{ (foF2} = 2.8 \times 10^6 \text{ Hz)}$$

$$K = \frac{3.6 \times (340)^2 \quad 10^6 \quad (6.9)^2}{15 \times 10^{10} \quad (2.8)^2} = 17$$

For the range in K of 0.5 to 20 the corresponding Δv_E values are shown in Table B.3 for τ = 1 msec, integration time 16 minutes, as a function of θ. The height resolution is also shown.

This table indicates clearly that for higher densities and lower heights of reflection, the optimum elevation angle is close to 30° but does not vary much between say 25 and 35°. For nighttime conditions and/or when densities are lower and the layer is higher, the optimum elevation angle increases, being close to 60° at K = 20. The height resolution may be reduced by using a pulse length τ = 0.5 msec and

Table B.3 Drift Velocity Uncertainties
Δv_E (m/sec)

	K							
θ^o	0.5	1	2	5	10	15	20	Δh (km)
15	8	16	31	77	155	232	310	39
18	6	11	22	55	111	166	220	46
25	4	7	13	31	61	92	123	63
30	4	5	10	23	46	69	92	75
35	4	5	8	19	37	56	75	86
45	5	6	8	15	29	43	57	106
60	9	9	11	16	28	41	53	130
75	20	20	21	28	45	62	85	145

increasing the integration time to 32 minutes. Furthermore, by assigning the value 15×10^{10} to the radar constant K_1 (foF2 = 6.9) as a mean value, the uncertainty constant K may be expressed by

$$K = 11.4 \times 10^{-4} \left(\frac{h_{max}}{foF2}\right)^2 \qquad (B.6)$$

where h_{max} is the height of the F2 peak in km, and foF2 is expressed in MHz.

In practice we have to assure that the S/N value is greater than 0.1. This implies a minimum in K_1 at $\theta = 60^{\circ}$.

$$K_1 = 0.1 \times (3.9)^2 \times 10^{10} = 1.54 \times 10^{10}$$

which corresponds to $foF2_{min} \cong 2.2$ MHz, and

$$K = \frac{3.6 \times 11.5}{1.54} \cong 27$$

Thus at $\theta = 60^{\circ}$, K less than 27 assures a signal-to-noise greater than 0.1 (h_{max} = 340 km).

For $\theta = 45^{\circ}$ we would have

$$K_1 = 0.1 \times (4.8)^2 \times 10^{10} = 2.3 \times 10^{10}$$

which corresponds to $foF2_{min} \cong 2.7$ MHz and

$$K = \frac{3.6 \times 11.5}{2.3} = 18$$

and thus for $\theta = 45^{0}$, K less than 18 assures us an S/N value greater than 0.1 (for $h_{max} \leq 340$ km).

This can be checked with measured values on 27 February 1973. At 20:54 local time, the peak was at about 365 km and with $\theta = 45^{\circ}$, the largest K admissible (i.e. S/N= 0.1, $K_1 = 2.3 \times 10^{10}$) is

$$K = 3.6 \times \frac{(3.65)^2}{2.3} = 21$$

Using Equation (B.6) for K, with foF2 = 2.5 MHz

$$K = 11.4 \times 10^{-4} \left(\frac{3.65}{2.5}\right)^2 \times 10^4 = 24$$

and we would thus be very close to the threshold with S/N close to or even less than 0.1. Checking the data for this day confirms the prediction by showing an S/N value of 0.1 at a time delay of 3.5 msec (R = 525 km).

Therefore it is possible to make nighttime F-region drift velocity measurements at Millstone Hill.

APPENDIX C

DESCRIPTION OF THE F-REGION DRIFT VELOCITY CALCULATION

Figure C. 1 shows the basic flow chart diagram describing the drift velocity calculations. Block 1 initializes the program with the definition of basic constants like the inclination angle, day number, declination, earth's radius, etc. In block 2 the northern latitude and local standard time are defined. Blocks 3, 8, 11 and 16 are memo variables to direct the flow to the right loop. In block 4 the neutral parameters are calculated and in block 5 the conductivities. In block 7 the height integrated layer conductivities are determined after which the southern latitude is defined and again the flow goes through blocks 4 and 5 to find the southern conductivities. In block 12 the eastward winds are defined and consequently the voltage generators acting in the north-south direction. Thus we can now find the loop currents for the north-south direction (block 13) from which the northward E-region current is found. With the equatorward winds defined (block 17) again the loop currents are calculated, this time for the east-west direction and the eastward current (block 18) is found. Given the currents and conductivities the Hall generators can be found (block 19) and finally the electric field and F-region drifts (block 20) after which a new local time is defined and the process may repeat itself. The basic sub-programs used are the CIRA (1972) model for the neutral properties and the Ching and Chiu (1973) model for the calculation of electron densities. The basic assumptions on these models and the input parameters are given in Section 3.6. Following is a listing of the main program.

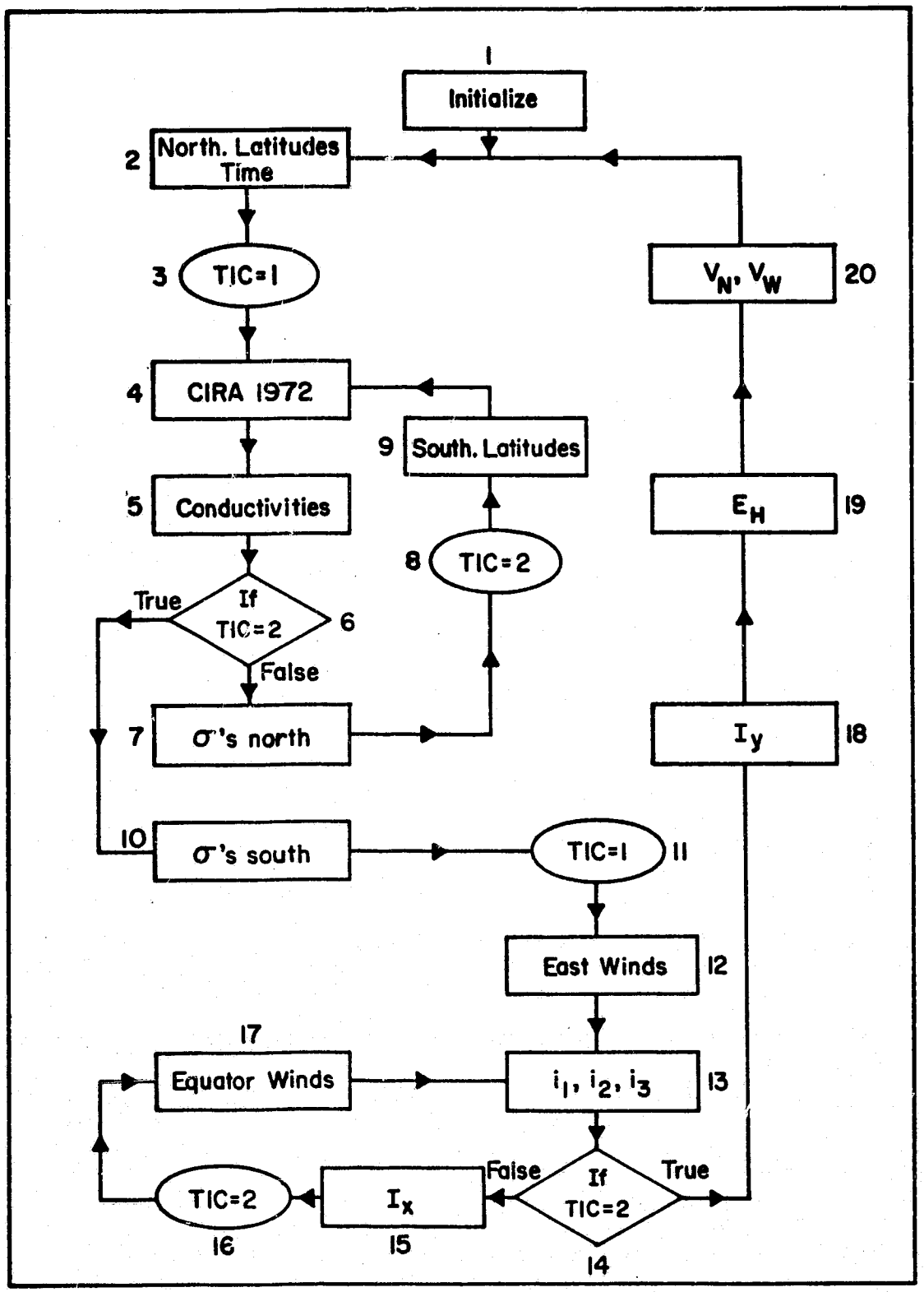

Figure C.1 Flow chart diagram for the conjugate E-F model

```
// EXEC FWCLG,PARM=NOSOURCE
//SYSIN DD *
C    ++++++++
C    ++++++++ THIS IS A PROGRAM TO CALCULATE DRIFT VELOCITIES
      X++++++++
C    CONDUCTIVITIES AND HEIGHT INTEGRATED CONDUCTIVITIES IN
      XTHE
C    IONOSPHERE. CIRA 1972 IS USED FOR THE NEUTRAL MODEL,CHI
      XNG
C    AND CHIU MODEL FOR ELECTRON DENSITIES.  MKS UNITS.
C    CREATED JUNE 75 BY V. KIRCHHOFF.
       DIMENSION QI(3),UEN(30),UEQN(30),TEN(30),TEQN(30),UES
      X(30),
      *UEQS(30),TES(30),TEQS(30)
       COMMON/JAC/ALAT,AKP,DAYNO,AHT,AF107,AFQ107,JA,TIME(10
      X0),RO1(350),H
      *F
       COMMON/ARRAY1/NN(5,350),TN(350),TL,RHO(350),G(350)
       COMMON HN(100),AN(100),A(100),MDEG,NPTS
       COMMON/ELAY/RE,PI,BLAT,HEMAX,HE,ENMAX
       REAL B(200),H(200),WI(200),WE(200),ANIUIN(200),ANIUEN
      X(200),
      *ANE(200),SIGPAR(200),SIGPED(200),SIGHAL(200),ATN(10),
      XARO(10)
      *,T(200),R(200),ZE(200)
C
C
C    LAST HEIGHT FOR NEUTRAL MODEL CALCULATIONS(AHT)
       AHT=910.
       PI=3.141593
       RE=6356.766*1.E 03
       Q=1.6*1.E-19
       AMI=16./6*1.E-26
       AME=9.11*1.E-31
       BE=5.*1.E-05
       DEC=-15.*PI/180.
       AINC=72.*PI/180.
       READ(5,2) DAYNO, AKPSUM,AF107,AFQ107,AR
     2 FORMAT(5F10.2)
       WRITE(6,3) DAYNO
       WRITE(6,4) AKPSUM
       WRITE(6, 5) AF107,AFQ107,AR
     5 FORMAT(' ',15X,'SOLAR FLUX,S.F.AVER.,SUNSP.NUMBER',3F
      X10.2,//)
     4 FORMAT(' ',30X,'KP(SUM) IS ', F10.2)
     3 FORMAT('1',30X,' DAY NUMBER IS', F10.2)
C
       AKP=AKPSUM/8.
C    ATN IS NEUTRAL TEMPERATURE FROM 90 TO 120 KM
C    ARO IS NEUTRAL DENSITY FROM 90 TO 120 KM
       READ(5,8)(ATN(I),I=1,7)
       READ(5,9)(ARO(I),I=1,7)
    8  FORMAT(7F10.2)
    9  FORMAT(7E10.3)
```

```
C    NEUTRAL THERMOSPH. WINDS INPUT,EVERY 2 HOURS, BEGIN AT
      X2.
       READ(5,6)(UEN(I),I=1,12)
       READ(5,6)(UEQN(I),I=1,12)
       READ(5,6)(UES(I),I=1,12)
       READ(5,6)(UEQS(I),I=1,12)
    6  FORMAT(7F10.2/5F10.2)
C    DEFINITION OF SALAH'S NEUTRAL E-REGION WINDS,EVERY 2 HO
      XURS,BEGIN AT
C    2 LOCAL STANDARD TIME.
       DO 112 I=1,12
       TEN(I)=25.*COS(PI/6.*2.*I-PI/2.)
       TEQN(I)=25.*COS(PI/6.*2.*I-PI)
       TES(I)=20.*COS(PI/6.*2.*I-PI/2.)
       TEQS(I)=20.*COS(PI/6.*2.*I-PI)
  112 CONTINUE
       JA=1
   13  CONTINUE
       ALAT=42.6
       BLAT=ALAT*PI/180.
       CLAT=54.*PI/180.
       BBLAT=BLAT
       TIME(JA)=2.*JA
       IF(TIME(JA).GT.24.)GO TO 100
       PHI=TIME(JA)*2.*PI/24.
       ANTIME=(DAYNO+15)/30.4
C    WINDS FROM GEOGRAPHIC TO MAGNETIC COORDINATES.
       DO 111 I=1,12
       UXN=UEN(I)*COS(DEC)+UEQN(I)*SIN(DEC)
       UYN=UEN(I)*SIN(DEC)-UEQN(I)*COS(DEC)
       UEN(I)=UXN
       UEQN(I)=-UYN
       UXS=UES(I)*COS(DEC)-UEQS(I)*SIN(DEC)
       UYS=UES(I)*SIN(DEC)+UEQS(I)*COS(DEC)
       UES(I)=UXS
       UEQS(I)=UYS
       TXN=TEN(I)*COS(DEC)+TEQN(I)*SIN(DEC)
       TYN=TEN(I)*SIN(DEC)-TEQN(I)*COS(DEC)
       TEN(I)=TXN
       TEQN(I)=-TYN
       TXS=TES(I)*COS(DEC)-TEQS(I)*SIN(DEC)
       TYS=TES(I)*SIN(DEC)+TEQS(I)*COS(DEC)
       TES(I)=TXS
       TEQS(I)=TYS
  111 CONTINUE
       TIC=1.
  101  CALL JAC71
C
C    TO REARRANGE INDICES OF NEUTRAL PARAMETERS
       DO 11 I=1,158
       J=I*2
       T(I)=TN(J)
       R(I)=RO1(J)
    11 CONTINUE
```

```
      DO 12 I=1,158
      J=I+7
      TN(J)=T(I)
      RO1(J)=R(I)
   12 CONTINUE
      DO 15 I=1,7
      TN(I)=ATN(I)
      RO1(I)=ARO(I)
   15 CONTINUE
C
C
      Z=1.
      CALL IONDEN(QTOT,QI,Z,AR,CLAT,BBLAT,PHI,ANTIME)
      DO 17 I=1,83
      H(I)=(90.+(I-1)*5.)
      Z=H(I)
      CALL NEWZ(QTOT,Z)
      ANE(I)=QTOT*1.E 11
   17 CONTINUE
      DO 7 I=1,83
      B(I)=(3.1*1.E-05*SQRT(1.+3.*(SIN(BLAT))**2))/((1.+H(I
     X)/RE)**3)
      WI(I)=B(I)*Q/AMI
      WE(I)=B(I)*Q/AME
      ANIUIN(I)=7.5*1.E-16*RO1(I)
      ANIUEN(I)=5.4*1.E-16*TN(I)**(.5)*RO1(I)+
     *(59.+4.18*ALOG10(TN(I)**3/ANE(I)))*1.E-06*TN(I)**(-1.
     X5)*ANE(I)
      S1=WI(I)/(WI(I)**2+ANIUIN(I)**2)
      S2=WE(I)/(WE(I)**2+ANIUEN(I)**2)
      SIGPAR(I)=ANE(I)*Q**2/(AME*ANIUEN(I))
      SIGPED(I)=ANE(I)*Q*(S1*ANIUIN(I)+S2*ANIUEN(I))/B(I)
      SIGHAL(I)=ANE(I)*Q*(1./(1.+(WI(I)/ANIUIN(I))**2))/B(I
     X)
    7 CONTINUE
C
C  CALCULATE HT INTEG. PED.(SIGE1) AND HAL(SIGE2) CONDUCT.(
     X90-150 KM)
      SIGE1=(SIGPED(1)+SIGPED(13))*5.*1.E 03/2.
      SIGE2=(SIGHAL(1)+SIGHAL(13))*5.*1.E 03/2.
      DO 19 I=2,12
      SIGE1=SIGE1+SIGPED(I)*5.*1.E 03
      SIGE2=SIGE2+SIGHAL(I)*5.*1.E 03
   19 CONTINUE
C  CALCULATE FOR F REGION
      SIGF1=(SIGPED(13)+SIGPED(83))*5.*1.E 03/2.
      SIGF2=(SIGHAL(13)+SIGHAL(83))*5.*1.E 03/2.
      DO 21 I=14,82
      SIGF1=SIGF1+SIGPED(I)*5.*1.E 03
      SIGF2=SIGF2+SIGHAL(I)*5.*1.E 03
   21 CONTINUE
      IF (TIC.EQ.2.)GO TO 121
      RFN=1./SIGF1
      S1N=1.1*SIGE1
```

```
      S2N=1.05*SIGE2
      S4N=SIGE1
      ALAT=-66.
      BLAT=ALAT*PI/180.
      CLAT=-54.*PI/180.
      BBLAT=BLAT
      TIC=2.
      GO TO 101
  121 CONTINUE
      RFS=1./SIGF1
      S1S=+1.1*SIGE1
      S2S=-1.05*SIGE2
      S4S=SIGE1
      N=1
      EHNN=0.
      EHNS=0.
      EHEN=0.
      EHES=0.
  120 CONTINUE
C
      TIC=1.
      REN=1./S4N
      RES=1./S4S
      EHN=EHNN
      EHS=EHNS
      VFN=UEN(JA)*BE*COS(PI/2.-AINC)
      VEN=TEN(JA)*BE*COS(PI/2.-AINC)
      VFS=-UES(JA)*BE*COS(PI/2.-AINC)
      VES=-TES(JA)*BE*COS(PI/2.-AINC)
   30 DEL=(REN+RFN)*(RFS+RFN)*(RFS+RES)-RFN*RFN*(RFS+RES)-
     *RFS*RFS*(REN+RFN)
      AN1=(VFN-VEN-EHN)*(RFS+RFN)*(RFS+RES)+(VFS-VFN)*RFN*(
     XRFS
     *+RES)+(EHS+VES-VFS)*RFN*RFS-RFS*RFS*(VFN-VEN-EHN)
      AN2=(REN+RFN)*(VFS-VFN)*(RFS+RES)+
     *(VFN-VEN-EHN)*RFN*(RFS+RES)+
     *RFS*(EHS+VES-VFS)*(REN+RFN)
      AN3=(REN+RFN)*(RFS+RFN)*(EHS+VES-VFS)+
     *RFN*RFS*(VFN-VEN-EHN)-
     *RFN*RFN*(EHS+VES-VFS)+
     *RFS*(VFS-VFN)*(REN+RFN)
      AI1=AN1/DEL
      AI2=AN2/DEL
      AI3=AN3/DEL
      IF(TIC.EQ.2.)GO TO 40
      AINN=-AI1
      AINS=AI3
      TIC=2.
      REN=1./S1N
      RES=1./S1S
      EHN=EHEN
      EHS=EHES
      VFN=UEQN(JA)*BE*SIN(AINC)
      VEN=TEQN(JA)*BE*SIN(AINC)
```

```
      VFS=UEQS(JA)*BE*SIN(AINC)
      VES=TEQS(JA)*BE*SIN(AINC)
      GO TO 30
40    AIEN=-AI1
      AIES=AI3
      EHNN=(S2N*S2N*AINN-S4N*S2N*AIEN)/(S4N*S2N*S2N+S4N*S4N
     XX*S1N)
      EHNS=(S2S*S2S*AINS-S4S*S2S*AIES)/(S4S*S2S*S2S+S1S*S4S
     XX*S4S)
      EHEN=(S2N*S2N*AIEN+S1N*S2N*AINN)/(S1N*S2N*S2N+S4N*S1N
     XX*S1N)
      EHES=(S2S*S2S*AIES+S1S*S2S*AINS)/(S1S*S2S*S2S+S4S*S1S
     XX*S1S)
      N=N+1
      IF((N-08).LT.0.)GO TO 120
      VW=-(-AINN*REN+EHNN+TEN(JA)*BE)/BE
      VN=-(-AIEN*REN+EHEN+TEQN(JA)*BE)/BE
      WRITE(6,16)TIME(JA),VN,VW
16    FORMAT(' ',20X,'TIME IS ',F10.2,5X,'VN',F10.0,5X,'VW'
     XX,F10.0,//)
      JA=JA+1
      GO TO 13
100   STOP
      END
```

REFERENCES

Amayenc, P. and G. Vasseur, Neutral winds deduced from incoherent scatter observations and their theoretical interpretation, J. Atmos. Terr. Phys., 34, 351-364, 1972.

Axford, W. I. and C. O. Hines, A unifying theory of high-latitude geophysical phenomena and geomagnetic storms, Can. J. Phys., 39, 1433-1464, 1961.

Baker, W. G. and D. F. Martyn, Electric currents in the ionosphere. I. Conductivity, Phil. Trans. Roy. Soc. London, A246, 281-294, 1953.

Banks, P. M., J. R. Doupnik and S. I. Akasofu, Electric field observations by incoherent scatter radar in the auroral zone, J. Geophys. Res., 78, 6607-6622, 1973.

Banks, P. M., C. L. Rino and V. B. Vickwar, Incoherent scatter radar observations of westward electric fields and plasma densities in the auroral ionosphere, 1, J. Geophys. Res., 79, 187-198, 1974.

Behnke, R. A., Vector measurements of the ion transport velocity with applications to F-region dynamics, Rice University Ph. D. Thesis, 1970.

Behnke, R. A. and T. Hagfors, Evidence for the existence of nighttime F-region polarization fields at Arecibo, Radio Science, 9, 211-216, 1974.

Behnke, R. A. and R. M. Harper, Vector measurements of F-region ion transport at Arecibo, J. Geophys. Res., 78, 8222-8234, 1973.

Behnke, R. A. and H. Kohl, The effects of neutral winds and electric fields on the ionospheric F2-layer over Arecibo, J. Atmos. Terr. Phys., 36, 325-333, 1974.

Bhargava, B. N. and A. Yacob, Local time and solar cycle features of day-to-day variability in geomagnetic horizontal intensity, Ann. Geophys., 30, 487-492, 1974.

Block, L. P., On the distribution of electric fields in the magnetosphere, J. Geophys. Res., 71, 855, 1966.

Brekke, A., J. R. Doupnik and P. M. Banks, Incoherent scatter measurements of E-region conductivities and currents in the auroral zone, J. Geophys. Res., 79, 3773-3790, 1974.

Butler, S. T. and K. A. Small, The excitation of atmospheric oscillations, Proc. Roy. Soc. London, A247, 91-121, 1963.

Carlson, H. C. and J. C. G. Walker, Electrodynamic drift in the nocturnal F-region ionosphere caused by conjugate point sunrise, Planet. Space Sci., 20, 141-148, 1972.

Carpenter, D. L., Whistler studies of the plasma pause in the magnetosphere. I. Temporal variations in the position of the knee and some evidence on plasma motions near the knee, J. Geophys. Res., 71, 693-709, 1966.

Carpenter, D. L., Whistler evidence of the dynamic behavior of the duskside bulge in the plasmasphere, J. Geophys. Res., 75, 3837-3847, 1970.

Carpenter, D. L. and N. T. Seely, Cross-L plasma drifts in the outer plasmasphere; quiet time patterns and some substorm effects, submitted to J. Geophys. Res., 1975.

Carpenter, D. L., K. Stone, J. C. Siren and T. L. Crystal, Magnetospheric electric fields deduced from drifting whistler paths, J. Geophys. Res., 77, 2819-2834, 1972.

Carpenter, L. A. and S. A. Bowhill, Investigation of the physics of dynamical processes in the topside F-region, University of Illinois, Urbana, Illinois, Aeronomy Report No. 44, 1971.

Carpenter, L. A. and V. W. J. H. Kirchhoff, Daytime three-dimensional drifts at Millstone Hill Observatory, Radio Science, 9, 217-222, 1974.

Carpenter, L. A. and V. W. J. H. Kirchhoff, Comparison of high-latitude and mid-latitude ionospheric electric fields, J. Geophys. Res., 80, 1810-1814, 1975.

Carpenter, L. A. and V. W. J. H. Kirchhoff, F-region drift velocities from incoherent scatter measurements at Millstone Hill, PSU-IRL-SCI-437, The Pennsylvania State University, 1975a.

Carru, H., M. Petit and P. Waldteufel, Mis en evidence de mouvements dans l'ionosphere au moyen de la diffusion incoherente, C. r. Acad. Sci. Paris, 264, 560-563, 1967.

Chapman, S., On the diurnal variations of the earth's magnetism produced by the moon and sun, Phil. Trans. Roy. Soc. London, A213, 279-321, 1913.

Chapman, S., The solar and lunar diurnal variations of terrestrial magnetism, Phil. Trans. Roy. Soc. London, A218, 1-118, 1919.

Chapman, S. and J. Bartels, Geomagnetism, Oxford University Press, London and New York, 1940.

Chapman, S. and R. S. Lindzen, Atmospheric Tides, Gordon and Breach, New York, pp. 131, 1970.

Ching, B. K. and Y. T. Chiu, A phenomenological model of global ionospheric electron density in the E, F1 and F-2 regions, J. Atmos. Terr. Phys., 35, 1615-1630, 1973.

Chiu, Y. T., Self consistent electrostatic field mapping in the high latitude ionosphere, J. Geophys. Res., 79, 2790-2802, 1974.

Cho, H. R. and K. C. Yeh, Neutral winds and the behavior of the ionospheric F-2 region, Radio Science, 5, 881-894, 1970.

CIRA 72, COSPAR International Reference Atmosphere, Akademie Verlag, Berlin, 1972.

Doupnik, J. R., P. M. Banks, M. J. Baron, C. L. Rino and J. Petriceks, Direct measurements of plasma drift velocities at high magnetic latitudes, J. Geophys. Res., 77, 4268-4271, 1972.

Dungey, J. W., Interplanetary magnetic field and the auroral zones, Phys. Rev. Letters, 6, 47-48, 1961.

Evans, J. V., Electron temperatures and ion composition in the F1 region, J. Geophys. Res., 72, 3343-3355, 1967.

Evans, J. V., Sunrise behavior of the F-layer at midlatitudes, J. Geophys. Res., 73, 3489-3504, 1968.

Evans, J. V., Theory and practice of ionosphere study by Thomson scatter radar, Proc. IEEE, 57, 496-529, 1969.

Evans, J. V., Observation of F-region vertical velocities at Millstone Hill, 1, evidence for drifts due to expansion, contraction, and winds, Radio Science, 6, 609-626, 1971.

Evans, J. V., Measurements of horizontal drifts in the E and F-regions at Millstone Hill, J. Geophys. Res., 77, 2341-2352, 1972.

Evans, J. V., Upgrading the Millstone Hill radar for International Magnetosphere Studies, a proposal to NSF, 1974.

Evans, J. V., R. A. Brockelman, R. F. Julian, W. A. Reid and L. A. Carpenter, Determination of F-region vertical drifts at Millstone Hill, Radio Science, 5, 27-38, 1970.

Evans, J. V., R. F. Julian and W. A. Reid, Incoherent scatter measurements of F-region density, temperatures and vertical velocity at Millstone Hill, Lincoln Laboratory Technical Report No. 477, 1970a.

Farley, D. T., A theory of electrostatic fields in a horizontally stratified ionosphere subject to a vertical magnetic field, J. Geophys. Res., 64, 1225-1233, 1959.

Forbes, J. M., Wind estimates near 150 km from the variation in inclination of low-perigee satellite orbits, Planet. Space Sci., 23, 726-731, 1975.

Geisler, J. E., Atmospheric winds in the middle latitude F-region, J. Atmos. Terr. Phys., 28, 703-720, 1966.

Gold, T., Motions in the magnetosphere of the earth, J. Geophys. Res., 64, 1219-1224, 1959.

Hagfors, T. and R. A. Behnke, Measurement of three-dimensional plasma velocities at the Arecibo Observatory, Radio Science, 9, 89-93, 1974.

Helliwell, R. A., Whistlers and Related Ionospheric Phenomena, Stanford University Press, Stanford, California, 1965.

Heppner, J. P., Electric field variations during substorms: OGO-6 measurements, Planet. Space Sci., 20, 1475-1498, 1972.

Heppner, J. P., Polar cap electric field distributions related to the interplanetary magnetic field direction, J. Geophys. Res., 77, 4877-4887, 1972a.

Heppner, J. P., High latitude electric fields and the modulations related to interplanetary magnetic field parameters, Radio Science, 8, 933-948, 1973.

Hines, C. O., Diurnal tide in the upper atmosphere, J. Geophys. Res., 71, 1453-1459, 1966.

Hirono, M., On the influence of the Hall current to the electric conductivity of the ionosphere, J. Geomagn. Geoelec., 2, 113-120, 1950.

Hirono, M., A theory of diurnal magnetic variations in equatorial regions and conductivity of the ionospheric E-region, J. Geomagn. Geoelec., 4, 7-21, 1952.

Hirono, M., A theory of diurnal magnetic variations in equatorial regions and conductivity of the ionospheric E-region, II, J. Geomagn. Geoelec., 5, 22-38, 1953.

Jacobs, J. A., Y. Kato, S. Matsushita and Y. A. Troitskaya, Classification of geomagnetic micropulsations, J. Geophys., Res., 69, 180, 1964.

Kirchhoff, V. W. J. H. and L. A. Carpenter, Dominance of the diurnal mode of horizontal drift velocities at F-region heights, J. Atmos. Terr. Phys., 37, 419-428, 1975.

Kohl, H. and J. W. King, Atmospheric winds between 100 and 700 km and their effects on the ionosphere, J. Atmos. Terr. Phys., 29, 1045-1062, 1967.

Lemaire, J., The "Roche-Limit" of ionospheric plasma and the formation of the plasmapause, Planet. Space Sci., 22, 757-766, 1974.

Lindzen, R. S., Reconsideration of diurnal velocity oscillations in the thermosphere, J. Geophys. Res., 72, 1591-1598, 1967.

Maeda, H., The vertical distribution of electrical conductivity in the upper atmosphere, J. Geomagn. Geoelec., 5, 94-104, 1953.

Maeda, H., Horizontal wind systems in the ionospheric E-region deduced from the dynamo theory of the geomagnetic Sq variation, I, J. Geomagn. Geoelec., 7, 121-132, 1955.

Maeda, H., Daily variations of the electrical conductivity of the upper atmosphere as deduced from the daily variations of geomagnetism, II, Rept. Ionosph. Space Res. Japan, 10, 49-68, 1956.

Maeda, H., World-wide pattern of ionization drifts in the ionospheric F-region as deduced from geomagnetic variations, Proc. Conf. Ionosphere 1962, Inst. Phys. and Phys. Soc. London, 187-190, 1963.

Martyn, D. F., Atmospheric tides in the ionosphere, IV, Proc. Roy. Soc. London, A194, 445-463, 1948.

Matsushita, S., Dynamo currents, winds, and electric fields, Radio Science, 4, 771-780, 1969.

Matsushita, S., Interactions between the ionosphere and the magnetosphere for Sq and L variations, Radio Science, 6, 279-294, 1971.

Matsushita, S., Ionospheric F2 motions interacting with the Sq and L fields, Space Res. XII, 1087-1093, 1972.

Matsushita, S. and W. H. Campbell, Physics of Geomagnetic Phenomena, Academic Press, Vol. II, 1967.

Matsushita, S. and J. D. Tarpley, Effect of dynamo region electric fields on the magnetosphere, J. Geophys. Res., 75, 5433-5443, 1970.

Maynard, N. C., Electric field measurements across the Harang discontinuity, Goddard Space Flight Center Report X-625-74-67, 1974.

Mendillo, M., Magnetospheric convection at ionospheric heights, AFCRL-TR-73-0358, 1973.

Mozer, F. S., Electric field mapping in the ionosphere at the equatorial plane, Planet. Space Sci., 18, 259-263, 1970.

Mozer, F. S., Balloon measurements of vertical and horizontal electric fields, Pure Appl. Geophys., 84, 32, 1971.

Mozer, F. S., Simultaneous electric field measurements on nearby balloons, J. Geophys. Res., 77, 6129-6132, 1972.

Mozer, F. S., Electric fields and plasma convection in the plasmasphere, Rev. Geophys. Space Phys., 11, 755-765, 1973.

Mozer, F. S. and P. Lucht, The average auroral zone electric field, J. Geophys. Res., 79, 1001-1006, 1974.

Mozer, F. S. and R. Serlin, Magnetospheric electric field measurements with balloons, J. Geophys. Res., 74, 4739-4754, 1969.

Nair, K. N., R. G. Rastogi and V. Sarabhai, Daily variation of the geomagnetic field at the dip equator, Nature, 226, 740-741, 1970.

Nishida, A., N. Iwasaki and T. Nagata, The origin of fluctuations in the equatorial electrojet; a new type of geomagnetic variation, Ann. Geophys., 22, 478-484, 1966.

Park, C. G., Methods of determining electron concentrations in the magnetosphere from nose whistlers, Technical Report 3454-1, Radio Science Laboratory, Stanford University, 1972.

Park, C. G. and M. Dejnakarintra, Penetration of thundercloud electric fields into the ionosphere and magnetosphere, 1, middle and sub-auroral latitudes, J. Geophys. Res., 78, 6623, 1973.

Rishbeth, H., The F-layer dynamo, Planet. Space Sci., 19, 263-267, 1971.

Rishbeth, H., Thermospheric winds and the F-region: A review, J. Atmos. Terr. Phys., 34, 1-47, 1972.

Rishbeth, H. and O. K. Garriott, Introduction to Ionospheric Physics, Academic Press, New York, 1969.

Saito, T., Oscillation of geomagnetic field with the progress of Pt-type pulsations, Sci. Rep. Tohoku Univ. 5, Geophys., 13, 53, 1961.

Saito, T. and S. Matsushita, Solar cycle effects on geomagnetic Pi 2 pulsations, J. Geophys. Res., 73, 267-286, 1968.

Salah, J. E., R. H. Wand and J. V. Evans, Tidal effects in the E-region from incoherent scatter radar observations, Radio Science, 10, 347-355, 1975.

Sarabhai, V. and K. N. Nair, Daily variation of the geomagnetic field and the deformation of the magnetosphere, Nature, 223, 603-604, 1969.

Schuster, A., The diurnal variation of terrestrial magnetism, Phil. Trans. Roy. Soc. London, A 180, 467-512, 1889.

Schuster, A., The diurnal variation of terrestrial magnetism, Phil. Trans. Roy. Soc. London, A 208, 163-204, 1908.

Spreiter, J. R. and B. R. Briggs, Theory of electrostatic fields in the ionosphere at polar and middle geomagnetic latitudes, J. Geophys. Res., 66, 1731-1744, 1961.

Stening, R. J., Calculation of electric currents in the ionosphere by an equivalent circuit method, Planet. Space Sci., 16, 717-728, 1968.

Stening, R. J., An assessment of the contribution of various tidal winds to the Sq current system, Planet. Space Sci., 17, 889-908, 1969.

Stening, R. J., Longitude and seasonal variations of the Sq current system, Radio Science, 6, 133-137, 1971.

Stening, R. J., The electrostatic field in the ionosphere, Planet. Space Sci., 21, 1897-1910, 1973.

Stening, R. J., private communication, 1974.

Stewart, B., Terrestrial Magnetism, Encyc. Brit., 9th ed., 159-184, 1882.

Storey, L. R. O., An investigation of whistling atmospherics, Phil. Trans. Roy. Soc. London, 246, 113, 1953.

Swift, D. W., Effective height integrated conductivity of the ionosphere, J. Geophys. Res., 77, 1279-1285, 1972.

Tarpley, J. D., The ionospheric wind dynamo, I, Planet. Space Sci., 18, 1075-1090, 1970a.

Tarpley, J. D., The ionospheric wind dynamo, II, Planet. Space Sci., 18, 1091-1103, 1970b.

Taylor, G. N., Meridional F-2 region plasma drifts at Malvern, J. Atmos. Terr. Phys., 36, 267-286, 1974.

Taylor, G. N., H. Rishbeth and P. J. S. Williams, Multistatic incoherent scatter measurements of ionospheric drift velocity, Nature, 242, 109-111, 1973.

Vasyliunas, V. M., Mathematical models of magnetospheric convection and its coupling to the ionosphere, ed. B. M. McCormac, Particles and Fields in the Magnetosphere, 60-71, 1970.

Volland, H., Mapping of the electric field of the Sq current into the lower atmosphere, J. Geophys. Res., 77, 1961-1965, 1972.

Walbridge, E., The limiting of magnetospheric convection by dissipation in the ionosphere, J. Geophys. Res., 72, 5213-5230, 1967.

Watt, T. M., Incoherent scatter observations of the ionosphere over Chatanika, Alaska, J. Geophys. Res., 78, 2993-3006, 1973.

Woodman, R. F., Vertical drift velocities and east-west electric fields at the magnetic equator, J. Geophys. Res., 75, 6249-6259, 1970.

Woodman, R. F., East-west ionospheric drifts at the magnetic equator, Space Res. XII, 969-974, 1972.

Woodrum, A. and C. G. Justus, Atmospheric tides in the height region 90 to 120 kilometers, J. Geophys. Res., 73, 467-478, 1968.